SEDIMENT MANAGEMENT IN LOW ENERGY ESTUARIES: THE LOXAHATCHEE, FLORIDA

By

RASHMI RANJAN PATRA

A THESIS PRESENTED TO THE GRADUATE SCHOOL
OF THE UNIVERSITY OF FLORIDA IN
PARTIAL FULFILLMENT OF THE REQUIREMENTS
FOR THE DEGREE OF MASTER OF SCIENCE

UNIVERSITY OF FLORIDA

2003

ACKNOWLEDGMENTS

My sincere gratitude is reserved for Dr. Ashish J. Mehta for his guidance in my education and research, which made my studies very precise and rewarding, as well as the entire Coastal and Oceanographic Engineering Program faculty. Also deserving my gratitude for their guidance and assistance are Dr. John Jaeger, Dr. William McDougal, and Kim Hunt. Most of the analysis in the study was made possible by the valuable assistance provided by Mr. Sidney Schofield, who taught me the basics of analysis. Special thanks are due to Dr. Earl Hayter for setting up, supporting and guiding me through the numerical model in its entirety.

Thanks are also due to Dr. Zal S. Tarapore, for his encouragement and guidance, which marked my initial years as a coastal engineer and my studies here possible. My wife Sumitra and my friend Anjana also deserve special kudos for their emotional and editorial support. Finally, my mother and father merit unlimited praise for providing me with mind, body and soul, as do my other friends and families for developing it.

TABLE OF CONTENTS

LIST OF TABLES

LIST OF FIGURES

LIST OF SYMBOLS

A	area
A_v	vertical turbulent viscosity
B	width of the basin
C	wave celerity
C_0	uniformly distributed initial sediment concentration (kg/m^3)
C_s	sediment concentration (kg/m^3)
C_{cue}	constant multiplier for u-velocity conversion to true east
C_{cun}	constant multiplier for u-velocity conversion to true north
C_{cve}	constant multiplier for v-velocity conversion to true east
C_{cvn}	constant multiplier for v-velocity conversion to true north
D	sediment deposition under reduced flow
D_{en}	deposition at the entrance to the channel
D_{ex}	deposition at the exit of the channel
D_p	dimensionless projected vegetation area
H	total water column depth
L	length of the channel/trap
K	coefficient of conductance
Q_H	volume source or sink
R_q	Richardson number

T	time
U	steady mean flow velocity
$\overline{U}$	velocity vector
W	width of the channel in equation 5.8
W_s	settling velocity
b	buoyancy
c_p	vegetation resistance
f	Darcy-Weishbach friction factor
f_e	coriolis acceleration
g	acceleration due to gravity
h	water depth
m_x	scale factor along x-axis
m_y	scale factor along y-axis
q	turbulent intensity
$(q_s)_i$	amount of sediment in influent
$(q_s)_e$	amount of sediment in effluent
r	removal ratio
u	velocity along the channel (x-axis)
u_*	friction velocity
u_c	velocity amplitude under current
$u_{c(en)}$	current at the entrance
$u_{c(ex)}$	current at the exit

u_{cr}	critical velocity for erosion
u_{co}	curvilinear-orthogonal horizontal velocity
u_{te}	velocity in true east direction
v	velocity across the length of the channel(y-axis)
v_{co}	curvilinear-orthogonal horizontal velocity
v_{tn}	velocity in true north direction
z	variable water depth
ρ	water density
ρ_0	reference water density
τ_s	bed erosion shear stress
τ_{bx}	x-component shear stress
τ_{by}	y-component shear stress
τ_b	bed bottom shear stress
η_c	mid-tide elevation
η_{HT}	high-tide elevation
η_{LT}	low tide elevation
ε	vertical diffusivity
κ	Karman constant
ϕ	free surface potential
θ	velocity angles

Abstract of Thesis to the Graduate School
of the University of Florida in Partial Fulfillment of the
Requirements for the Degree of Master of Science

SEDIMENT MANAGEMENT IN LOW ENERGY ESTUARIES: THE LOXAHATCHEE, FLORIDA

By

Rashmi Ranjan Patra

December 2003

Chairman: Ashish J. Mehta
Major Department: Civil and Coastal Engineering

Implementation of schemes for sediment entrapment and self-cleaning channels was examined in the micro-tidal estuarine environment containing both sand and fine sediment. The central embayment of the micro-tidal Loxahatchee River estuary on the Atlantic Coast of Florida was chosen as the candidate location due to its unique characteristics with respect to the influx of sand and fine sediment in its central embayment, and concerns regarding the potential for long term impacts of this flux on the embayment. An ideal sediment trap captures all of incoming sediment, i.e., the removal efficiency is 100%. A self-cleaning channel allows no net deposition of incoming sediment, which passes through, so that its removal efficiency is nil.

Hydrodynamic model simulations were carried out for selected trap/channel alternatives, and their efficiency was calculated by relating sediment deposition to change in the flow regime due to implementation of these alternatives. Calculations indicated

that the concepts of sediment entrapment and of self-cleaning can operate only imperfectly in the study area due to the low prevailing forcing by tide and the episodic nature of freshwater discharges in the tributaries.

Fine sediment accumulation in the central embayment can be reduced by dredging the C-18 canal, as the trapped sediment would account for more than half of the total fine sediment entering the bay. A channel close to the southern bank of the embayment could improve bay flushing by ebb flow, reduce bay-wide sedimentation and serve as a navigation route. Careful design with regard to channel alignment would be required to avoid sea grass beds in the area. Long term simulations of flow and sediment transport are required to assess sediment circulation patterns and the formation of shoals in the central embayment and the Northwest Fork.

CHAPTER 1
INTRODUCTION

1.1 Problem Statement

Sedimentation due to the influx of fine and coarse particles is an issue affecting numerous estuaries and coastal waterways. Often enough, these particles originate far inland, and are transported into the coastal zone by runoff and stream flow. In the estuarine regime, inorganic sediment almost never occurs in isolation, as it is complemented by measurable organic fraction produced by either indigenous sources (e.g., native phytoplankton, swamp vegetation, wind blown material), or allochthonous sources (e.g., river-borne phytoplanktons, swamp vegetation, windblown material) (Darnell, 1967). In turn, such organic-rich sediments can degrade water quality by oxygen uptake and a reduction in light penetration. In this study, the question of preemptive dredging of sediment prior to its deposition in an area of concern or, as an alternative, preventing its deposition in the area of concern by channelizing flow, was studied. The candidate water body was the estuarine segment of the Loxahatchee River on the east coast of Florida.

Loxahatchee River, which discharges mainly through its Northwest Fork, supplies mainly quartz sand and organic detritus. Clay mineral makes up less than 5% of the mud in the estuary, but because this mud is rich in organic matter, its accumulation has become a matter of concern in the central embayment of the estuary. This flow, in addition to controlled discharges from the S-46 structure in the C-18 Canal at the head of

the Southwest Fork, brings in much of the sediment (mean concentration 0.014 kg/m^3; Sonnetag and Mcpherson, 1984) in the central embayment.

A commonly employed solution to reduce sedimentation is the implementation of a trap scheme by trenching the submerged bottom. Such a trench-trap is a means to increase the depth at the chosen location by dredging. Increased depth results in a decreased flow velocity (and associated bed shear stress), thereby allowing incoming sediment to settle in the trap, instead of being carried further downstream. The removal of sediments becomes much easier as it can be then be removed from the trap, rather than dredging the otherwise distributed deposits from a considerably broader area. As an alternative to sediment entrapment, creating a self-cleaning channel in the area of concern for sedimentation would mean that sediment would pass through the system, without deposition. The degree to which both approaches can function depends on the flow conditions, type of sediment and the morphology of the estuary.

Given the above background, the objectives of this study were: 1) to determine the efficiency of traps installed at selected locations in the estuary, and 2) to evaluate the efficiency of channels as a means to pursue the goal of a self-cleaning sedimentary environment.

Shoaling has occurred the Loxahatchee in many areas, especially near the confluences of the major tributaries (Northwest Fork and Southwest Fork) in the central embayment where the velocities are typically low (Sonntag and McPherson, 1984). Recent studies (Jaeger et al., 2002) suggest internal recirculation of sediments as an important factor governing sediment transport within the estuarine portion of the river. Accordingly, in order to manage sedimentation in the central embayment, it may be

desirable to test trap/channel deployments at multiple locations. The performance of these schemes was evaluated with regard to efficiency of sediment removal.

1.2 Study Tasks

The tasks undertaken included:

1. Data collection from the site and scrutiny of data from the existing literature to characterize the nature of flow, sediment transport and sedimentation. This included measuring tidal elevations, current velocities, sediment concentrations and bed sediment distribution (Jaeger et al., 2002) in the estuary, and obtaining stream flow data for the tributaries from the literature.

2. Simulating the flow field using a hydrodynamic model, in order to determine the velocities, water surface elevations and bed shear stress distributions.

3. Introduction of trap schemes in the calibrated flow model to determine flow velocities with and without the trap, and development of relationships for calculating trap efficiency.

4. Introduction of self-cleaning channels and an assessment of their viability.

5. A qualitative assessment of the usefulness of the approaches based on selected criteria.

1.3 Outline of Chapters

Chapter 2 describes the sediment management alternatives including existing conditions and the proposals for implementation. Chapter 3 deals with the field data collection for this study including data analysis and interpretation. Flow model calibration and validation is included in Chapter 4 and evaluation of management alternatives is described in Chapter 5. Summary of the results and conclusions are made in Chapter 6, followed by a bibliography of studies cited.

CHAPTER 2
SEDIMENT MANAGEMENT ALTERNATIVES

2.1 Present Condition of the Loxahatchee Estuary

Loxahatchee River empties to the Atlantic Ocean through the Jupiter Inlet located in northern Palm Beach County on the south coast of Florida, about 28 km south of St. Lucie Inlet and 20 km north of Lake Worth Inlet. The three main tributaries, which feed the estuary, are the Northwest Fork, the North Fork, and the Southwest Fork. In addition, the Jones Creek and Sims Creek, which are far lesser tributaries than the others, also feed the estuary through the Southwest Fork. Figures 2.1 shows the general location map of the study area.

The major surface flow in to the estuary historically was through the Northwest Fork draining the Loxahatchee Marsh and Hungry land slough (refer Fig 2.1). The upstream reach of the Southwest Fork, referred to as the C-18 canal, was created in 1957/58 in the natural drainage path in order to lengthen the area of influence of the Southwest Fork and facilitate drainage of the westward swampland (Refer Figure 2.1 and Figure 2.2). The flow in the canal is regulated by the S-46 automated sluice gate structure. Whereas, the Southwest and the Northwest fork converge on the estuary approximately 4 km west of the inlet, the North fork joins the central bay about 3 km west of the inlet. Down stream of the Florida East coast Railroad (FECRR) Bridge the Intracoastal Waterway (ICWW) intersects the estuary in a dogleg fashion. Five navigation/access channels exist on the south shore of the central embayment

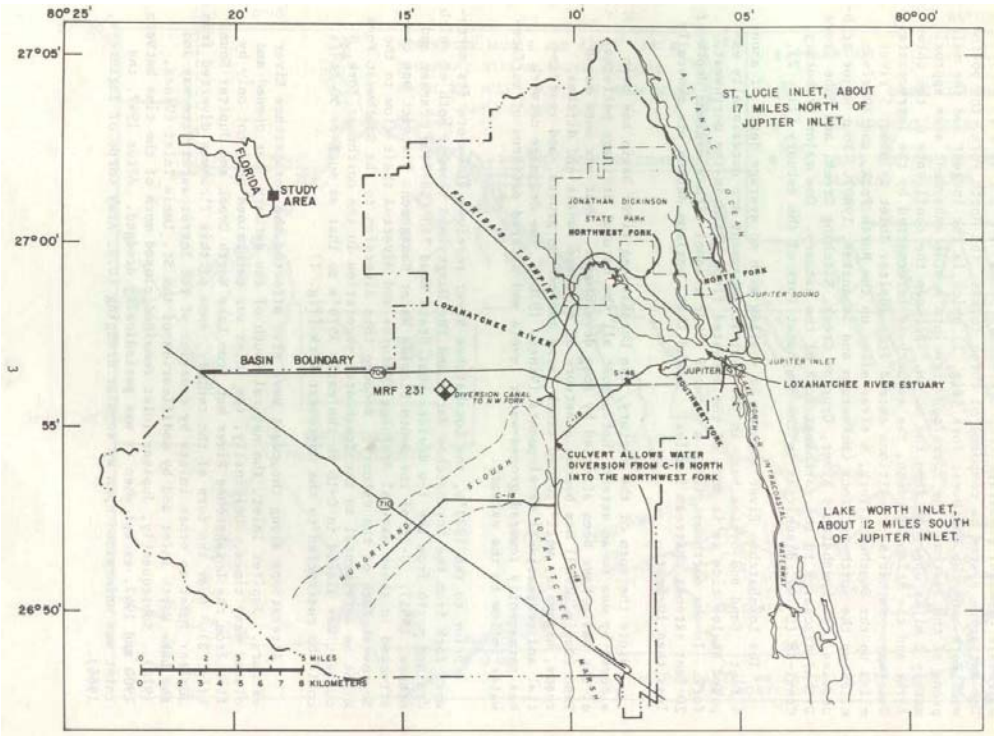

Figure 2.1 Location map of the study area (Source: U.S. Geological Survey report no.84-4157, 1984)

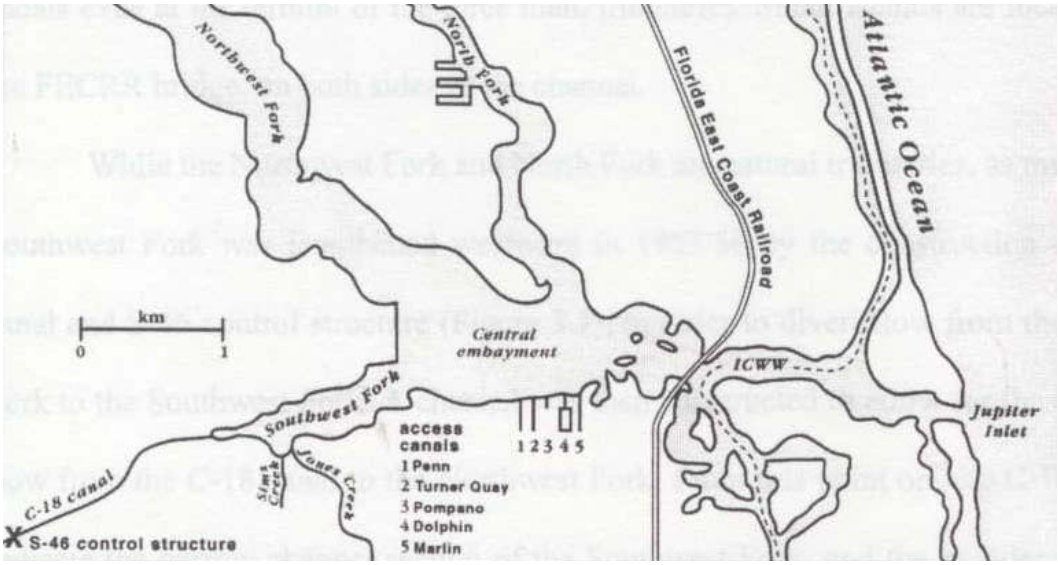

Figure 2.2 Loxahatchee River estuary and tributaries

A detailed hydrographic survey of the central embayment (Figure 2.3) and the Northwest and Southwest Forks carried out in November' 2001 (Lidberg Land Surveying, Inc) indicates the depths in the estuary, which range between 0 m (reference to North Atlantic Vertical Datum 1988, (NAVD 88)) near the sandy shoals to almost 6 m

in the entrance channel near the FECRR Bridge. The average depth over the embayment is just over 1 m. The navigation channel (maintained by the Jupiter Inlet District) runs westward from the Inlet, under the FECRR bridge, and through the central embayment approximately 14 km upstream from the Inlet. The navigation Channel has a bottom width of about 30.5m (100 feet) and is maintained at - 1.75m(5.74feet) (reference to National Geodetic Vertical Datum 1929, (NGVD 29) and – 2.21m (7.24feet) with reference to NAVD 88) with a side slope of 1:3. Flood shoals, which approximately bisects the central embayment exists mainly due to the sand influx from the ocean, and smaller shoals exist at the termini of the three main tributaries. Small shoal islands are located west of the FECRR bridge, on both sides of the channel.

The Northwest Fork and North Fork are natural tributaries draining in to the central embayment. However, as mentioned the Southwest Fork was lengthened westward by construction of C-18 canal with a control structure (S-46), in order to divert flow from the Northwest Fork to the Southwest Fork. A channel was then constructed allowing the diversion of flow from the Northwest Fork to the Southwest Fork. For easy reference from this point on, the C-18 canal will be indicated as the narrow channel section and the broader section at the root will be called Southwest Fork (Figure 2.2).

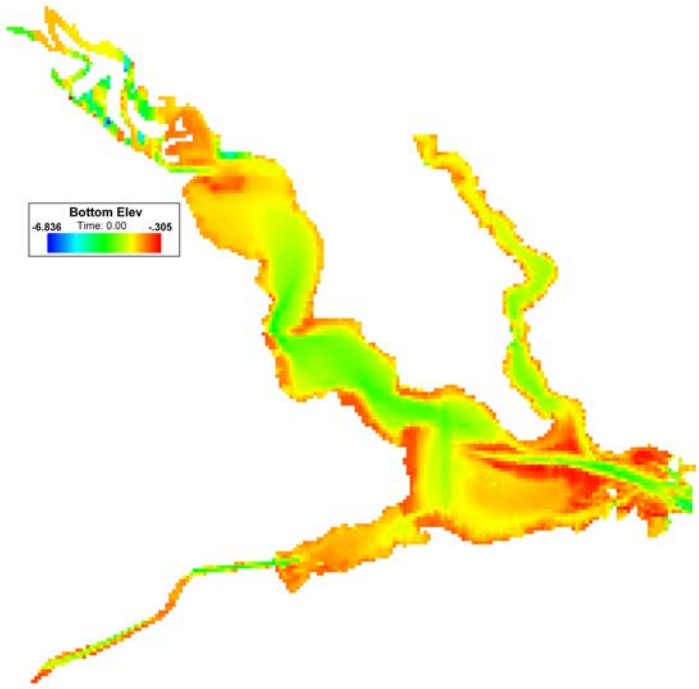

Figure 2.3 Hydrographic survey of the estuary (November 2001)

The Loxahatchee River estuary drains over 1000 km^2 of land through the three main tributaries, the ICWW, and several minor tributaries. The individual watershed basins are shown in Figure 2.4 and listed in Table 2.1. The watershed constitutes residential areas, agricultural lands, and uninhabited marsh and slough areas.

Table 2.1 Basin area distributions in the Loxahatchee River estuary watershed

Basin	Area (km^2)
Intracoastal Water way	545
C – 18 Canal	278
Jonathan Dickinson	155
South Indian River	65
Loxahatchee Rive	6

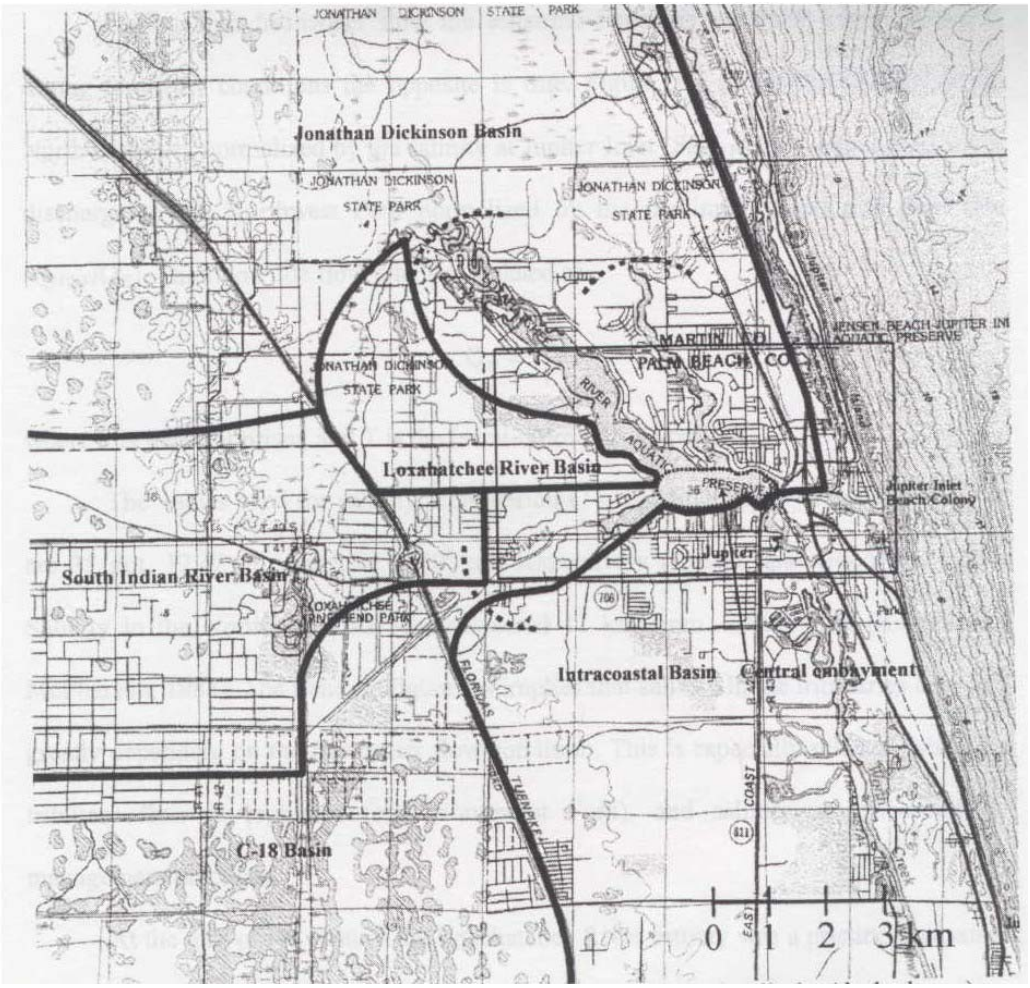

Figure 2.4 Loxahatchee River estuary watershed basins, estuarine limits (dashed arcs) and central embayment

Unlike more northerly estuaries, upland drainage in to the Loxahatchee provides only quartz sand and organic detritus. Clay mineral makes up less than 5% of the mud in the estuary (McPherson, 1984). Earlier studies indicate that the estuary was periodically open and closed to the sea due to various reasons. Originally, flow from the Loxahatchee River along with that from Lake Worth Creek and Jupiter Sound kept the inlet clean. With the construction of the ICWW and the Lake Worth inlet and the modifications of the St.Lucie Inlet in 1970, some flow was diverted. Subsequently, Jupiter Inlet generally remained closed until 1947, except when it is dredged periodically. After 1947, it was

maintained open by dredging by the Jupiter Inlet District and the U.S. Army Corps of Engineers.

Dredge and fill operations have also been carried out in the estuary embayment and forks. In the early 1900's, there was significant amount of filling at the present FECRR Bridge, which narrowed the estuary from 370 m to 310 m. The areas east and west of the bridge (and also under the bridge) were dredged in mid-1930's, and also in 1942. The material was high is shell content and was used in construction of roads. In 1976-77, additional estimated 23,000 m^3 materials were removed from the estuary at the bridge and from an area extending 180 m from the west. Some dredging was also carried out in the Southwest Fork near the C-18 canal in the early 1970's (Wanless, Rossinsky and McPherson, 1984). In 1980, three channels were dug in the embayment, and an estimated 23,000 m^3 of sediment were removed.

After 1900, the estuary was greatly influenced by the dredging and alteration of the drainage to the basin. With gradual lowering of the water table and resultant effect on the water quantity, the direction and pattern of inflow (McPherson and Sabanskas, 1980) were considerably affected. Historically, the major surface flow to the estuary was in to the Northwest Fork from the Loxahatchee Marsh and the Hungry-land Slough (Figure 2.1), both of which drained north. A small agricultural canal was dug before 1928 to divert a small amount of water from the Loxahatchee Marsh to the Southwest Fork. As noted, in 1957-58, C-18 canal was constructed along the natural drainage way to divert flow from the Northwest Fork to the Southwest Fork of the estuary.

Jaeger et al., (2001) carried out extensive studies in the estuary to reevaluate the nature of environmental sedimentology in the lower Loxahatchee River Estuary and as a

companion study to Ganju et al. (2001). Specifically, new samples were collected in order to 1) examine changes in surficial sediment types between 1990 and 2000, 2) attempt to determine the sources of fine-grained muddy sediments accumulating within the estuary; and 3) examine rates of sedimentation within the central embayment and three forks (North, Northwest, and Southwest/C-18 canal) by collecting a suite of ~1-m long pushcores and ~3 m long vibracores within the estuary. Grab samples were collected in all regions of the estuary and were analyzed. One of the main findings of the study was the internal movement of the sediments in the estuary system. With the growth of the population on the shoreline and associated human activities the mangroves dotting the shoreline started vanishing. The removal of these Mangrove cover from the shoreline released a large quantity of sediments, which was otherwise trapped in their roots. Essentially fine grained, these sediments moved with the flow and started getting deposited in the estuarine bounds. According, to this study new shoals were developed/grown by this process, especially the submerged one in the Northwest Fork, down stream of the shoal identifiable from a satellite map and Figure 4 of the Report (Jaeger et al., 2001). The aerial photograph reproduced in Figure 2.5 also indicates an additional shoal developing from the root of the existing shoal, suggesting that the general nature sediments being fed by the Northwest Fork is coarse grained with the fine grained ones carried downstream with the current before deposition.

Tidal flow into and out of the estuary is much larger than freshwater inflow from all the major tributaries. Fresh water flow is reported to be about 2 percent of the total tidal inflow (Sonnetag and McPherson, 1984). Tides are mixed semidiurnal (twice daily with varying amplitude) with a tidal range of about 0.6 to 0.9 m. Tidal waves advances

up the estuary at a rate of 2.23 m/s to 4.46 m/s (McPherson and Sonnetag, 1984) and shows little change in the tidal amplitudes over to about 16 km river km. Winds have a significant effect on the tidal ranges especially the strong northeast winds which prevails during autumn and winter for example can push in additional water into the estuary affecting the tidal ranges.

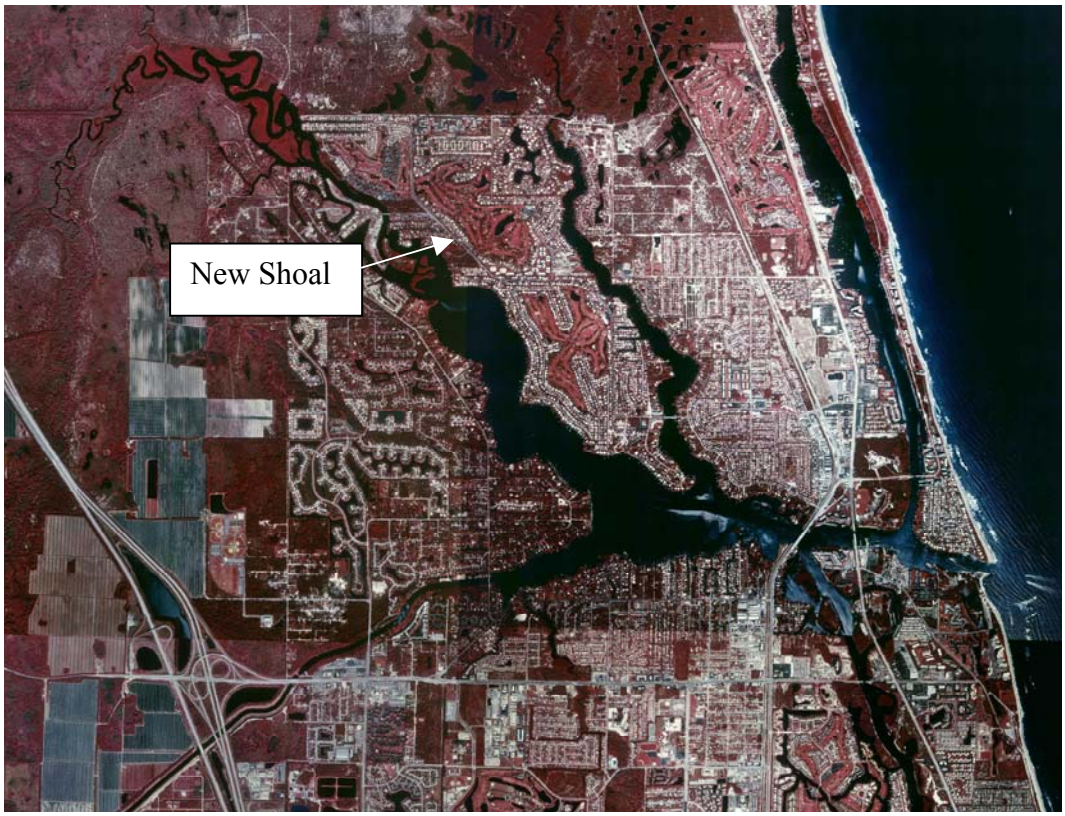

Figure 2.5 Ariel photograph showing development of new shoal

Estuarine conditions extends in the estuary from the inlet for about 8 river km into Southwest Fork, 9.6 river km in to the North fork and 16 river km into the Northwest Fork.

Of late, the environmental condition of the Loxahatchee River and the estuary has become a matter of great concern. The major factor affecting the environmental health is the sediment transported in to the estuary. Large amount of the sediments settling in the

basin might affect the bottom life, alter circulation patterns, and accumulate shoals, thereby impeding boat traffic (McPherson, Wanless and Rossinsky, 1984).

2.2 C-18 Canal

2.2.1 Present Condition

The C-18 canal drains the Loxahatchee Slough, a shallow swamp-like feature containing diverse flora and fauna. However, estuarine conditions persist for 8 km up the Southwest Fork/C-18 canal measured from the inlet.

Flow data obtained from USGS stream flow gage data, for all available years (1971-2002 N.W. Fork, 1980-1982 N. Fork, and 1959-2002 S.W. Fork) indicate that C-18 canal/Southwest Fork carries a maximum discharge of 61.54 m^3/sec. Cumulative frequency distribution curves were constructed to designate (Figure 2.6 a-c) median and extreme flow events (Table 2.2) for all the tributaries. The C-18 canal is regulated at S-46 structure, which is basically a gated sluice. The criterion for controlling the flow at the S-46 structure is based on water level behind the structure. When the level exceeds a predetermined mark, the sluice gates are opened until the level recedes by 30 cm (Russell and McPherson, 1984), at which point the gates are closed. This regulation has resulted in a discontinuous flow record; with weeks of no flow passing the structure, and days when storm flows have been released. During normal wet season, the level behind the S-46 structure is not always sufficiently high for releasing flow, while the other tributaries are freely discharging to the estuary.

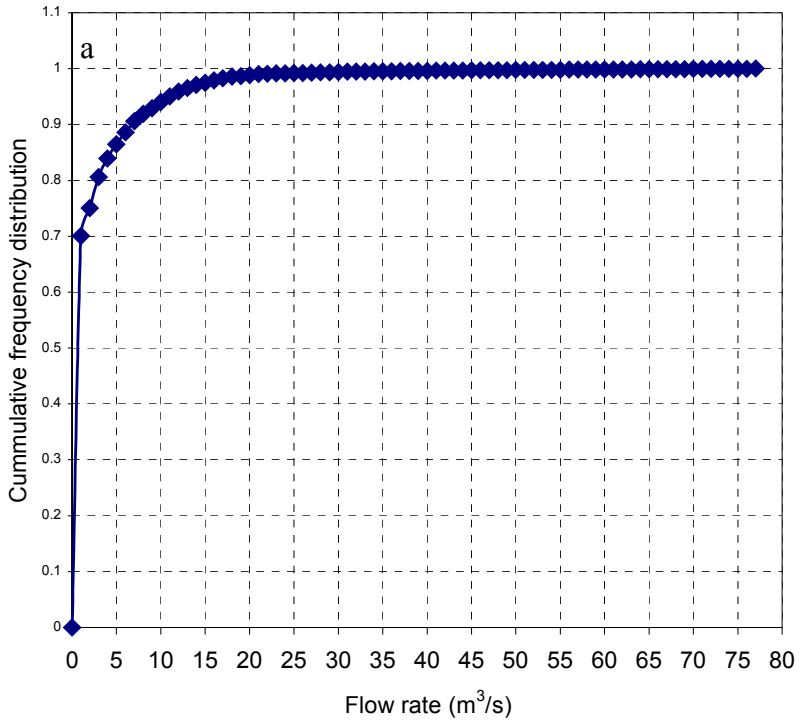
a
Cummulative frequency distribution
Flow rate (m3/s)
0
0.1
0.2
0.3
0.4
0.5
0.6
0.7
0.8
0.9
1
1.1
0
5
10
15
20
25
30
35
40
45
50
55
60
65
70
75
80

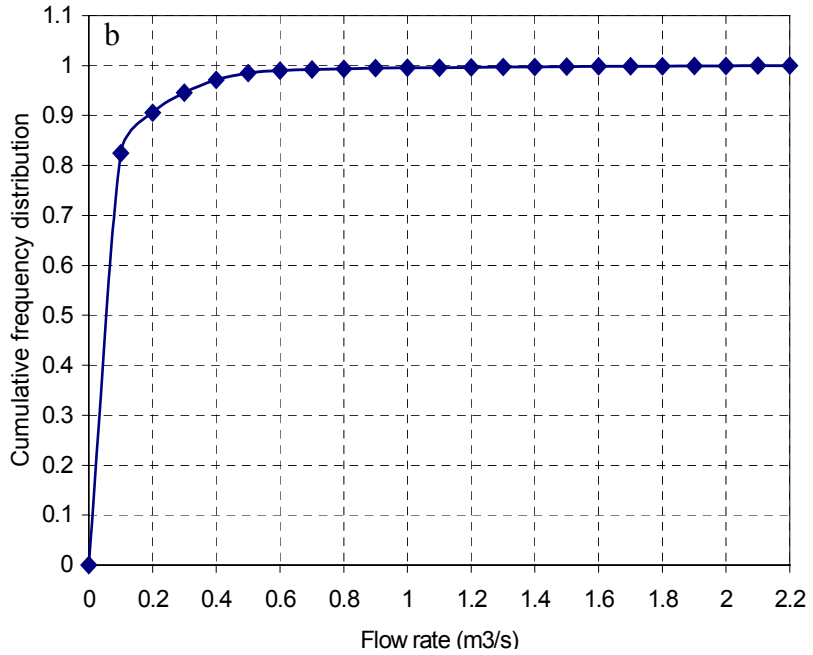
b
Cumulative frequency distribution
Flow rate (m3/s)
0
0.1
0.2
0.3
0.4
0.5
0.6
0.7
0.8
0.9
1
1.1
0
0.2
0.4
0.6
0.8
1
1.2
1.4
1.6
1.8
2
2.2

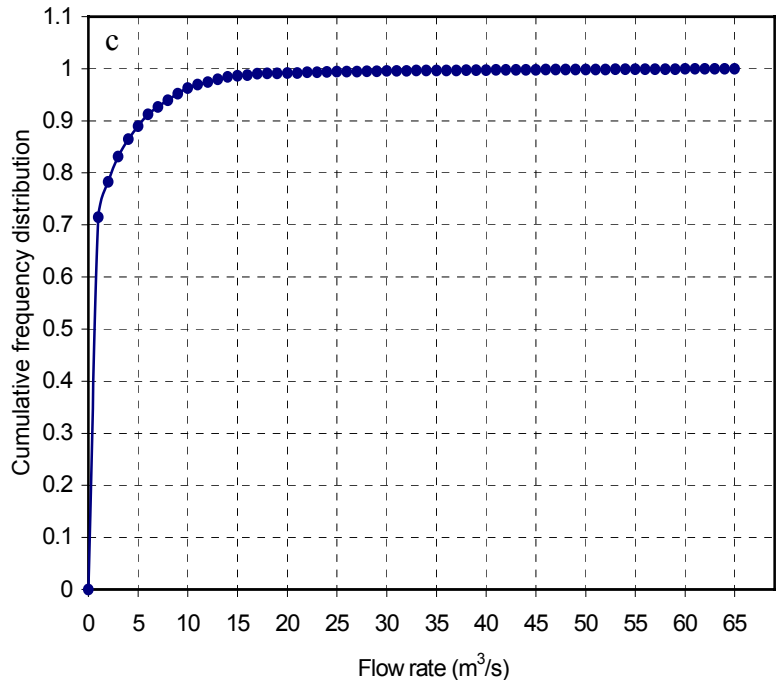

Figure 2.6.Cumulative discharge plot. a) Northwest Fork. b) North Fork. c) Southwest Fork.

Table 2.2 Statistical tributary flow (based on Figures 2.6 a-c)

Tributary	Median Flow (50%) (m^3/s)	High Flow (90%) (m^3/s)	Maximum Flow (98%) (m^3/s)
Northwest Fork	0.7	4.1	76
North Fork	0.1	0.21	1.9
Southwest Fork	1.3	7.8	61

Sonnetag and McPherson (1984) reported two values of suspended solid sediment concentration (0.059 kg/m^3, 0.017 kg/m^3) with corresponding flow data for the C-18 canal (31 m^3/s, 28 m^3/s, respectively) and a mean concentration value for duration (1980-82) of their study (0.014 kg/m^3). The median flow for the C-18 canal (1.3 m^3/s) from the Figure 2.6c was correlated to this mean value of concentration in the present study. A fit in the form of (Müller and Föstner, 1968)

$$C = a_s Q^{b_s} \tag{2.1}$$

was used (Ganju et al., 2001), where a_s and b_s are site specific coefficients, with a_s is indicative of the erodibility of the upstream banks/bed and exponent b_s is indicative of the intensity of the erosional forces in the river.

Table 2.3 Median and high flow concentration data and coefficients for equation 2.1

Tributary	Median flow Concentration (kg/m3)	High flow Concentration (kg/m3)	a_s Coefficient	b_s Coefficient
Northwest Fork	0.011	0.023	0.012	0.27
North Fork	0.01	0.018	0.018	0.02
Southwest Fork	0.014	0.059	0.012	0.49

Fieldwork, consisting of bottom profiling and sampling, was carried out during July 2001 (Jaeger et al.,) by collecting a suite of ~1-m long push cores and ~3 m long vibracores within the estuary. A total of 110 samples were collected from sampling locations covering the entire estuary and river (Figure 1, Final Report on Sedimentary processes in the Loxahatchee River Estuary, 5000 Years ago to the Present, Jaeger et al., 2001) including from outcrops of regional surficial geological unit (undifferentiated 1.8 million year-old Pleistocene sediments) in order to examine the potential sediment sources (Loxahatchee River, C-18 canal, Inlet, and Pleistocene-Age (last 1.8 million years) sediments exposed along the banks of the C-18 canal. 56 of the samples were reoccupations of sites sampled in 1990 and were reported (Mehta et al.,1992). These new samples were collected to examine the changes in sediment characteristics pattern over a 10-year period. Positions of all sampling sites were determined by differential GPS providing a position accuracy of ~1 m. Each grab sample recovered approximately 1,000-2,000 cm^3 of sediment, removing approximately the uppermost 1-5 cm of the sediment surface. Sediment distribution maps produced from these grab samples indicate

particle sizes reveal that the majority of the estuary is dominated (by weight) of fine, well-sorted sand in the ~150 micron (3 phi; 0.15 mm) size range (Jaeger et al., 2001)

In the same study conducted by Jaeger et al., (2001), poling depths (obtained by pushing a graduated pole into bottom until a hard substrate is reached) in the C-18 canal were determined to estimate sedimentation rates along the length of the canal. Since the bottom was dredged at the time of construction of the canal in 1957/58, the bed thickness can be considered to represent the subsequent accumulation. This is because, the dredging of the canal in 1958 would have most likely left behind a hard, sand rich horizon that could not be easily penetrated with the solid rod. Figure 2.7 shows these thicknesses along the canal length. Sediment thickness increases with the distance from the S-46 structure, possibly due to the large erosional forces near the structure (when flow is released), and reduction of these forces as the flow moves along the canal, allowing more deposition of sediment.

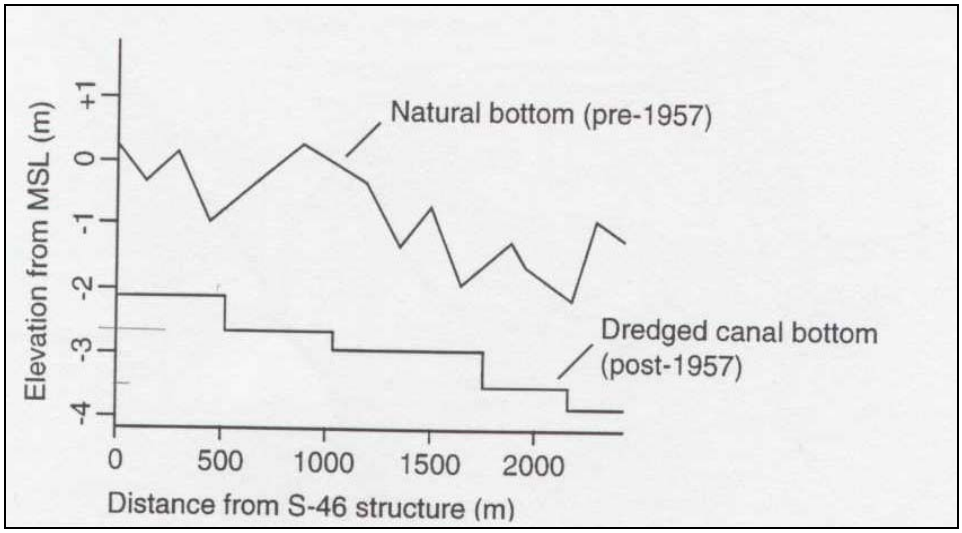

Figure 2.7 Dredging Plans for C-18 canal, 1956 *(Source: Ganju et al., 2001)*

This coarse sand layer was sampled at the base of push cores (see Figures 21 and 22 from Jaeger et al., 2001). There appears to be a trend of increasing thickness away

from the S-46 control structure (Figure 19). Modeling of sediment transport in the canal (Ganju et al., 2001) also supports such a trend. The overall sedimentation rates (10-50 mm/yr) in the canal are very high for most coastal areas, where sedimentation has kept pace with the rise in sea level (3-5 mm/yr) (Davis, 1994). However, this sampling technique of poling only provides mean sedimentation rates over this 42-year (1958-2001) time period. Analyses of push cores collected in the canal document alternating layers of clean sand and muddy sand/sandy mud (see Figures 21-22, Jaeger et al., 2001). This inter-layering of sediment types is characteristic of time-varying deposition rates/erosion rates. When the sluice gates are opened, fast currents can erode the sediment surface followed by rapid deposition of sand and mud. The best way to evaluate time-varying sedimentation rates is with either accurate annual bathymetric profiles or by measuring naturally occurring radioisotopes in the sediment cores (Jaeger et al., 2001).

2.2.2 Management Options

Dredging plans for the C-18 canal from 1956 is shown in Figure 2.7 (U.S. Army Corps of Engineers, 1956). The existing bottom was deepened to 3 m at some locations to facilitate drainage. The depths refer to the National Geodetic Vertical datum of 1929 (NGVD). The present mean depth of the canal as measured along the length is 1.2 m. Hence there has been substantial sedimentation in the canal, which in turn means that it no longer serves as a sediment trap and allows sediment to be transported to the central embayment. One way of maintaining the depth in the canal is to devise a suitable dredging option coupled with a designed flow regime in order to maintain the canal in the self-cleaning mode. However**,** one of the main difficulties in this is the lack of continuous supply of water. As described earlier, the flow in the canal is erratic and controlled by the S-46 control structure. Accordingly, although the median flow in this canal is higher than

the other tributaries, the flow is episodic and therefore not enough to overcome the bed shear resistance of the deposited sediments. This situation can be illustrated by data collected during between April 4th and April 24th, 2002.

Figure 2.8 indicates the dependence of the current velocity on the released discharge. The sudden jump in the over all current magnitude recorded downstream of the structure therefore exhibit strong erosional trend as can be seen from the Figure 2.9. In addition, it indicates that, sediment concentrations in the bottom layers are much more pronounced due to the obvious reason of erosion of the bed. It can therefore be concluded that, a sustained and regular flow regime would help keeping the canal sediment free.

An option is to increase the depth in the canal by dredging part or all of it, thereby recreating the sediment trap. As an alternative, a detailed study of the flow pattern can be undertaken and a suitable flow regime worked out. This would involve redesigning of the control structure and a better regulation of the flow. However, the following points should be noted:

1. The capacity of flow from the structure appears to be insufficient to flush out sediment beyond 1.2 km (Ganju et al., 2001) from the structure even under "high" discharges when the gates are open.

2. A potential option is to change the gate configuration but not the flow regulation schedule. If changing the gate configuration from sluice to weir is successful, it would create a sediment trap upstream of the gate, which would "buy time" for the downstream reach of the canal, but this upstream trap would eventually have to be dredged to maintain it effectiveness. The volume of material trapped will be restricted the weir height. Over-depth dredging upstream is a viable option.

3. However, because sediment transported across the gate is believed to be quite heterogeneous (ranging from fine sand to clay and organic matter) and the organic material is presently not found in the bed there, *predictive* modeling the transport of sediment across the gate will be an uncertain exercise without extensive data collection on both sides of the gate. An option would be to carry out gate conversion and work with the new system based on a rough estimation of the new flow/sediment regime. It is likely that some modification of gate opening schedule may also have to be carried out to improve the efficiency of the upstream trap.

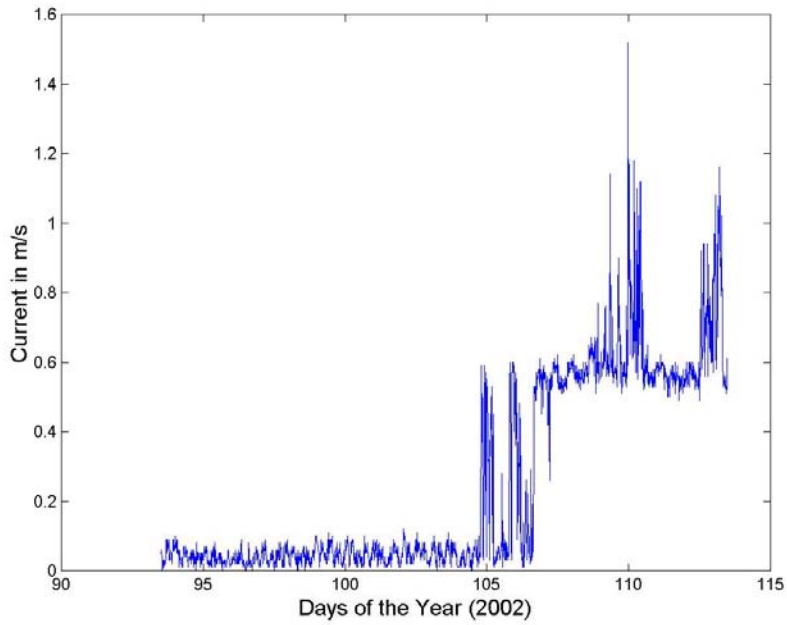

Figure 2.8 Current variation under the effect of released discharge from the S-46 structure.

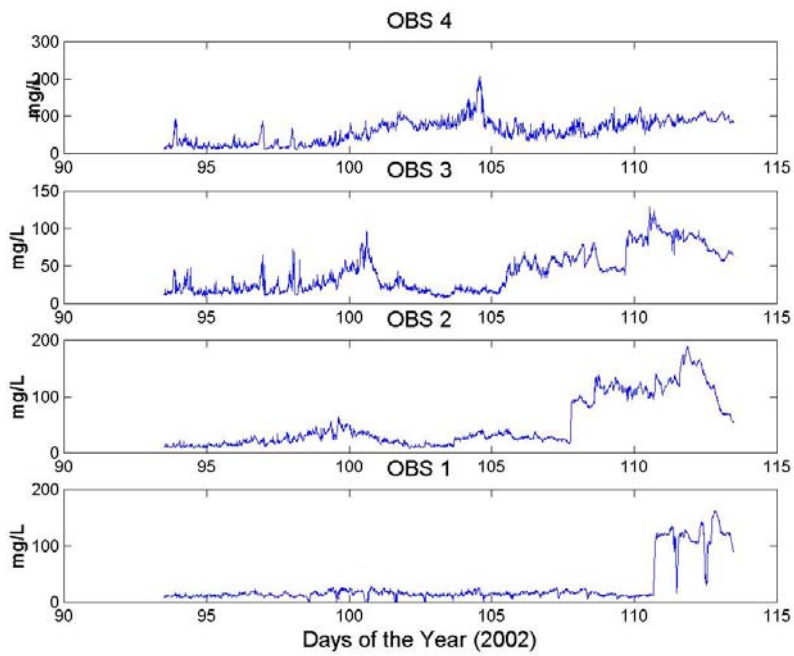

Figure 2.9 Effect of S-46 discharge on the suspended sediment concentration

The present study envisages examining the option dredging the downstream canal. Ganju (2001) carried out such an exercise by testing the effectiveness of a comparatively

short sediment trap. The trap design and results of the investigation are summarized below.In order to quantify the sedimentation rate as a function of discharge in the C-18 canal investigations were carried out using calibrated sediment transport models. The boundary conditions were designed to simulate the episodic unsynchronized (with Northwest and North Fork discharges) discharges from the S-46 structure. The results indicated that as discharge increases the change in the rate of sedimentation rate decreases. However, they do not share a direct straight-line relationship. For instance, doubling of flow from 2.5 m^3/s to 5 m^3/s results an increase of 71% in the sedimentation rate and similar increase from 10 to 20 m^3/s changes the rate only by 25% indicating that, the sedimentation rate is more sensitive to lower discharges. This is evidently due to increasing discharge is associated with increased concentration. The regulation of the C-18 canal by the S-46 structure is manifested in the high frequency of zero-discharge periods (54% of the days) and the spikes. The deposition rates were found to be 0.15 m for a period of 10 years, which compared well with the poling results.

The study also compares the sedimentation in a regulated C-18 canal to that of hypothetically unregulated canal by applying flow record for the Northwest fork for the same period pro-rated so that the discharges over the 10 year flow period remains identical. Resulting in a 10-year deposition thickness of 0.22m (0.022m/yr), implying that the episodic discharges in actuality reduced the rate of sedimentation. This is a direct consequence of near constant high discharge attenuating the increasing trend of sedimentation.

The study incorporates a trap near the area of greatest post dredging thickness, with a poling depth of approximately 1.2 m. A dredging depth of 3 m (from the original bed

level) width of 60 m, and a length of 180 m were chosen for the trap, which was considered sufficient to reduce the velocity in the canal, and allow a measurable amount of sediments to settle. This trap configuration reduced the current magnitude by 67% over the trap. As a consequence a number of factors were evaluated by the study namely,

- Simulations showed that the removal ratio, i.e., the ratio of sediment influx (into the trap) minus out flux divided by influx), was maximum at an S-46 discharge of approximately 1.7 m^3/s. At higher discharges sediment was transported beyond the trap, while at lower discharges sediment settled before the trap.

- The second simulation involved testing the trap efficiency as a function of sediment concentration. It was observed that increase in sediment concentrations in the free settling range in general increases the settlement. The increase in trapped load followed a linear trend up to concentrations of 0.25 kg/m^3 (free settling zone), which is explained by the increase of deposition flux with concentration (with constant settling velocity). Above this concentration, and below 7 kg/m^3 (flocculation range), the increase in settling velocity yields a similarly increasing trend for trapped load. In the hindered settling zone, however, (which lies above this concentration) trapped load decreases as the settling velocity deceases. It was therefore be inferred that trapped load is a function of concentration because settling velocity (and hence the deposition flux) is also a function of concentration at values greater than 0.25 kg/m^3.

- The simulations on varying organic content indicated that, increase in organic content led to decease in settling velocity, which resulted in lower removal ratio. Sedimentation rate in the trap increased with increased organic content, due to corresponding decease in dry density. In addition, the increase in influent load with increasing organic content as less sediment was deposited upstream of the trap at higher organic content.

2.3 Central Embayment

2.3.1 Present Condition

Jupiter Inlet, which is about 112 m wide and 3.9 m deep at the jetties, allows the tidal flow in and out of the estuary. The channel starting at the jetties leading up to the Florida East Coast Railroad Bridge is fairly uniform, with width varying from 206 m to 247 m and the mean depth varying between 3.92 m at the inlet and 2.6 m near the FECRR Bridge. The ICWW meets the channel down stream of the FECRR bridge.

Upstream of the FECRR Bridge the embayment widens and the channel is divided in to two parts by shoals often exposed under low water conditions. These shoals, presumably created by the sands introduced in to the system through the inlet and the tributaries, and carried by the flood tide, occur where the sediment carrying capacity of the flow reduces with the reduction of current at wider sections. In addition, east of these sandy shoals there occurs a small mangrove island. Similar Islands occur near the north bank close to the FECCR Bridge. The deepest portion of the embayment lies to the north of the sandy shoal, easily identifiable even from a areal photograph (Figure 2.9) is currently used for navigation. The shoreline is basically sandy with little or no clay present. The percentage of clay and silt is barely 5%. The average depth in the central embayment is 1.2 m. The depth in the deeper portions along the flood channel however exceeds 3 m in patches. A similar deep channel can be found along the south bank, which has been presumably created by the ebb circulation. A clear ebb channel can also be seen from the satellite photographs to the south of the sandy shoal. Boats returning to their docks use this channel at high water. There are many private wooden docks along the entire coastline.

At the turn of the century, the Loxahatchee River estuaries along with its immediate environ was a pristine ecosystem consisting of mangroves, salt marshes, and scrubland. Prior to Word War II, agricultural interests transformed the area in to a rural landscape with citrus groves and vegetable farms. As a result, a significant increase in residential population occurred around this time. These developments ultimately prompted the declaration of the estuary an aquatic preserve in 1984. Nonetheless, the construction activities, especially of the residential homes, still continue along the shoreline and the entire estuarial shoreline of the central embayment as well as a

significant portion of the tributary shorelines is residentially occupied. Recreational boating is widely practiced in the estuary by the local residents. Access is necessary to the upstream areas for recreational activities, and also to the open sea and the ICWW. Many of the natural and artificial access routes have shoaled in recent years (Antonini et al., 1998), leading to hazardous boating practices such as high-speed entry/ exist to prevent grounding of vessels. The channels adjacent to the south shore of the central embayment are more susceptible to shoaling (Sonntag and McPherson, 1984), directly affecting the boaters who rely on these channels for access**.**

Figure 2.10 Arial Photograph showing the Central Embayment, the Inlet and the Tributaries

Estimates with regard to grain size, composition and age of bottom sediments are given by McPherson et al. (1984) for the entire estuary. The samples collected by vibro-core boring were analyzed in the laboratory for micro-faunal and macro-faunal assemblages, grain size distributions, constituent composition and radiocarbon age. With regard to the grain size it was seen that, the characteristics of the bed material were identical to those of the underlying sediments in the core. Fine-grained sediments dominate the central bar at the lower reaches of the estuary; whereas medium to coarse-grained sand dominates upper reaches of the bar. Patches of fine to medium sand draping

the muddy sediment surface can be seen in the main body of the estuary. The shell content in the bed material varies from 0 to 5% at the eastern end to 20 to 30% at the western end.

Grain-size analysis reveals that there are two distinct different populations. The first, well-sorted sediment with a mode between 62.5 to 125 microns, and the second, poorly sorted sediment commonly showing bimodality. The bimodal distributions generally have one mode at about 300 microns and the other at 100 microns.

Jaeger et al, (2001) measured the particle sizes in the estuary, which, reveal that the majority of the estuary is dominated (by weight) of fine, well-sorted sand in the ~150 micron (3 phi; 0.15 mm) size range. This size sand is ubiquitous in the estuary and is observed in Pleistocene-age coastal deposits exposed in outcrops within the study area. The ultimate source of the sand accumulating within the upper estuary is from erosion of these older deposits. The amount of mud-sized sediment (<63 microns) is minimal with the exception of the upper reach of the Northwest Fork, the North Fork, and near the junction of the C-18 canal and the Southwest Fork. Clay mineral analyses on the mud fraction accumulating throughout the estuary reveals that the ultimate source of the clay-sized sediment is from erosion of the Pleistocene-age deposits.

Comparison of the sediment characteristics (median particle-size, sorting) between 1990 and 2000 within the Central Embayment reveal that this region has not changed significantly over the past decade. However, the navigation channels have become coarser apparently due to the removal of fine sediment. Portions of the lower Northwest Fork and the Southwest Fork have gotten finer.

Based on the analyses of 20 push cores, there does not appear to be a widespread organic-rich flocculent “muck” layer within the three major forks of the estuary. Although mud is a common component of the sediments in these locations, by weight it usually represents less than 20% of the total core mass.

In addition, study by Jaeger et al., (2001) indicate that in the main navigation channels, the sediments have become coarser and more poorly sorted over the last ten years. The study attributes this to the likely inclusion of shelly material in the 2000 samples that was not sampled in 1990. It is possible that maintenance dredging during this time period resulted in the exposure of older shelly material or that changes in the shape of the navigation channel has led to stronger currents that have removed the finer sands. Although the western portion of the Central Embayment has seen no change in the median particle diameter, it has gotten marginally better sorted, and could reflect a decrease in fine sediments accumulating.

Freshwater runoff enters the Loxahatchee River estuary by river and canal discharges, by storm drains, and by overland subsurface inflow. Most of the freshwater from the tributaries is discharged from the Northwest Fork of the estuary. These flows, as expected, vary seasonally, occurring chiefly in the wet season. The median, high and maximum flow discharges are given in Table 2.2.

Tidal flow into and out of the estuary is much larger than the freshwater inflow from all the major tributaries. The combined freshwater flow into the estuary is found to be about 2% or less of the average tidal inflow at the Jupiter inlet (McPherson, Sonnetag, 1984). However, during tropical storm Dennis, freshwater inflow per tidal cycle increased to 18% of average tidal inflow (McPherson, Sonnetag, 1983). Tides are mixed

semi-diurnal with varying amplitudes, with a tidal range of approximately 0.6 to 1 m. The tidal wave advances to the estuary at a rate of about 2.3 m/s to 4.5 m/s. Higher than usual tides can be noted during the autumn and winter when strong northeast winds pushes additional water in to the estuary causing higher than average tides.

Ultrasonic water level gauges (Model 220, Infinities USA, Daytona Beach, FL) with stilling walls were installed to measure tidal elevations between September 14th and October 18th, at three locations in the estuary one each in the Central embayment (tied to the FECRR bridge pier), Northwest Fork, and Southwest Fork. The gauge locations are shown in Figure 2.10. Tidal elevations were recorded with respect to North Atlantic Vertical Datum 1988 (NAVD 88) and are reproduced in Table 2.3. Tidal ranges indicate the total change in water surface elevation between low and high tides and phase lag refers to the difference in time between high/low tide at UFG1 gauge and the other gauges. In Figure 2.12 sample records from three tidal gauge locations are shown.

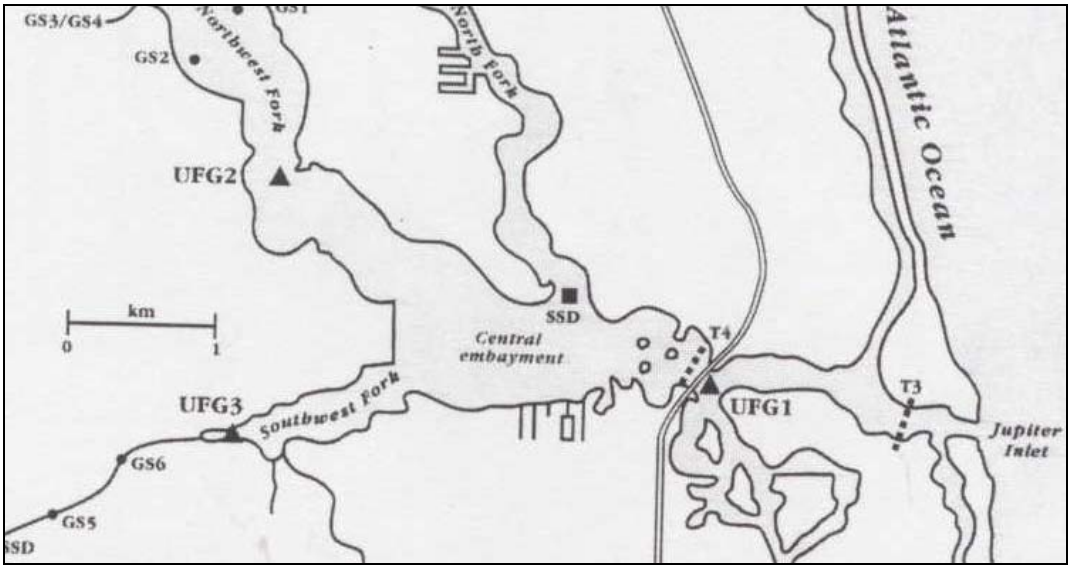

Figure 2.11 Location of tide gauges marked UFG1, UFG2 and UFG3

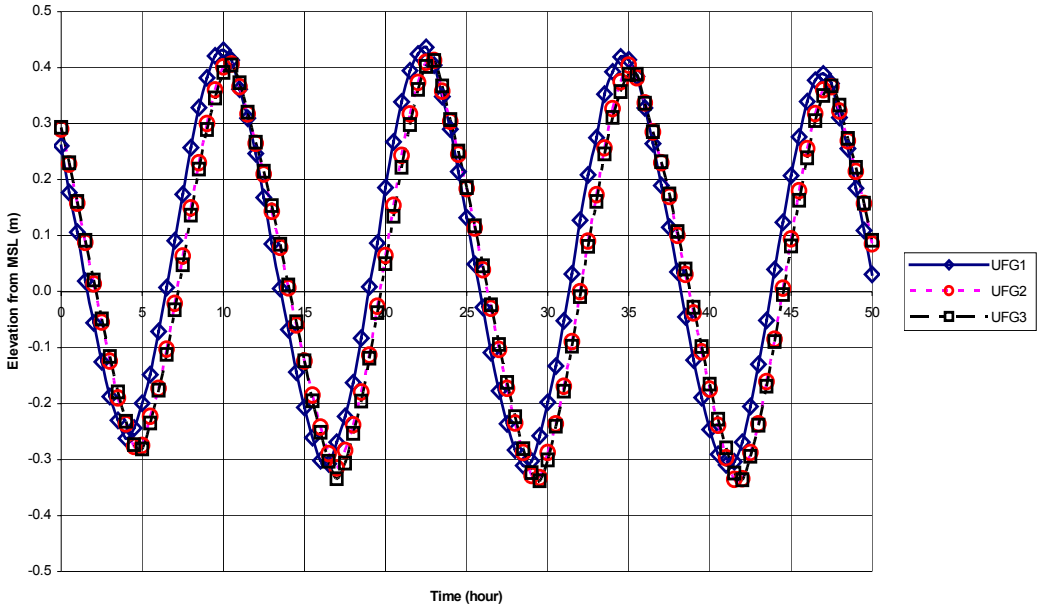

Figure 2.12 Sample records of tidal measurements at three locations (09/14/00-09/15/00)- Datum NAVD 88.

Table 2.4 Spring/neap tidal ranges and phase lags for three gauges

Gauge ID	Spring range (m)	Neap range (m)	Phase lag from UFG1 (min)	
UFG1	0.90	0.66	0	0
UFG2	0.85	0.65	21	60
UFG3	0.86	0.64	28	60

Ganju et al., (2001) compared the data obtained from these gauges to a station on the Northeast Florida coast and inferred that trends in water surface elevation followed similar increases and decreases in mid-tide elevations and the increased elevations in side the estuary is a direct result of onshore winds. The wind records from two offshore stations were averaged and correlated with the mid-tide elevation, resulting in a positive correlation. Accordingly, mid-tide elevation was subtracted from the measured elevations (filtering) in order to obtain tidal data without any variation.

2.3.2 Management Option:

Presently, the dredged spoil from the embayment is disposed on land. Land disposal of marine sediment is often times not optimal for the environment, especially for

the ground water. According to earlier studies by Sonnetag and McPherson (1984) the central embayment receives sediment from two main sources, the inlet and upland discharge. Regular maintenance of the navigation channel is a clear indication of this supply. Ideally, a large enough central shoal (if developed to correct contours) could serve the process of self-cleansing of the bay. The shoal when developed would decrease the water flow area and thereby, increasing the velocity of flow. The increased current in the limiting case would develop erosional stresses equal to the critical bed shear of the sediment and therefore would be able to prevent the further sedimentation of the bay. However, numerical modeling for such an examination is outside the scope of this study. The present study will however deal with the development of an additional navigation/flow channels for improvement of ebb flow.

2.4 Northwest Fork:

2.4.1 Present Condition:

The Northwest Fork meanders through typical South Florida swampland within the Jonathan Dickinson State Park (JDSP). The extensive swampland and scrubland east of JDSP is drained by the North Fork. It is therefore evident that the watershed is biologically productive, and the sediment carried by the runoff is rich in organic content eventually finds its way in to the estuary (Sonnetag and McPherson, 1984).

Most of the freshwater from is discharged through this fork. From February 1st, 1980, to the September 30th, 1981, for example, 77.3 percent of the freshwater was discharged into the Northwest Fork, 20.5 percent in to the Southwest Fork (C-18 Canal), and 2.2 percent into the North Fork (Sonnetag and McPherson, 1984). The Loxahatchee River (i.e., Northwest Fork) at SR-706, site 23 as shown in Figure 2.14 (*Figure 2*, *U.S.*

Geological report no 83-4244, 1984), contributed the greatest percentage of flow to the estuary (37.4 percent) of all the tributaries.

Vertical variation of the sediments in the Northwest fork is Found at site 5 and 5E (*Figure 2, U.S. Geological report no 84-4157, 1984*) during both incoming and outgoing tides. Presumably, greater water velocities, particularly at 0.6 m above the bottom at the mid depth, associated with higher tide stages contributed to the greater vertical variation of suspended sediments (Sonnetag and McPherson, 1984). Concentration of the suspended sediments and the percentage of sediments of organic origin were variable with season and weather conditions as indicated by the data collected and listed in U.S Geological Survey report 84-4157 (Sonnetag and McPherson, 1984). The greatest increases were observed in Cypress Creek, lying upstream of the Northwest Fork. Concentration of the suspended sediment in the tributaries also changed as a result of man's upstream activities. During September 1981, suspended sediment concentration in the Cypress Creek and Hobe Grove Ditch increased as much as 21 times over concentrations in early September (Sonnetag and McPherson, 1984). Cleaning and dredging operations on the irrigation canal connected to the Cypress Creek and Hobe Grove Ditch were presumably responsible**.**

Suspended sediment load from the tributaries are highly seasonal and storm related. The 5 major tributaries to the Loxahatchee estuary Loxahatchee River at SR-706, Cypress Creek, Kitching Creek, Hobe Grove Ditch, and C-18 at S-46 discharged 1,904 tons of suspended sediments to the estuary during the 20-month period (February 1, 1980 to September 30, 1981) (Table 2.3). During the 61 days period of the above-average rainfall (August 1 to September 30, 1981) that included tropical storm Dennis, the major

tributaries discharged 926 tons of suspended sediment to the estuary. This accounted for 49 percent of the suspended sediment discharged to the estuary during the 20-month period and about 74 percent of the suspended sediment discharged during 1981 water year (Sonnetag and McPherson, 1984). Sediment loads from C-18, Loxahatchee River at SR-706, and Cypress Creek accounted for more than 94 percent of the total tributary input of the sediment load.

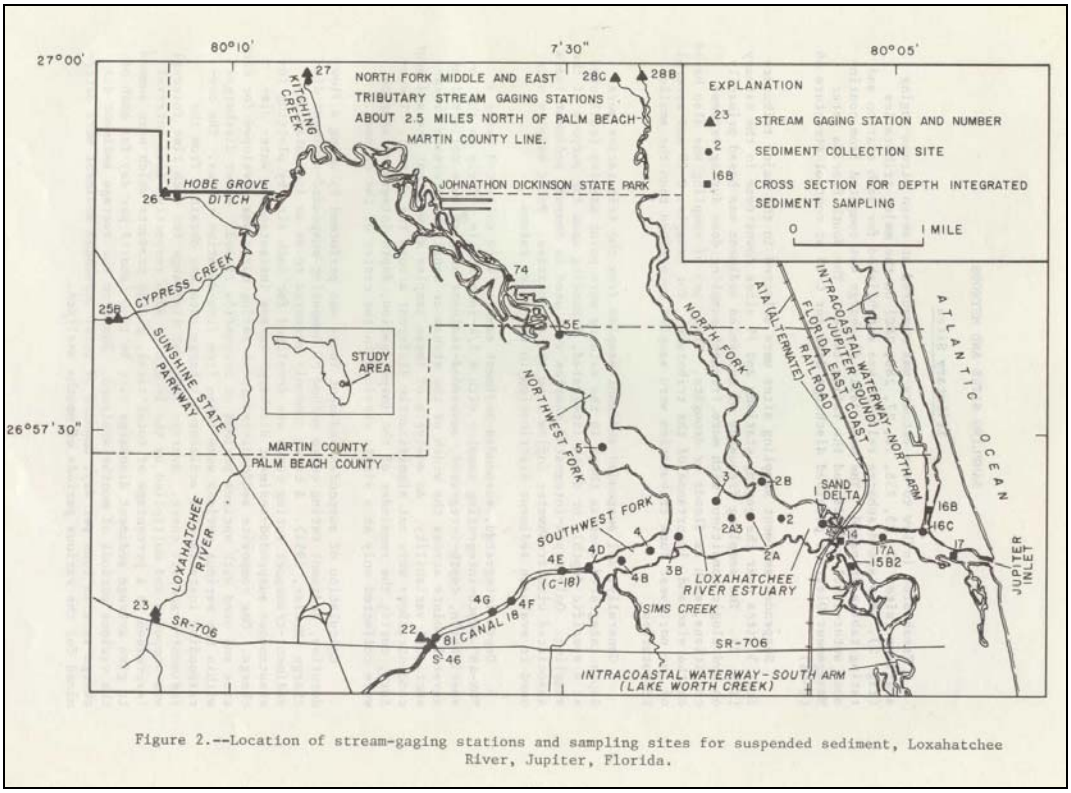

Figure 2.--Location of stream-gaging stations and sampling sites for suspended sediment, Loxahatchee River, Jupiter, Florida.

Figure 2.13 Location of stream-gauging stations and sampling site for suspended sediments, *(Source U.S. Geological report no 83-4244 and 84-4157)*

Unlike the central embayment concentration of mud was quite high (~50%) in the Northwest Fork (Jaeger et al., 2001). The study by Jaeger et al., (2001) also analyses vibracores takes which, reveal that there has been roughly 0.5-1 cm/yr of sedimentation within a part of the Northwest Fork when compared to data from a USGS-sponsored

study completed, in 1984 (Sonnetag and McPherson). The study further concludes that, these accumulation rates are close to those averaged over the past 50 years, assuming that an observed change in the cores from layered sediment not mixed by organisms to those that are well mixed by organisms occurred in 1947 when the inlet was stabilized. Inlet stabilization would have led to increased tidal flushing that allowed for better oxygenation of bottom waters and sediments permitting occupation of sediments by organisms. However, this datum has not been substantiated as pre 1947 and the accumulation rates are bulk averages. A comparison of the collected data and studies by Ganju et al., (2001) showed that accumulation rates within the upper reaches of the three Forks are about 2-3 times higher than the modeled fine-sediment budget prepared by Ganju et al. (2001). Accordingly, the study concludes that, this discrepancy could be due to poor age constraints of the core layers or to the substantial presence of sand in the core sections, which was measured in this stratigraphic (i.e., core layering) approach but not in the fine-sediment budget.

Upstream of the outfall point of the Northwest Fork is marked by a horseshoe-shaped shoal (Figure 2.14). Presumably this shoal is formed due to the reduction in current velocity of the sediment-laden flow by the ebb tide. In addition, the ebb flow velocity gets reduced upon meeting a large body of water (central embayment). Upstream of this shoal there occur a series of sand shoals also formed by the same processes. Downstream of the shoal however, the depths are uniform gradually increasing as moves in to the central embayment area. Formation of deposits presumably from the erosion of old deposits in side the estuary was also reported by Jaeger et al., (2001). Figure no 4 of

the report are reproduced here for reference with regard to the deposition and material composition.

In Figure 2.15 the mass percent of the mud (particles smaller than 63 microns) in the upper ~5 cm of the sediment surface is shown. Location of the sampling sites are shown as dot symbols.

2.4.2 Management Options

Discounting the sedimentation from the internal sources of erosion, the Northwest Fork contributes the maximum discharge as well as the maximum sediment into the central embayment (Sonnetag and McPherson, 1984). However, Jaeger et al, (2001) indicate that fresh deposits are found in the Fork (Figure 2.14), suggesting that the source of such deposits may be mostly internal to the estuary, and most likely due to the erosion of old deposits. Sediment from external sources entering the estuary with fresh water discharge as reported by McPherson (1984) would have deposited in the proximity of the horseshoe shoal.

In order to minimize the deposition of fine sediment in the area of high mud percentage in the Northwest Fork (Figure 2.14), a self-cleaning channel will be examined. According to Jaeger et al., (2001), the origin of deposits (Figure 2.14) is due to the erosion of old deposits. Therefore the channel is proposed to be located downstream of these deposits. Design aspects of the channel are considered in Chapter 4.

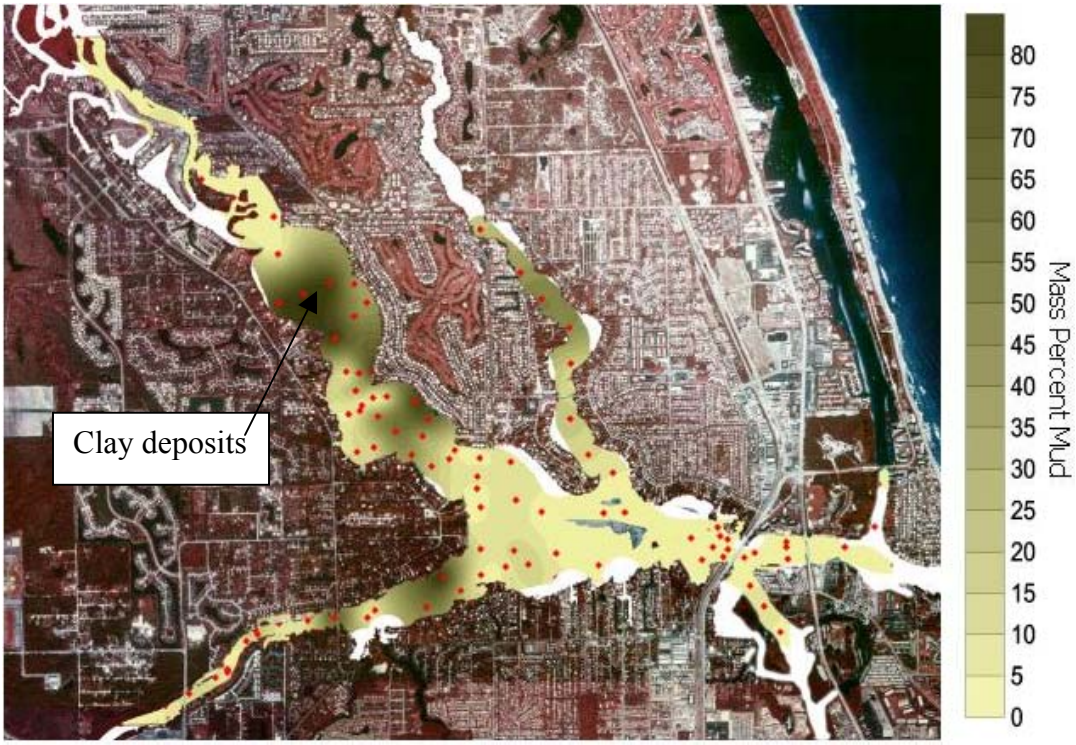

Figure 2.14 Location indicating fresh mud depositions and the Shoals the estuary. Source: Sedimentary Processes in the Loxahatchee River Estuary: 5000 Years Ago to the Present-FINAL REPORT, Jaeger et al., (2001)

2.5 North Fork

2.5.1 Present Condition

The North Fork is a natural tributary draining the eastern part of the Jonathan Dickson State Park. Discharge as given in Table 2.2 is the least of the three main tributaries (2.2% of total), and water depth is fairly uniform at around 2 m, with virtually no shoals. McPherson and Sonnetag (1983) reported that in the 1981 water year the tributaries of the North Fork were dry at the gauging stations (Figure 2.13) from March trough mid-August. During the rest of the year the average flow was 0.12 m^3/s, a very small value. Discharge following Tropical Storm Dennis was also small for the amount of rainfall associated with the storm. Daily discharges for the last 10 days of August 1981 averaged 0.31 m^3/s but increased to 0.71m^3/s in September. Jaeger et al. (2001) found

some mud deposits in the upper reaches. Depths in the fork appear to be adequate for the recreational boating.

2.5.2 Management Options

The North Fork as indicated above has the least river inflow as well as the least sediment contribution to the estuary. In addition, the depths are fairly uniform and good for the types of boats presently using it. Hence no additional facility is believed to be required for this area. Therefore no dredging is planned for this tributary nor appears to be required.

CHAPTER 3
DATA COLLECTION

3.1 Field Setup in the Southwest Fork

Field data were collected at two sites, one in the Southwest Fork and the other in the Northwest Fork. Section 3.3 collection effort and results in the Southwest Fork, and Section 3.4 in the Northwest Fork.

The field data collection set up in the Southwest Fork of the estuary had geographical coordinates of latitude 26° 56' 36.78" N and longitude 80° 07' 17.34" W. In the Northwest Fork the corresponding coordinates were 26° 59' 16.78" N and longitude 80° 07' 56.34" W. These two locations are shown in Figure 3.1. The locations of the tidal gages installed in the year 2000 were shown in Figure 2.11. The depth (below North Atlantic Vertical Datum, 1988, (NAVD88)) at the sites ware 2.1m and 2.18, respectively.

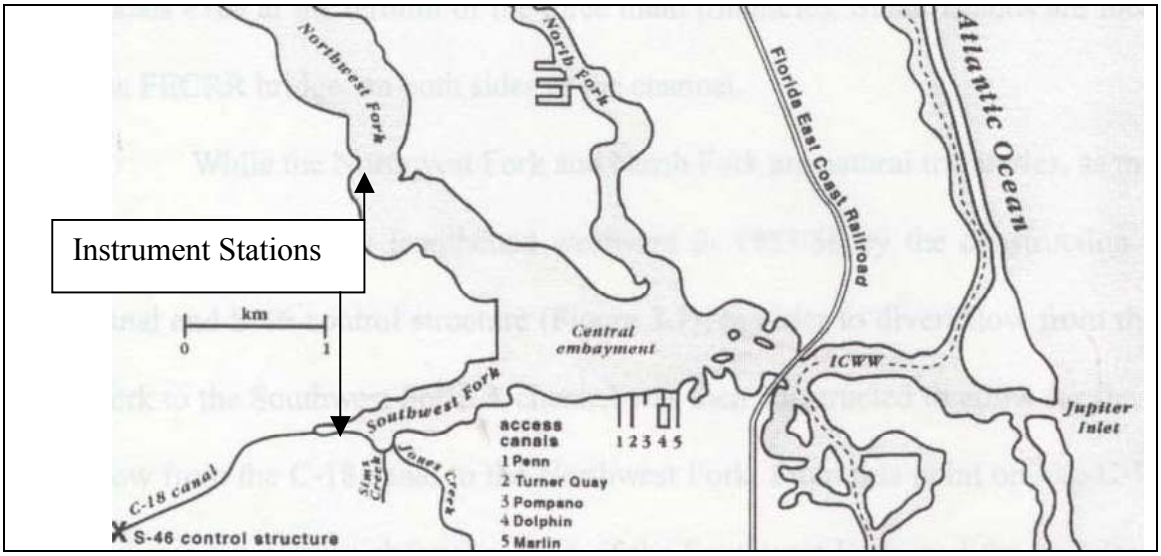

Figure 3.1 Location of instrument tower in the Southwest and Northwest Forks

Data in the Southwest Fork were collected in two phases. The first phase of the data collection was carried out between 4th and 24th April 2002, and the second phase was between 6th of February and 2nd of June 2003. The instrumentation deployed is given in Table 3.1.

Table 3.1 Instrumentation for data collection and data blocks

Instrument	Data	Date	
Data logger (*)	Current (mag.) – u	Apr 04 to Apr 24	Nov 27 to Jun 2
Data logger (*)	Current (dir.) – u	Apr 04 to Apr 24	Nov 27 to Jun 2
Data logger (*)	Current (mag.) - v	No data	Nov 27 to Jun 2
Data logger (*)	Current (dir.) - v	No data	Nov 27 to Jun 2
Data logger (*)	Tide levels	Apr 04 to Apr 24	Nov 27 to Jun 2
Data logger (*)	OBS 1	Apr 04 to Apr 24	Nov 27 to Jun 2 (Poor quality)
Data logger (*))	OBS 2	Apr 04 to Apr 24	Nov 27 to Jun 2
Data logger (*)	OBS 3	Apr 04 to Apr 24	Nov 27 to Jun 2
Data logger (*)	OBS 4	Apr 04 to Apr 24	No data collected
Data logger (*)	Temperature	Apr 04 to Apr 24	Nov 27 to Jun 2
Data logger (*)	Salinity	Apr 04 to Apr 24	Nov 27 to Jun 2

**With* *ultrasonic current meter in April 2002 replaced with an electromagnetic current meter*

Instruments were attached to a tower erected for this purpose and was powered by rechargeable batteries. The instrument assembly consisted of a Marsh-McBirney electromagnetic current meter, a Transmetrics pressure transducer for the measurement of water surface elevation, a Vitel VEC-200 conductivity/temperature sensor for measurement of salinity and temperature, and three Sea point Optical Backscatter Sensor (OBS) turbidity meters for measuring the sediment concentration at 3 different levels. In the first phase instrument setup, however, turbidity sensors were deployed at 4 different levels. In addition Lidberg Land Surveys, Inc. carried out a hydrographic survey and collected data with regard to the bottom bathymetry of the central embayment and the tributaries.

In the Northwest Fork the data collection started on 14th of August 2003, with 3 level OBS sensors, one Conductivity Temperature sensor and one Pressure gauge

3.2 Instruments Deployed

3.2.1 Current

Current data were collected using Marsh-McBirney electromagnetic current meter (Model 585 OEM). This meter consists of a 10 cm diameter spherical sensor, OEM motherboard, and signal processing electronics (Figure 3.5). The instrument senses water flow in a plane normal to the longitudinal axis of the electromagnetic sensor. Flow information is output as analog voltage corresponding to the water velocity components along the y-axis and x-axis of the electromagnetic sensor. The velocity sensor works on the Faraday principle of electromagnetic induction. The conductor (water) moving in the magnetic field (generated from within the flow probe) produces a voltage that is proportional to the velocity of water. The Marsh-McBirney requires periodic cleaning of the probe with mild soap and water to keep the electrodes free of non-conductive material.

Since the instrument has essentially a cosine response in the horizontal plane, the flow magnitude and the direction information are retained. In addition, the spherical electromagnetic sensor has an excellent vertical cosine response. This unique characteristic allows the sensor to successfully reject vertical current components that may be caused by mooring line motions. As the flow changes direction, the polarities of the output signal also change. So the u (velocity along axis of the channel flow) and the v (velocity across the channel) velocities are stored and can be combined to give the resultant magnitude and direction. It must however be noted that, the v velocity component was largely insignificant due to the width of the channel at the tower location.

3.2.2 Tide

Water surface elevation was measured using a Transmetrics pressure transducer installed at the instrument tower. The instrument incorporates three major design elements that allow it to measure pressure accurately and reliably; bonded foil strain gages configured in a Wheatstone bridge (for temperature stability), high precision integral electronics for signal amplification, and stainless steel construction for durability and corrosion resistance. The instrument was calibrated and temperature-compensated against standards applicable for the region.

3.2.3 Salinity/Temperature

Conductivity is the measurement of the ability of a solution to carry an electric current. It is defined as the inverse of the resistance (ohms) per unit square, and is measured in the units of Siemens/meter or micro-Siemens/centimeter. The measurement of conductivity is necessary for the determination of the salinity of a solution. Salinity is proportional to the conductivity and is expressed in terms of concentration of salt per unit volume (mg/l, or ppt). The field measurement of salinity was carried out following similar procedures using a Greenspan Electrical Conductivity (EC) sensor substantially eliminating a basic source of error arising out of the inaccuracies due to temperature and electrode effects. In this instrument the electrical conductivity is a function of the number of ions present and their mobility. The electrical conductivity of a liquid changes at a rate of approximately 2% per degree Centigrade for neutral salt and is due to the ionic mobility being temperature dependent. The temperature coefficient of the conductance (or K factor) varies for salts and can be in the range 0.5 to 3.0. As electrical conductivity is a function of both salt concentration and temperature, it is preferable to normalize the

conductivity measurement to a specific reference temperature (25^0C) so as to separate conductivity changes due to salt concentration from those due to temperature changes.

- The instrument deployed consisted of the following primary elements:
- Toroidal sensing head (conductivity sensor)
- Temperature sensor
- Microprocessor controlled signal conditioning and output device

The conductivity sensor uses an electromagnetic field for measuring conductivity. The plastic head contains two ferrite cores configured as transformers within an encapsulated open-ended tube. One ferrite core is excited with a sinusoidal voltage and the corresponding secondary core senses an energized voltage when a conductive path is coupled with primary voltage. An increase in charged ion mobility or concentration causes a decrease in the resistivity and a corresponding increase in the output of the sensor.

A separate PT100 temperature sensor independently monitors the temperature of the sample solution. This sensor provides both a temperature output and a signal to normalize the conductivity output.

3.2.4 Sediment Concentration

The instrument deployed was a Sea Point turbidity meter. This instrument measures turbidity by scattered light from suspended particles in water. The turbidity meter senses scattered light from a small volume within 5 centimeters of the sensor window. The light sources are side-by-side 880 nm Light Emitting Diodes (LED). Light from the LED shines through the clear epoxy emitter window into the sensing volume, where it gets scattered by particles. Scattered light between angles 15 and 150 degrees can pass through the detector window and reach the detector. The amount of scattered light that

reaches the detector is proportional to the turbidity or particle concentration in the water over a very large range.

The sensors were calibrated using a sample from the measurement site. Periodic calibrations were conducted in order to evaluate the conditions of the windows and the sensitivity to scattering. In addition, only black containers were used in calibration so as to prevent any probable scattering events due to reflection off the container wall. The calibration was carried out using known volume of sediments in known volume of water and the voltage output of the instrument recorded. A linear fit curve was generated in order to determine the accuracy of the calibration. The calibration plots are given below,

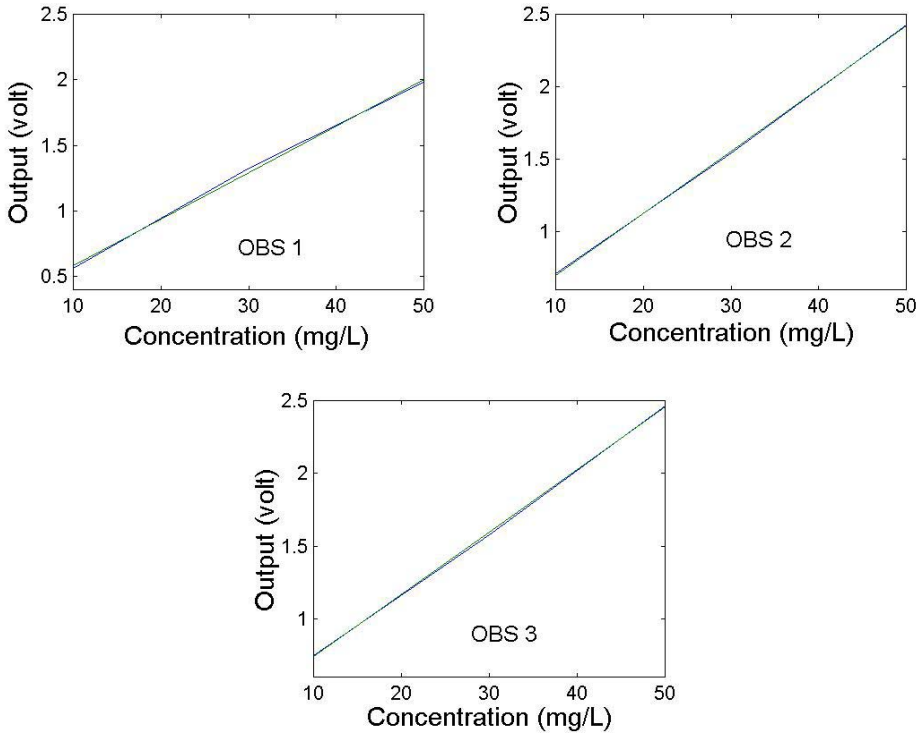

Figure 3.2 Calibration plots used for calibration of OBS sensors

3.3 Field Data Results in Southwest Fork

3.3.1 Current

The electromagnetic current meter was located at a height of 96.5 cm from the bed level. The velocity data in two directions, one parallel to the flow and the other perpendicular to it, were combined vectorially to find the resultant magnitude and direction. The ultrasonic current meter deployed in April 2002 collected the current magnitude and direction directly. Based on these data the depth-mean magnitude time series for Julian days 94-114 is shown in Figure 3.3 and the corresponding direction plot is given as Figure 3.4. A sudden increase in the current magnitude in the plot is attributable to the opening of control structure S-46. The directional plot indicates a uni-directional flow driven by the discharge from the structure. The discharge record for the period is given in Table 3.2 for ready reference.

Table 3.2 Discharge data for the period 04/14/2002 to 04/21/200

Date	Julian Days of 2002	Discharge (m^3/s)
04.14.2002	104	0.03171
04.15.2002	105	0.00821
04.16.2002	106	0.01416
04.17.2002	107	0.01501
04.18.2002	108	0.03483
04.19.2002	109	0.05777
04.20.2002	110	0.03568
04.21.2002	111	0.00934

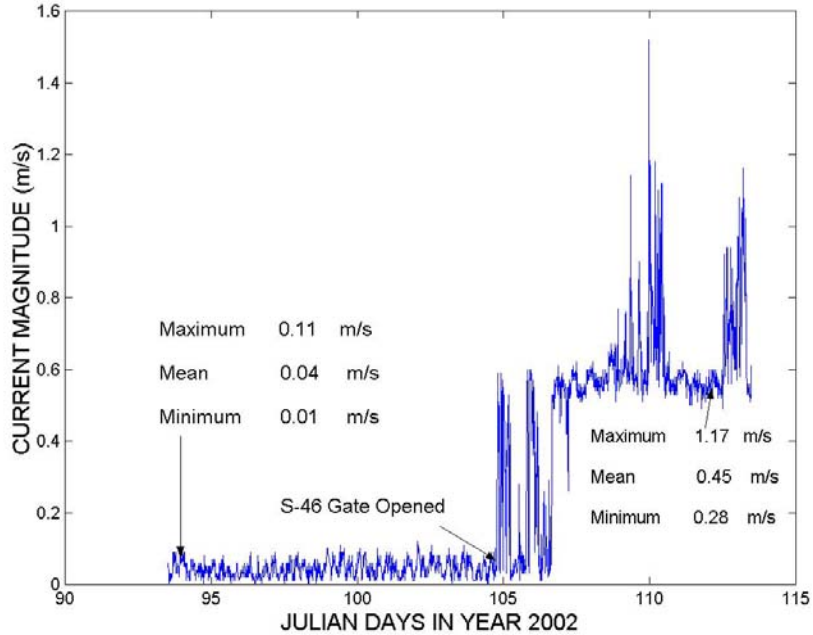

Figure 3.3 Record of current magnitude: Days 94-114 (year 2002).

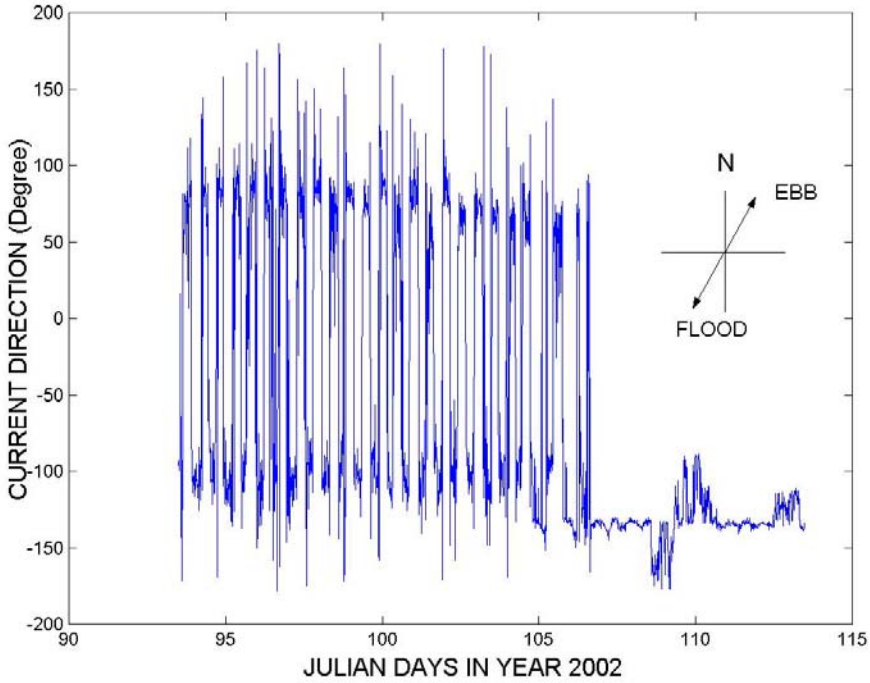

Figure 3.4 Record of current direction: Days 94-114 (year 2002).

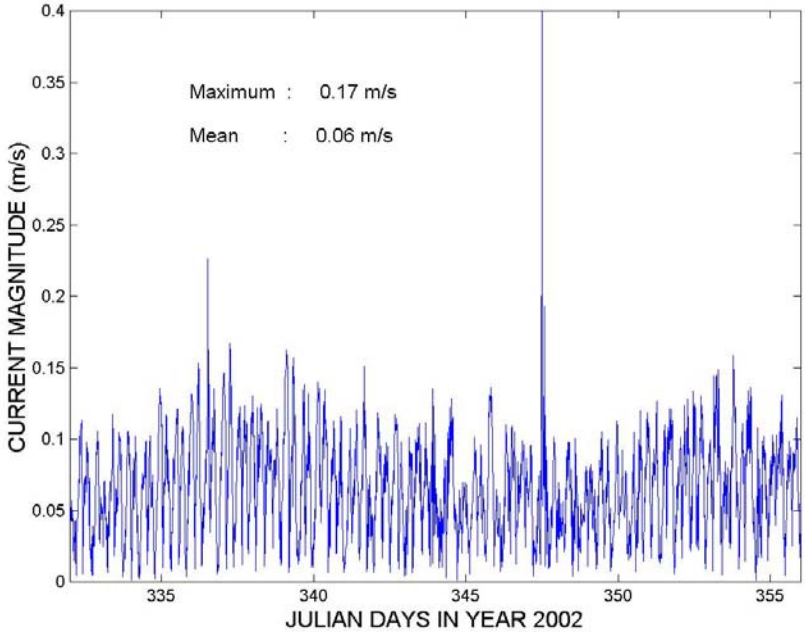

Figure 3.5 Record of current magnitude: Days 332-356 (year 2002).

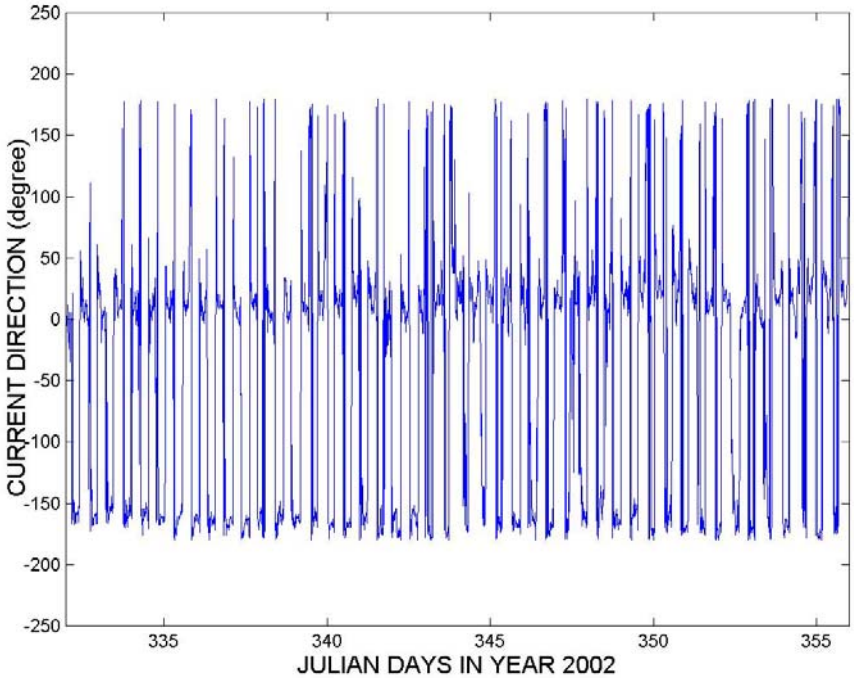

Figure 3.6 Record of current direction: Days 332- 356 (year 2002).

Figure 3.5 is a representative plot of the current magnitude for the second data block. This plot indicates a more uniform velocity pattern driven by the tidal flow in the

estuary. The current magnitudes reach a maximum value of 0.17 m/s with the mean value at 0.06 m/s. In addition it is seen that the flow is predominantly along the estuary with very low values observed for transverse current (v). In Table 3.3 typical mean current values are summarized.

Table 3.3 Typical mean current magnitude values for data blocks

Julian days in 2002	Current magnitude (m/s)		Velocity u (m/s)	Velocity v (m/s)
	With S-46 discharge	Only tidal flow		
94 - 114	0.25	0.04	[a] -	[a] -
332 - 356	[a] -	0.06	0.057	0.018

a No data

3.3.2 Tidal Level

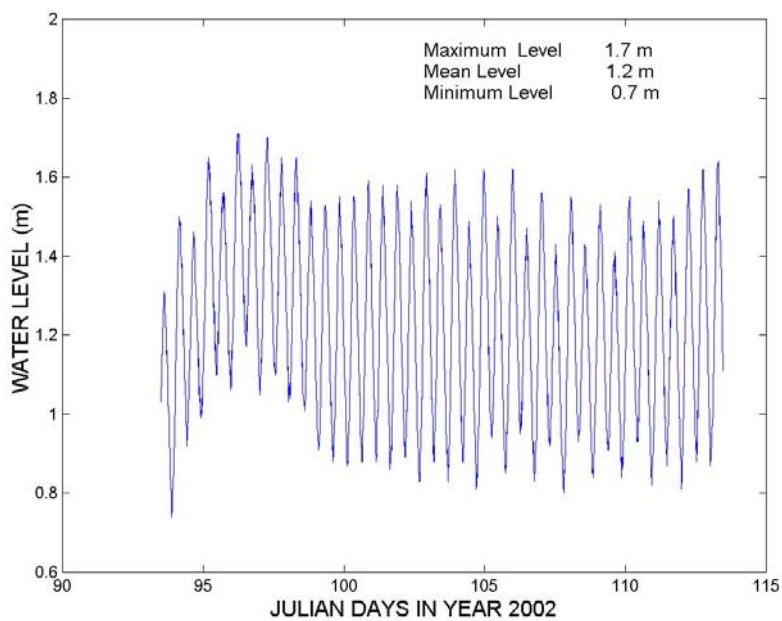

Figure 3.7 Water level time-series: All levels relative to NAVD 88. Days 94-114 (2002).

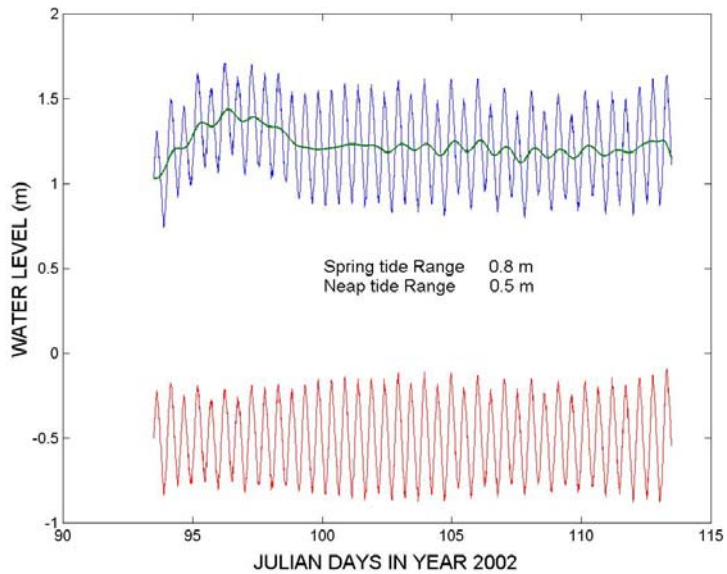

Figure 3.8 Water level time series. Upper plot shows original time series with mean trend and the lower plot is without the mean oscillations. All levels relative to NAVD 88. Days 94-114 (2002).

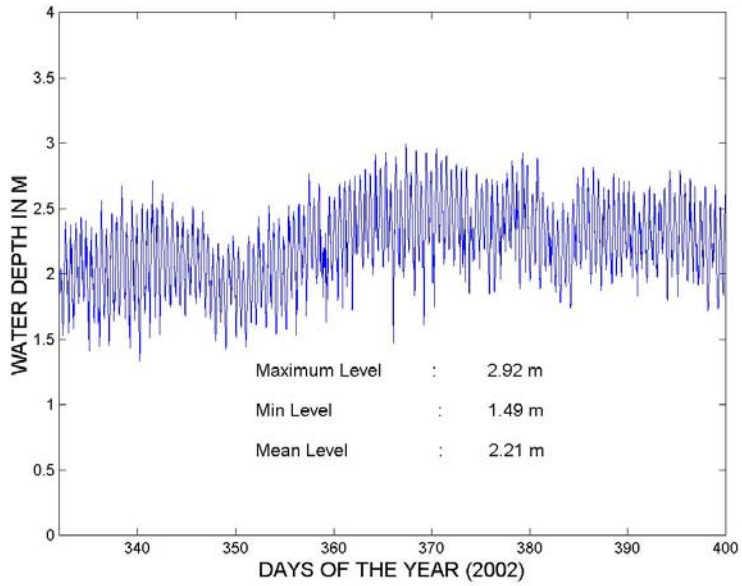

Figure 3.9 Water level time-series. All levels relative to NAVD88. Days 332- 365 (2002) and Days 01-35 (2003).

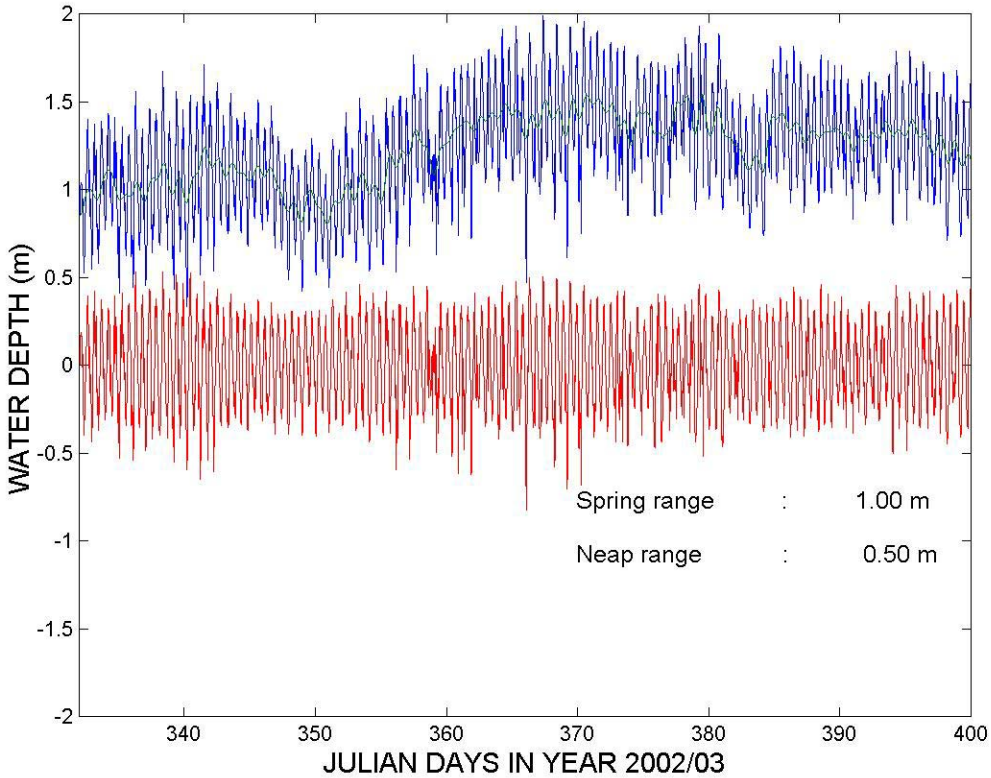

Figure 3.10 Water level time series. Upper plot shows original time series with mean trend and the lower plot is without this trend. All level relative to NAVD 88. Days 332-365 (2002) and Days 01 – 35 (2003).

In Figure 3.7 the raw tidal time-series is shown for the period April 4th to April 24th, 2002. In Figure 3.8 the upper plot shows the original time series with the tidal trend and the lower plot is with the tidal trend removed.

The tidal plots indicated in the Figure 3.7 to Figure 3.10 are representative plots from the phase II and I. The characteristic values of the tidal data are given in Table 3.4. In addition it can be noted that the tidal ranges compares well in both the phases with the spring range equal to 1.0m and the neap range around 0.5m. As will be explained later, the tidal fluctuations (as could be noted from Figure 3.9) between Julian days 360 to 365 in Year 2002, 01 to 5 and 17 to 25 in Year 2003, is likely to affect the sediment concentration in the estuary.

Table 3.4 Characteristic values of the tidal data

Julian days in 2002/03	Mean water depth (m)	Water level/Tidal range			
		Water level (m)		Spring/neap range (m)	
		Maximum	Minimum	Spring	Neap
94-114	1.20	1.70	0.30	0.90	0.50
332-365 01 - 35	1.20	1.90	0.30	1.00	0.50

3.3.3 Total Suspended Solids

Total Suspended Solid (TSS) was recorded at four elevations in the first phase and three elevations in the second phase. The elevation of the OBSs relative to the bed level was OBS-4 = 1.17 m, OBS-3 = 0.80 m, OBS-2 = 0.48 m and OBS-1 = 0.22 m. The corresponding total suspended solid time series are reported in Figures 3.11 and 3.12 for days 94-114 (Phase I) and 352- 365 in 2002 and 01 to 35 in year 2003 (Phase II), respectively.

Table 3.5 provides the maximum, mean and minimum values of sediment concentrations at different levels for each data block. Depth-mean concentration averaged every 12 hours is presented in Figures 3.13 and 3.14. The mean concentration figures (Figure 3.13 and 3.14) indicate the average variations in the concentration over time with out the instantaneous variations (spikes).

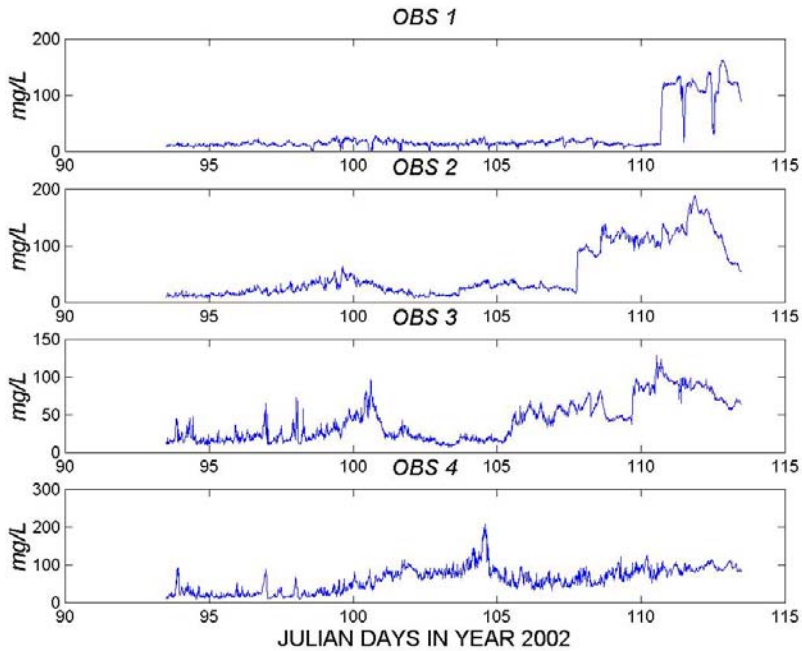

Figure 3.11 TSS time-series at four elevations: Days 94-114 (year 2002).

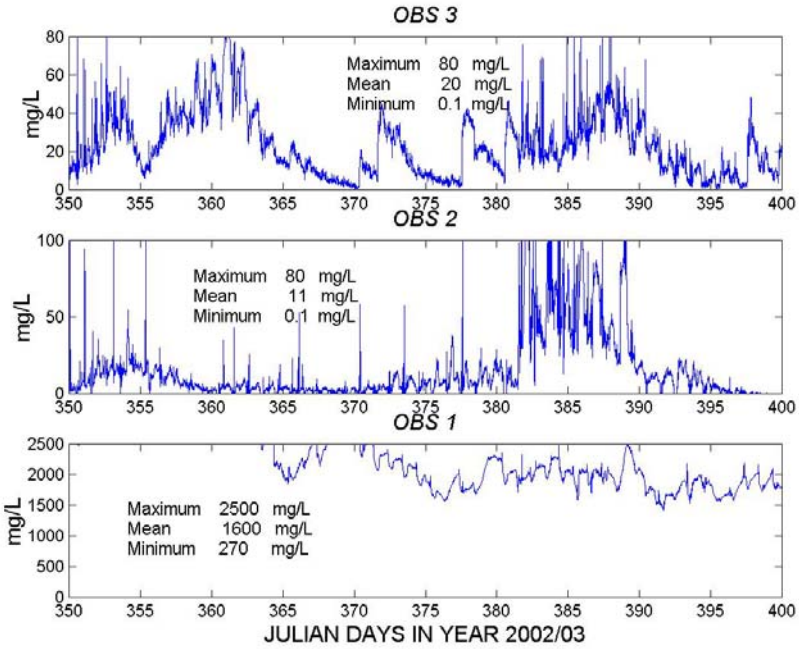

Figure 3.12 TSS time-series at three elevations: Days 352- 365 (year 2002) and 01–35 (year 2003).

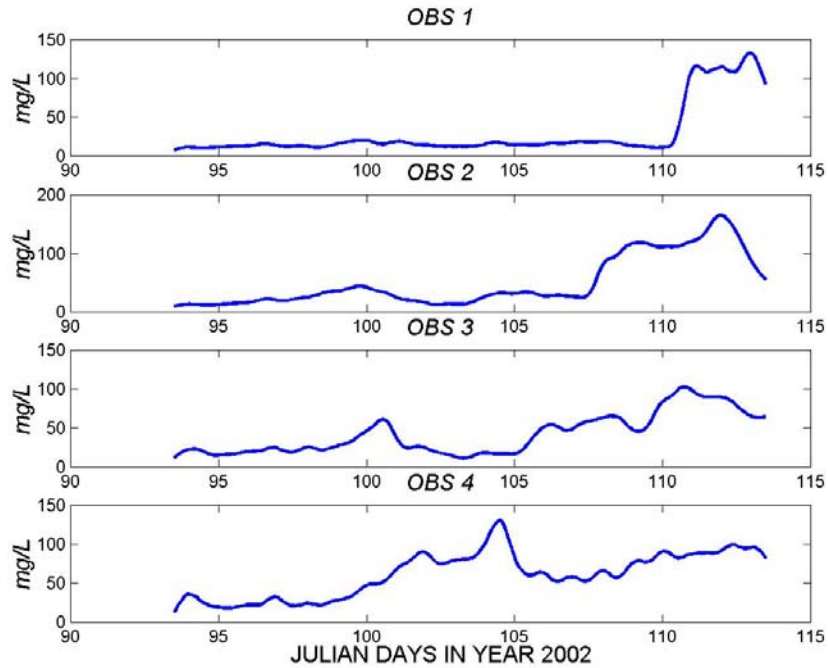

Figure 3.13 Depth-mean TSS concentration time series: Days 94-114 (year 2002)

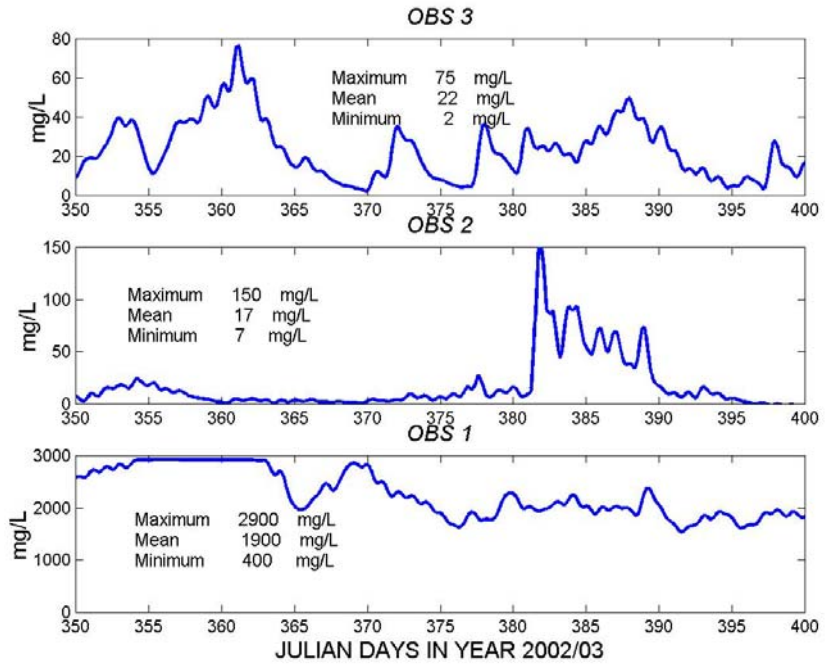

Figure 3.14 Depth mean TSS concentration time series: Days 352- 365 (year 2002) and Days 01 – 35 (year 2003).

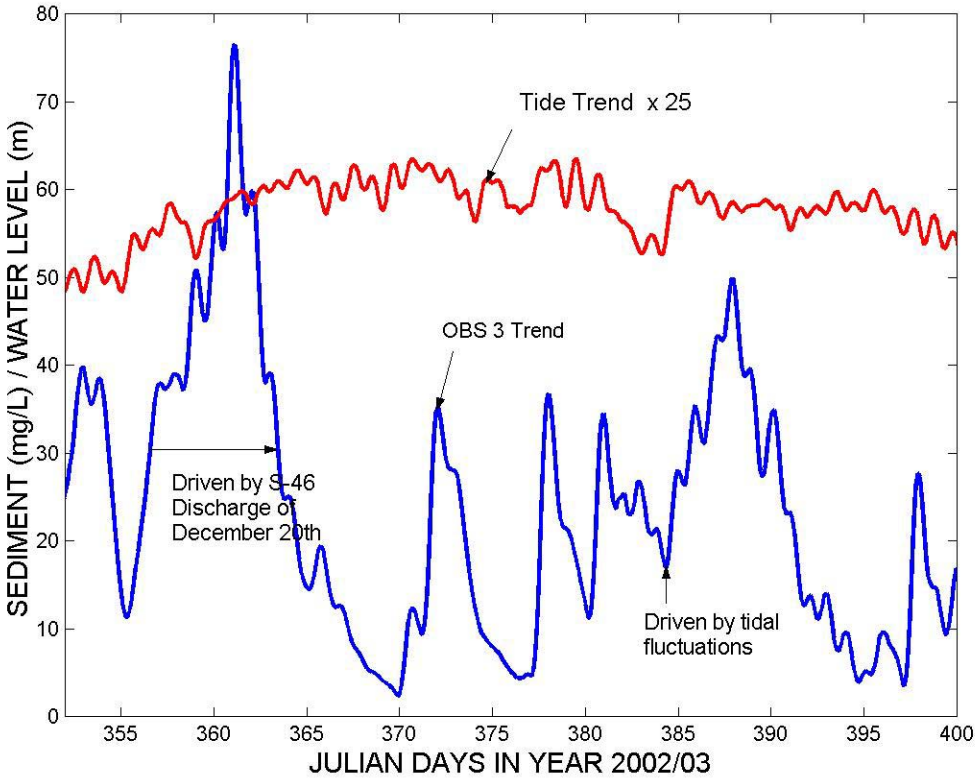

Figure 3.15 Depth mean TSS concentration time series and tidal trend indicating their dependence: Days 352- 365 (year 2002) and Days 01 – 35 (year 2003).

It can be noted from Figures 3.11 and 3.13 that there is a sudden increase in sediment concentration with the discharge from the S-46 structure on 14th of April 2002 (Refer Table 2.2 for discharge details). This clearly indicates that sediment concentration is discharge driven. Results of Figures 3.12 and 3.14 indicate that the lowest OBS1 sensor was too close to the bed and recorded almost saturated sediment content. There was no discharge from the structure between December 14th and February 20th, except for 0.01 m^3/s discharge on the December 20th, 2002, which explains the increase in sediment concentration recorded around Julian day 355 (December 20th). However, the increase in TSS reported between days 17 and 27 (Year 2003) without any discharge from S-46, could be attributed to spring tidal effects (Refer to Figure 3.15). In general, it appears that

TSS concentration is dependent on the local tidal current and flow discharges down the S-46 structure. The TSS concentrations with regard to other data blocks are given in Table 3.7 to 3.9.

Table 3.5 TSS concentrations for the representative data blocks

Julian Days in 2002/03	Maximum TSS concentration (mg/L)	Mean TSS concentration (mg/L)	Minimum TSS concentration (mg/L)
94-114	165	50	10
352-365 01-35	158	17	7

3.3.4 Salinity and Temperature

The conductivity and temperature measurements carried out for the location is presented in Figures 3.16 (days 94 –114 of 2002). The salinity curve indicates the effect of the fresh water discharge. Due to this flow fresh water from the S-46 structure the salinity values dropped to 11 mg/L from a mean value of about 28 mg/L. In order to examine this hypothecation the current magnitude and the salinity was plotted together in Figure 3.17, which, indicated a decrease in salinity with an increase in the current magnitude. Accordingly, it can be concluded that the fresh water discharge reduces the salinity in the estuary.

Table 3.6 Characteristic salinity values

Julian days in 2002/03	Maximum Salinity (mg/L)	Mean Salinity (mg/L)	Minimum Salinity (mg/L)
94-114	34.2	24.9	11.1
352-365 01-35	39.5	36.5	26.7

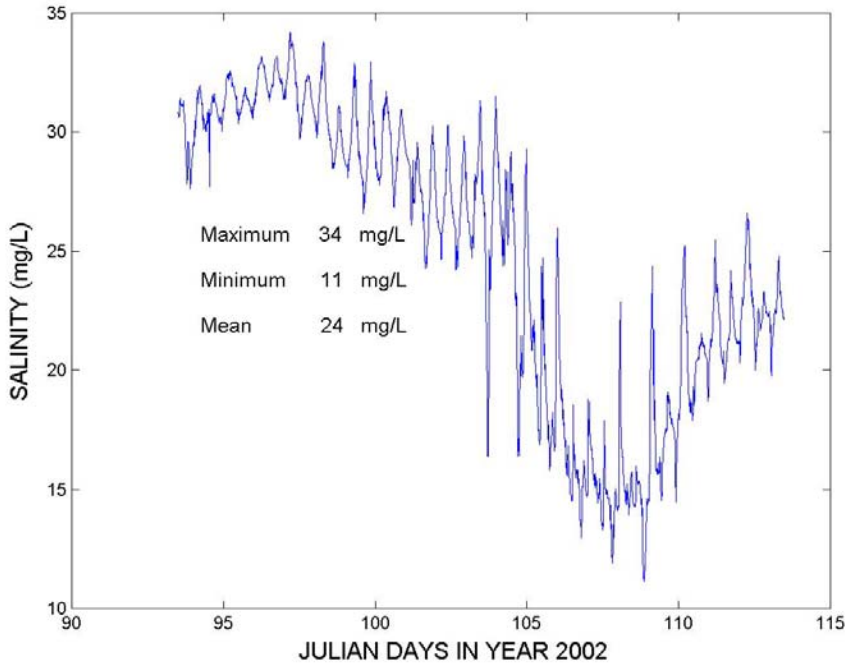

Figure 3.16 Salinity time series: Days 94-114 (year 2002).

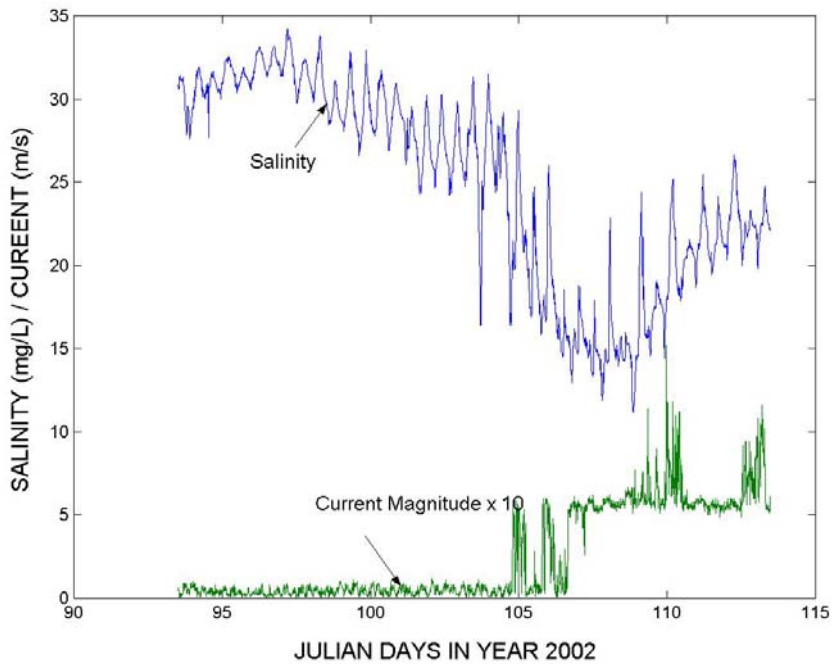

Figure 3.17 Salinity and Current magnitude time series: Days 94-114 (year 2002).

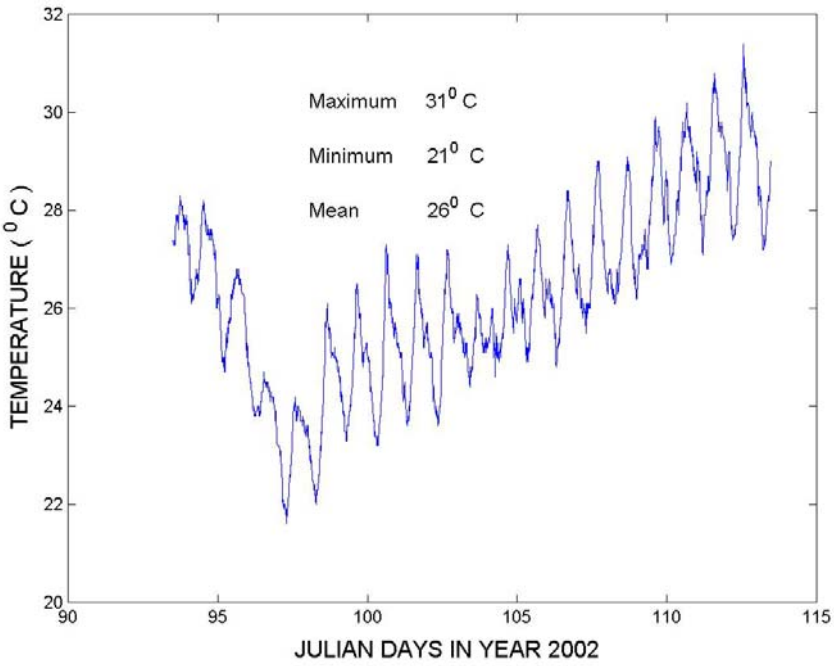

Figure 3.18 Temperature time series: Days 94-114 (year 2002).

Similarly the temperature time-series shows a positive correlation with the discharge, with temperature increasing with the discharge from S-46 structure. However any definite conclusion could not be deduced from this the absence of adequate data on temperature of the freshwater discharged.

For the second data block between days 352 and 365 (of year 2002) and days 01 and 35 (of year 2003) the Figure 3.19 indicates an apparent malfunctioning of the sensor that seems to have contaminated the conductivity time series that calculates the salinity by measuring its conductivity of the solution at a given temperature. Although the temperature time series for the same period appears to give correct reading consistent with the environment, the incorrect conductivity data have made the salinity determination inaccurate. Therefore salinity values reported in this period appear to be rather high. Tables 3.5 and 3.6 summarize the characteristic values of salinity and

temperature for both the data blocks. The results from the other data blocks are furnished in Table 3.7 to 3.9.

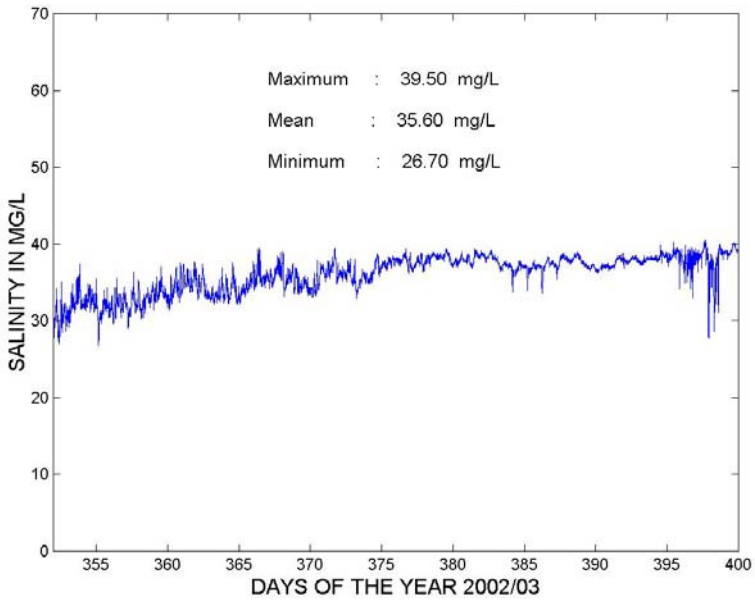

Figure 3.19 Salinity time series: Days 352- 365 (year 2002) and 01-35 (year 2003).

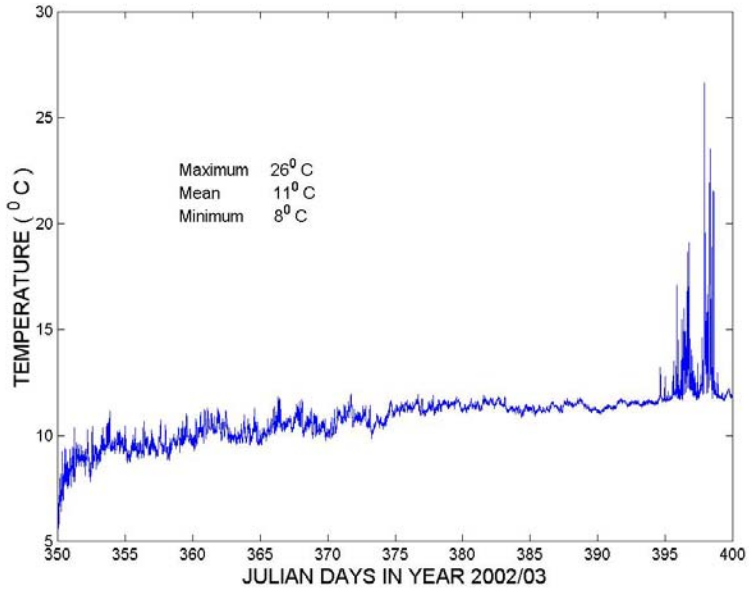

Figure 3.20 Temperature time series: 352- 365 (year 2002) and 01-35 (year 2003).

Table 3.7 Characteristic temperature values

Julian days in 2002	Maximum Temperature (^{0} C)	Mean Temp (^{0} C)	Minimum Temperature (^{0} C)
94-114	31.4	26.3	21.6
352-400	26.7	10.9	7.8

3.3.5 Other Data Blocks

The foregoing discussions included the various aspects of data collection their analysis and results for two representative data blocks (Julian Days 94 to 114, 330-365 in year 2002 and 01 to 35 in year 2003). However since the second phase data collection lasted from November 26th, 2002 to May 15th, 2003, it was considered necessary to include the characteristic values obtained from the other data blocks, which would offer a better insight in to the overall site conditions.

Table 3.8 Summary of parametric value (Days 37-59 in year 2003)

Parameter	Maximum	Mean	Minimum
Depth (m)	1.9	1.2	0.5
OBS 1 (mg/L)	*	*	*
OBS 2 (mg/L)	240	30	0.7
OBS 3 (mg/L)	110	20	1.0
Salinity (mg/L)	40	35	23
Temperature (^{0}C)	27	16	11
Current Magnitude (m/s)	*	*	*

** Poor quality data*

In Table 3.7 a summary of parametric values of the data collected between February 6th and February 28th is presented. The data obtained for the other two blocks are presented in Tables 3.8 and 3.9.

Table 3.9 Summary of parametric value (Days 90-101 in year 2003)

Parameter	Maximum	Mean	Minimum
Depth (m)	1.6	1.1	0.6
OBS 1 (mg/L)	2670	1710	1470
OBS 2 (mg/L)	80	50	1.0
OBS 3 (mg/L)	96	51	20
Salinity (mg/L)	*	*	*
Temperature (^{0}C)	20	11	3
Current Magnitude (m/s)	*	*	*

*-Bad Data

Table 3.10 Summary of parametric value (Days 101-135 in year 2003)

Parameter	Maximum	Mean	Minimum
Depth (m)	1.9	1.3	0.7
OBS 1 (mg/L)	2090	1670	1180
OBS 2 (mg/L)	170	46	2
OBS 3 (mg/L)	210	56	10
Salinity (mg/L)	26	19*	17*
Temperature (^{0}C)	22	12	4
Current Magnitude (m/s)	1.40	0.60	0.10

* *Bad Data*

3.4 Field Data Results in Northwest Fork

3.4.1 Field Setup

In the third phase of data collection, in the Northwest Fork, the instrument tower included three optical backscatter sensors (OBS), a pressure transducer (for water level) and a conductivity/temperature sensor. Data collection began on 08/14/2003. Data on water level and TSS are presented. The conductivity/temperature sensor malfunctions during this phase and yielded values of questionable accuracy. Hence these data are not reported.

3.4.2 Tidal Level

The pressure transducer was located 0.45 m from the bed. Figure 3.21 shows the original time series of the water level.

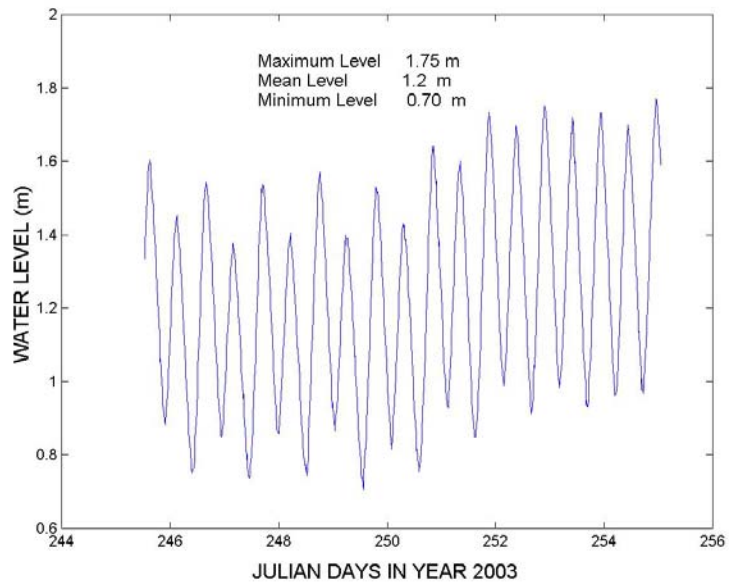

Figure 3.21 Record of water level variation. Days 245 – 255 (year 2003).

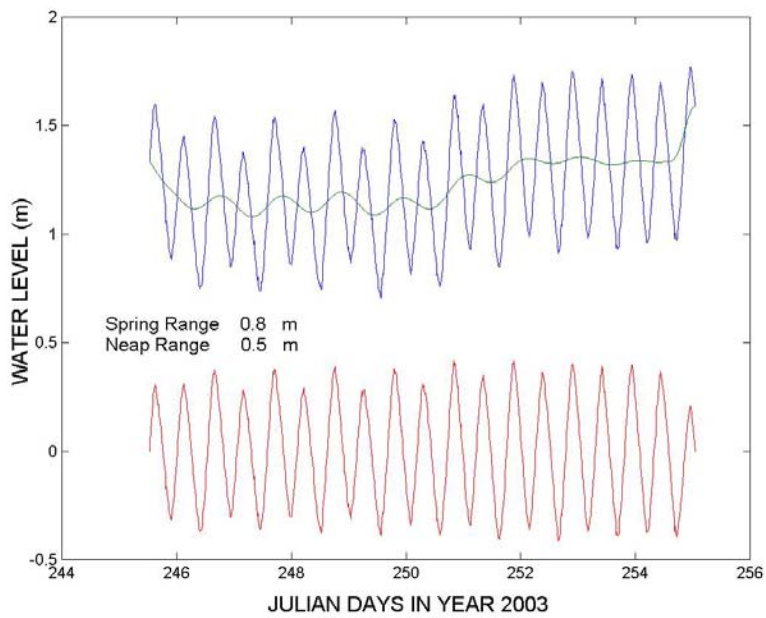

Figure 3.22 Water level time series. Upper plot shows original time series with mean trend and the lower plot is without the mean oscillations. All levels relative to NAVD 88. Days 245 -255 (year 2003).

In Figure 3.22 the upper plot shows 12-hourly mean trend with the original time series, and in the lower plot this trend is removed. As can be seen from the latter plot, the

rising mean trend indicates the effect of fresh water discharge. The tidal range was 0.80 m. Characteristic values are given in Table 3.10.

Table 3.11 Characteristic values of the tidal data

Julian days in 2003	Mean Water depth (m)	Water Level/Tidal range			
		Water level (m)		Spring/neap range (m)	
		Maximum	Minimum	Spring	Neap
245-255	1.20	1.75	0.70	0.80	0.50

3.4.3 Total Suspended Solids

Total suspended solids (TSS) concentration was recorded at three elevations. The elevations of the OBS sensors relative to the bed were OBS-1 = 1.04 m, OBS-2 = 0.66 m and OBS-3 = 0.30 m. The corresponding depth-mean concentration time series is reported in Figure 3.23. Characteristic values are given in Table 3.11.

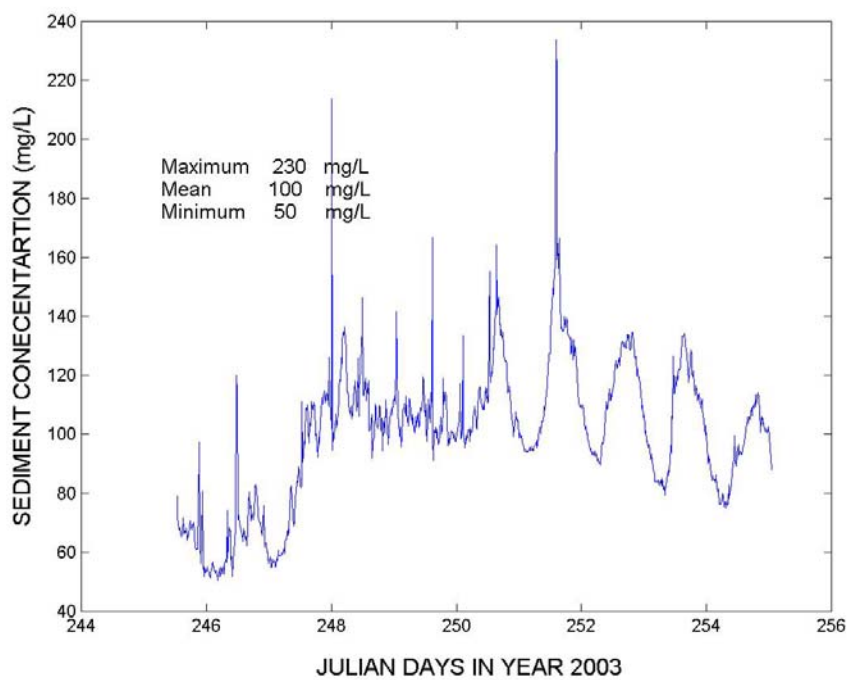

Figure 3.23 Depth-mean TSS concentration time-series: Days 245-255 (year 2003).

Table 3.12 TSS concentrations for the representative data blocks

Julian Days in 2003	Maximum TSS concentration (mg/L)	Mean TSS concentration (mg/L)	Minimum TSS concentration (mg/L)
245-255	230	100	50

3.4.5 Additional Data Blocks

3.4.5.1 Tidal Level

Two additional data blocks were collected between November 6th, 2003 and November 24th, 2003. Tide data for Julian days 310 and 313 are presented here. The remainder was found to be of poor quality.

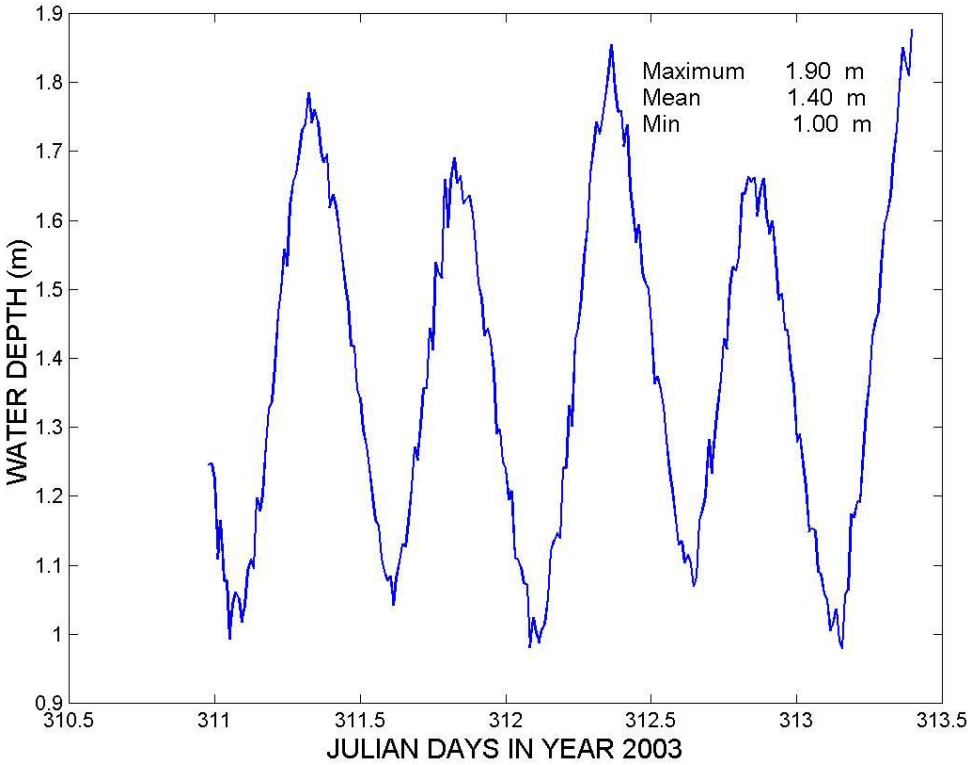

Figure 3.24 Record of water level variation. Days 310.5 – 313.5 (year 2003).

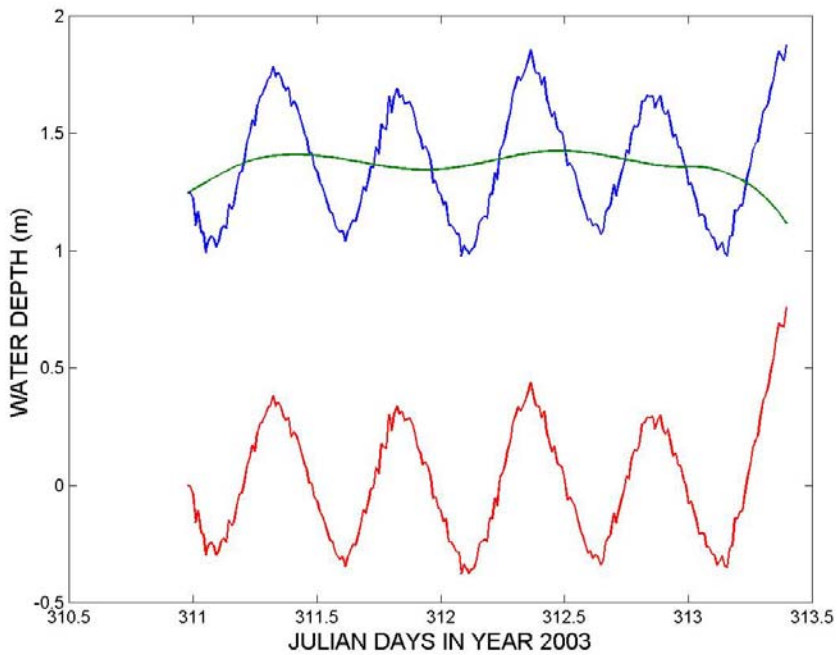

Figure 3.25 Water level time series. Upper plot shows original time series with mean trend and the lower plot is without the mean oscillations. All levels relative to NAVD 88. Days 310.5 – 313.5 (Year 2003).

Table 3.13 Characteristic values of the tidal data

Julian days in 2003	Mean Water depth (m)	Water Level/Tidal range			
		Water level (m)		Spring/neap range (m)	
		Maximum	Minimum	Spring	Neap
310.5-313.5	1.40	1.90	1.00	0.90	0.50

3.4.5.2 Total Suspended Solids

Two data blocks for the TSS concentration was collected and are presented below.

Characteristic values are presented in Table 3.14.

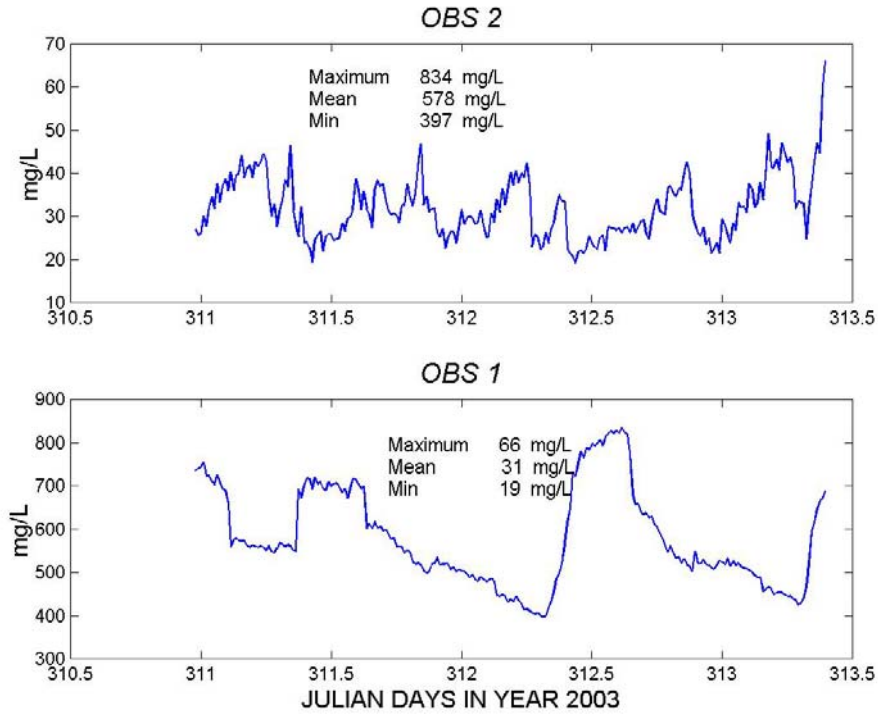

Figure 3.26 TSS time-series at two elevations: Days 310.5 – 313.5 (year 2003).

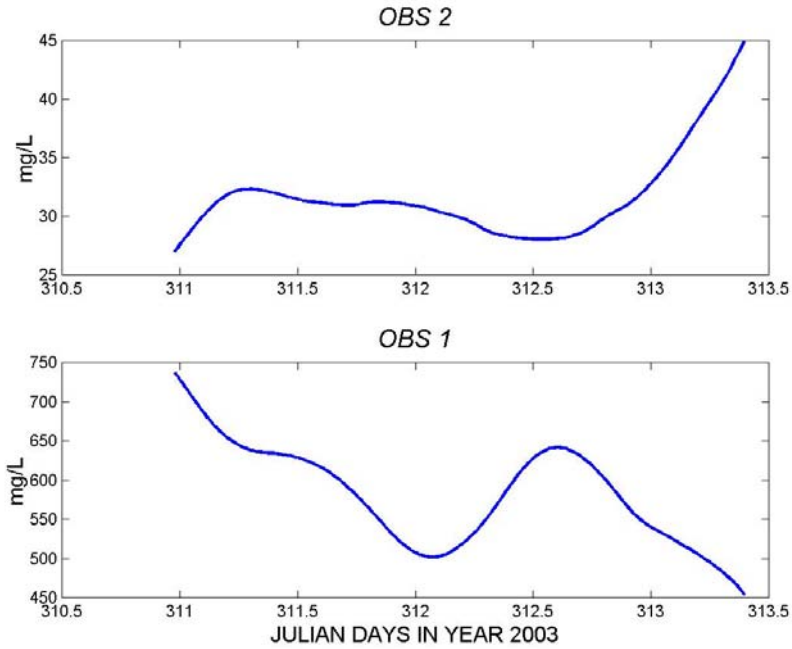

Figure 3.27 Depth mean TSS concentration time series: Days 310.5 – 313.5 (year 2003).

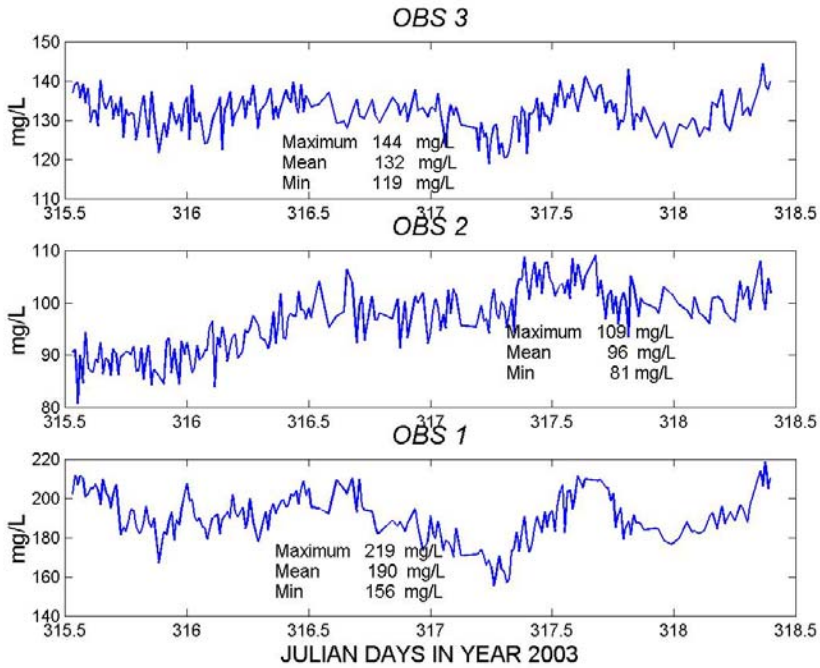

Figure 3.28 TSS time-series at three elevations: Days 315.5 – 318.5 (year 2003).

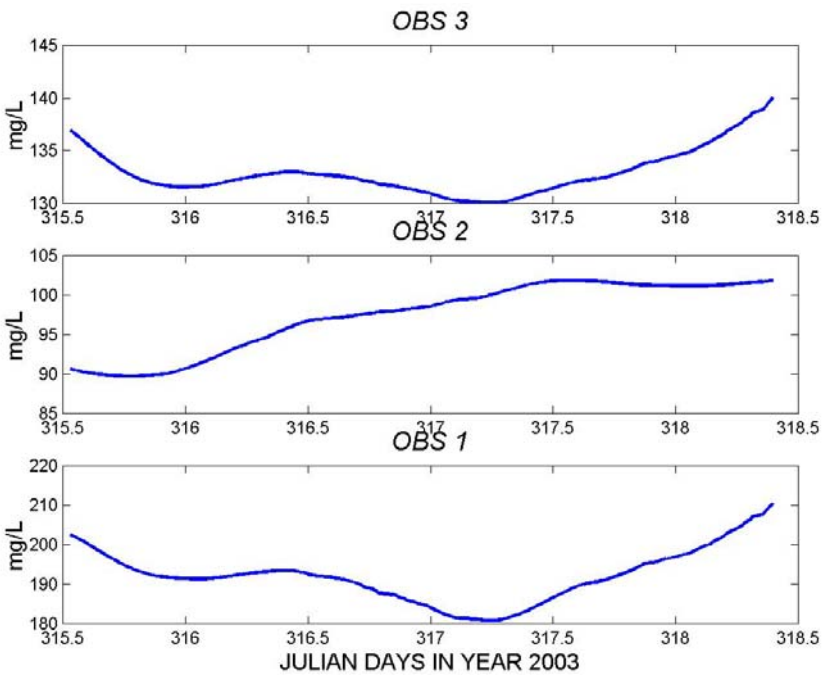

Figure 3.29 Depth-mean TSS concentration time series: Days 315.5 – 318.5 (year 2003).

Table 3.14 TSS concentrations for the representative data blocks

Julian Days in 2003	Maximum TSS concentration (mg/L)	Mean TSS concentration (mg/L)	Minimum TSS concentration (mg/L)
310.5 – 313.5	834	304	19
315.5 – 318.5	219	140	81

CHAPTER 4
MODEL CALIBRATION AND VALIDATION

The analyzed data presented in Chapter 3 give a qualitative insight into the prevailing environmental conditions. However, in order to have a quantitative understanding of the flow regime in the estuary, it is necessary to apply a numerical simulation technique. This chapter includes a brief description of the numerical model, generation of the computational grid, initial and boundary conditions and the model operational scheme. Model calibration and validation are then carried out.

Certain aspects of the estuary have been idealized in the formulation of the model in order to reduce the computational time and avoidance of potential errors. These idealizations are as follows:

1. The central embayment domain is terminated at the FECRR bridge excluding the ICWW (Intracoastal Waterway). This enables use of tide data from UFG1 gage installed at the bridge.
2. The traps and the navigation channels have rectangular cross-sections.

4.1 Model Description

Flow simulations were carried out using Environmental Fluid Dynamics Code (EFDC) maintained by the Environmental Protection Agency, and developed by Hamrick, 1992. This code works through a Microsoft Windows-based EDFC-Explorer pre- and post-processor. Developed on a Fortran platform, the physics of EFDC and many aspects of the computational scheme are equivalent to the widely used Blumberg-Mellor model (Blumberg and Mellor, 1987) and the U.S. Army Corps of Engineers' Chesapeake Bay model (Johnson, et al, 1993). EFDC solves the three-dimensional

hydrostatic, free surface, turbulent averaged equations of motion of a variable density fluid. The model uses a stretched or sigma vertical coordinate and Cartesian or curvilinear, orthogonal horizontal coordinates. Dynamically coupled transport equations for turbulent kinetic energy, turbulent length scale, salinity and temperature are also solved. Externally specified bottom friction can be incorporated in the turbulence closure model as a source term. For the simulation of flow in vegetated environments, EFDC incorporates both two and three-dimensional vegetation resistance formulations (Moustafa, and Hamrick 1995).

The numerical scheme employed in EDFC to solve the equations of motion uses second-order-accurate spatial finite difference on a staggered- or a C-grid. The model's time integration employs a second-order-accurate, three-time-level, finite-difference scheme with an internal-external mode splitting procedure to separate the internal shear or baroclinic mode from the external free surface gravity wave or barotropic mode. The external mode solution is semi-implicit, and simultaneously computes the two-dimensional surface elevation field by the preconditioned conjugate gradient procedure. The external solution is completed by the calculation of the depth averaged barotropic velocities using the new surface elevation field. The models' semi-implicit external solution allows large time steps that are constrained by the stability criteria of the explicit central difference or upwind advection scheme used for the nonlinear accelerations. Horizontal boundary conditions for the external mode solution include the option for simultaneously specifying the surface elevations, the characteristic of an incoming wave, free radiation of an outgoing wave or the volumetric flux on arbitrary portions of the boundary. The model's internal momentum equation solution, at the same time step as

the external, is implicit with respect to vertical diffusion. The internal solution of the momentum equations in terms of the vertical profile of shear stress and velocity shear, which results in the simplest and most accurate form of baroclinic pressure gradients, and eliminates the over-determined character of alternate internal mode formulations.

The model implements a second order accurate in space and time, mass conservation fractional step solution scheme for the Eulerian transport equation at the same time step or twice the time step of the momentum equation solution. The advective portion of the transport solution uses either the central difference scheme used in the Blumberg-Mellor model or hierarchy of positive definite upwind difference schemes. The highest accuracy up-wind scheme, second order accurate in space and time, is based on a flux corrected transport version of Smolarkiewicz's multidimensional positive definite advection transport algorithm, which is monotonic and minimizes numerical diffusion.

The EFDC model's hydrodynamic component is based on the three-dimensional hydrostatic equations formulated in curvilinear-orthogonal horizontal coordinates and a sigma or stretched vertical coordinate. The momentum equations are:

$$\begin{aligned}
&\partial_t\left(m_x m_y Hu\right)+\partial_x\left(m_y Huu\right)+\partial_y\left(m_x Hvu\right)+\partial_z\left(m_x m_y wu\right)-f_e m_x m_y Hv \\
&=-m_y H\partial_x\left(p+p_{atm}+\phi\right)+m_y\left(\partial_x z_b^*+z\partial_x H\right)\partial_z p+\partial_z\left(m_x m_y \frac{A_v}{H}\partial_z u\right) \\
&\quad+\partial_x\left(\frac{m_y}{m_x}HA_H\partial_x u\right)+\partial_y\left(\frac{m_x}{m_y}HA_H\partial_y u\right)-m_x m_y c_p D_p\left(u^2+v^2\right)^{1/2}u
\end{aligned} \tag{4.1}$$

$$\begin{aligned}
&\partial_t\left(m_x m_y Hv\right)+\partial_x\left(m_y Huv\right)+\partial_y\left(m_x Hvv\right)+\partial_z\left(m_x m_y wv\right)+f_e m_x m_y Hu \\
&=-m_x H\partial_y\left(p+p_{atm}+\phi\right)+m_x\left(\partial_y z_b^*+z\partial_y H\right)\partial_z p+\partial_z\left(m_x m_y \frac{A_v}{H}\partial_z v\right) \\
&\quad+\partial_x\left(\frac{m_y}{m_x}HA_H\partial_x v\right)+\partial_y\left(\frac{m_x}{m_y}HA_H\partial_y v\right)-m_x m_y c_p D_p\left(u^2+v^2\right)^{1/2}v
\end{aligned} \tag{4.2}$$

$$m_x m_y f_e = m_x m_y f - u\partial_y m_x + v\partial_x m_y \tag{4.3}$$

$$(\tau_{xz}, \tau_{yz}) = A_v H^{-1} \partial_z (u, v) \tag{4.4}$$

where u and v are the horizontal velocity components in the dimensionless curvilinear-orthogonal horizontal coordinates x and y, respectively. The scale factors of the horizontal coordinates are m_x and m_y. The vertical velocity in the stretched vertical coordinate z is w. The physical vertical coordinates of the free surface and bottom bed are z_s^* and z_b^* respectively. The total water column depth is H, and ϕ is the free surface potential which is equal to gz_s^*. The effective Coriolis acceleration f_e incorporates the curvature acceleration terms, with the Coriolis parameter, f, according to (4.3). The Q terms in (4.1) and (4.2) represent optional horizontal momentum diffusion terms. The vertical turbulent viscosity A_v relates the shear stresses to the vertical shear of the horizontal velocity components by (4.4). The kinematic atmospheric pressure, referenced to water density, is p_{atm}, while the excess hydrostatic pressure in the water column is given by:

$$\partial_z p = -gHb = -gH(\rho - \rho_o)\rho_o^{-1} \tag{4.5}$$

where ρ and ρ_o are the actual and reference water densities and b is the buoyancy. The horizontal turbulent stress on the last lines of (4.1) and (4.2), with A_H being the horizontal turbulent viscosity, are typically retained when the advective acceleration are represented by central differences. The last terms in (4.1) and (4.2) represent vegetation resistance where c_p is a resistance coefficient and D_p is the dimensionless projected vegetation area normal to the flow per unit horizontal area.

The three-dimensional continuity equation in the stretched vertical and curvilinear-orthogonal horizontal coordinate system is:

$$\partial_t\left(m_x m_y H\right)+\partial_x\left(m_y H u\right)+\partial_y\left(m_x H v\right)+\partial_z\left(m_x m_y w\right)=Q_H \tag{4.6}$$

with Q_H representing volume sources and sinks including rainfall, evaporation, infiltration and lateral inflows and outflows having negligible momentum fluxes.

The solution of the momentum equations, (4.1) and (4.2) requires the specification of the vertical turbulent viscosity, A_v, and diffusivity, K_v. To provide the vertical turbulent viscosity and diffusivity, the second moment turbulence closure model developed by Mellor and Yamada (1982) (MY model) and modified by Galperin *et al* (1988) and Blumberg *et al.* (1988) is used. The MY model relates the vertical turbulent viscosity and diffusivity to the turbulent intensity, q, a turbulent length scale, l, and a turbulent intensity and length scaled based Richardson number, R_q, by:

$$\begin{aligned}
A_v &= \phi_A q l \\
\phi_A &= \frac{A_o\left(1+R_1^{-1}R_q\right)}{\left(1+R_2^{-1}R_q\right)\left(1+R_3^{-1}R_q\right)} \\
A_o &= A_1\left(1-3C_1-\frac{6A_1}{B_1}\right)=\frac{1}{B_1^{1/3}} \\
R_1^{-1} &= 3A_2\frac{\left(B_2-3A_2\right)\left(1-\frac{6A_1}{B_1}\right)-3C_1\left(B_2+6A_1\right)}{\left(1-3C_1-\frac{6A_1}{B_1}\right)} \\
R_2^{-1} &= 9A_1A_2 \\
R_3^{-1} &= 3A_2\left(6A_1+B_2\right)
\end{aligned} \tag{4.7}$$

$$\begin{aligned}
K_v &= \phi_K q l \\
\phi_K &= \frac{K_o}{\left(1+R_3^{-1}R_q\right)} \\
K_o &= A_2\left(1-\frac{6A_1}{B_1}\right)
\end{aligned} \tag{4.8}$$

$$R_q=-\frac{gH\partial_z b}{q^2}\frac{l^2}{H^2} \tag{4.9}$$

where the so-called stability functions, ϕ_A and ϕ_K, account for reduced and enhanced vertical mixing or transport in stable and unstable vertically density stratified environments, respectively. Mellor and Yamada (1982) specify the constants A_1, B_1, C_1, A_2, and B_2 as 0.92, 16.6, 0.08, 0.74, and 10.1, respectively.

For stable stratification, Galperin *et al.* (1988) suggest limiting the length scale such that the square root of R_q is less than 0.52. When horizontal turbulent viscosity and diffusivity are included in the momentum and transport equations, they are determined independently using Smagorinsky's (1963) sub-grid scale closure formulation.

At the bed, the stress components are presumed to be related to the near bed or bottom layer velocity components by the quadratic resistance formulation

$$(\tau_{xz}, \tau_{yz}) = (\tau_{bx}, \tau_{by}) = c_b \sqrt{u_1^2 + v_1^2}\,(u_1, v_1) \tag{4.10}$$

where the 1 subscript denotes bottom layer values. Under the assumption that the near bottom velocity profile is logarithmic at any instant of time, the bottom stress coefficient is given by

$$c_b = \left(\frac{\kappa}{\ln(\Delta_1 / 2z_o)} \right)^2 \tag{4.11}$$

where κ is the von Karman constant, Δ_1 is the dimensionless thickness of the bottom layer, and $z_o = z_o^*/H$ is the dimensionless roughness height. Vertical boundary conditions for the turbulent kinetic energy and length scale equations are:

$$q^2 = B_1^{2/3} |\tau_s| : z = 1 \tag{4.12}$$

$$q^2 = B_1^{2/3} |\tau_b| : z = 1 \tag{4.13}$$

$$l = 0 \quad : \quad z = 0,1 \tag{4.14}$$

where the absolute values indicate the magnitude of the enclosed vector quantity which are wind stress and bottom stress, respectively.

4.3 Grid Generation

The first step in the setup of the modeling system is to define the horizontal plane domain of the region being modeled. The horizontal plane domain is approximated by a set of discrete quadrilateral and triangular cells. Developed on a digitized shoreline, the grid defines the precise locations of the faces of the quadrilateral cells in the horizontal as well as in the vertical plane. However, all the computations are carried out at the center of the cells. Since the model solves the hydrodynamic equations in a horizontal coordinate system that is curvilinear and orthogonal, grid lines also correspond to lines having a constant value of one of the horizontal coordinates. The shoreline as well as the cell reference is provided by a local set of Coordinates in MKS unit, as the code uses MKS system internally. Seven identification numbers were used to define the cell types. The cell identification details are given in Table 4.1.

Table 4.1 Definition of cell type used in the model input

Cell ID	Definition of cell type
0	Dry land cell not bordering a water cell on a side or corner of the model
1	Triangular cell with land to the northeast of the model
2	Triangular cell with land to the southeast of the model
3	Triangular cell with land to the southwest of the model
4	Triangular cell with land to the northwest of the model
5	Quadrilateral water cells of the model
9	Dry land cell bordering a water cell on a side or on a corner of the model

The type 9 dry land or fictitious dry land cell type is used in the specification of no flow boundary conditions. The horizontal geometric and topographic (bottom bathymetry) and other related characteristics of the region, files *dxdy.inp* and *lxly.inp* are used. The program then directly reads these quantities expressed in meters. The *lxly.inp*

provides cell center coordinates and components of a rotation matrix. Cell center coordinates are used only in graphics output and can be specified in the most convenient units for graphical display such as decimal degrees, feet, miles, meters or kilometers. The rotation matrix is used to convert pseudo east and north (curvilinear x and y) horizontal velocities (u and v respectively) to true east and north for graphics vector plotting, according to;

$$\begin{Bmatrix} u_{te} \\ v_{tn} \end{Bmatrix} = \begin{bmatrix} C_{cue} C_{cve} \\ C_{cun} C_{cvn} \end{bmatrix} \begin{Bmatrix} u_{co} \\ v_{co} \end{Bmatrix} \qquad 4.15$$

where the subscripts te and tn denote true east and true north, while the subscripts co denotes the curvilinear-orthogonal horizontal velocity components. The coefficient C is the multiplier term for conversion to true east and true north.

The width of the C-18 canal, which varies between 75 m at the Southwest Fork junction to less than 40m at the S-46 structure, dictated the dimensions of the cells. It was decided that a 25 x 25m cell would be accurate enough for representing the width of the C-18 canal resulting in desired level of accuracy. The same cell size was then conveniently extended to the rest of the model domain. The bottom bathymetry was based on the Hydrographic survey carried out in November ‘2001 by Lidberg Land Surveying, Inc. However additional data for areas not covered under this survey were obtained from other available surveys. The roughness coefficient of the bottom bathymetry in the model is composed of two components. A fixed component viscosity (for the present model fixed at 0.020m) and a variable component, which is varied uniformly on the entire model domain during calibration process, both the component together constitutes the factor z_0, defined in equation 4.11. The dimensionless thickness

of the bottom layer Δ_1, defined in the same equation, equals to 0.25, since four vertical layers are used. The fixed component of the roughness factor, how ever can be increased/decreased in the areas of vegetation or other special features. The details of sea grass locations in the central embayment can be referred from Drawing no LOX-001 (Cuthcher & Associates, Inc. Coastal Engineer, 2002) provided by the Jupiter Inlet District. The sea grass was input in the model as an overlay file. In this way the cells having the sea grasses are enclosed by a polyline so that, the roughness coefficient can be easily edited. The sea grass was represented as cells having more roughness (fixed component = 0.040m) than that of the surroundings. In Figure 4.1 the input bathymetry and the shoreline as generated by the model are shown.

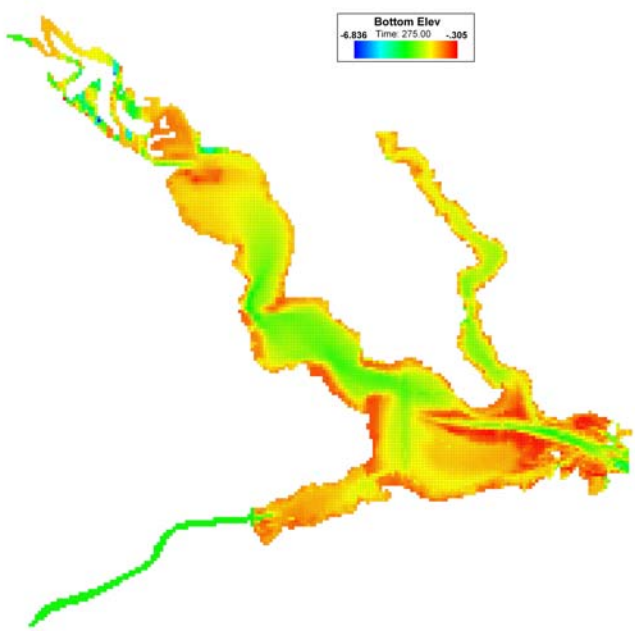

Figure 4.1 Model domain showing input bathymetry and shoreline

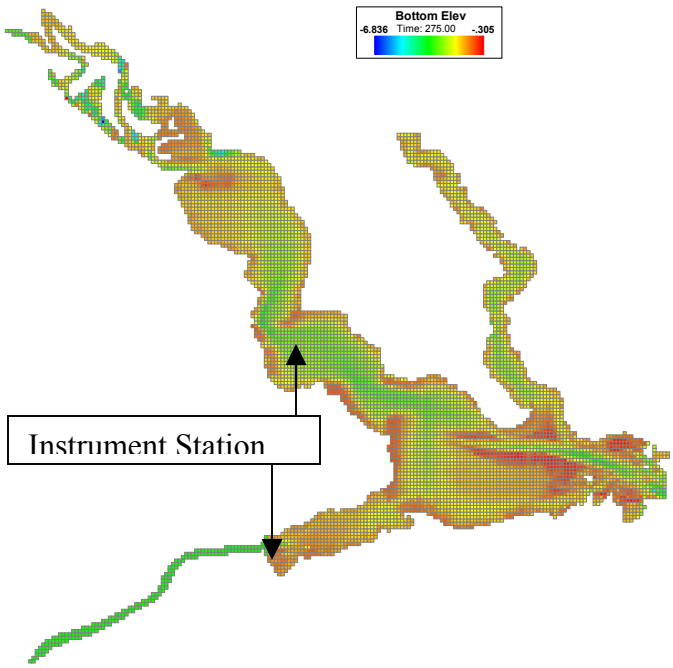

Figure 4.2 Computational grid showing the flow boundaries

In the computational grid (Figure 4.2), each land cell was assigned number zero or nine as the case may be and each water cell was assigned five. There were no triangular cells used for this grid. Figure 4.2, in addition, indicates the locations of the tide gages and the Instrument tower in the Southwest fork. The S-46 structure in the C-18 canal is a flow boundary (black cells), as are the two main tributaries, and the FECRR bridge on the East. The eastern boundary was restricted to the FECRR bridge. The flow boundaries were kept straight; so as to allow flows perpendicular to the cell faces, as the model does not allow non-orthogonal flows.

4.4 Boundary Conditions

In the beginning of the simulation, velocities throughout the model domain are considered to be zero. It was observed that a full tidal cycle was required before the water surface elevation reached a quasi-steady state. This was verified by recording water

surface elevations at the location of the two tide gauges (UFG2 and UFG3) over multiple tidal periods.

Tidal forcing at the FECRR bridge (eastern boundary) is perhaps the most important boundary condition in this system, because it is this mechanism by which the majority of the water flows through the estuary. The data obtained from the UFG1 gage (Figure 2.10) were used to simulate this forcing. The raw data were examined for the mean trends in the water surface elevation (Figure 4.3). The raw data contains a sub-tidal frequency trend, which was also noticed in the water surface elevation data of the Miami Harbor. The trends were of a similar in nature and therefore it was hypothesized that onshore winds may have created increased elevation in side the estuary. The wind records from two offshore sites (37 and 221 kilometer east of Cape Carnival, Florida) were correlated with the mid-tide elevation, which indicated a positive correlation (Ganju et al., 2001). In order to overcome the effects of these variations imposed on the astronomical tide, the mid-tide elevation was subtracted from each measured elevation in the same tidal cycle. The mid tide elevation η_c is given by Equation 4.1, where, η_{HT} and η_{LT} are the water surface elevation at high and low tides respectively.

$$\eta_c = \frac{\eta_{HT} + \eta_{LT}}{2} \tag{4.16}$$

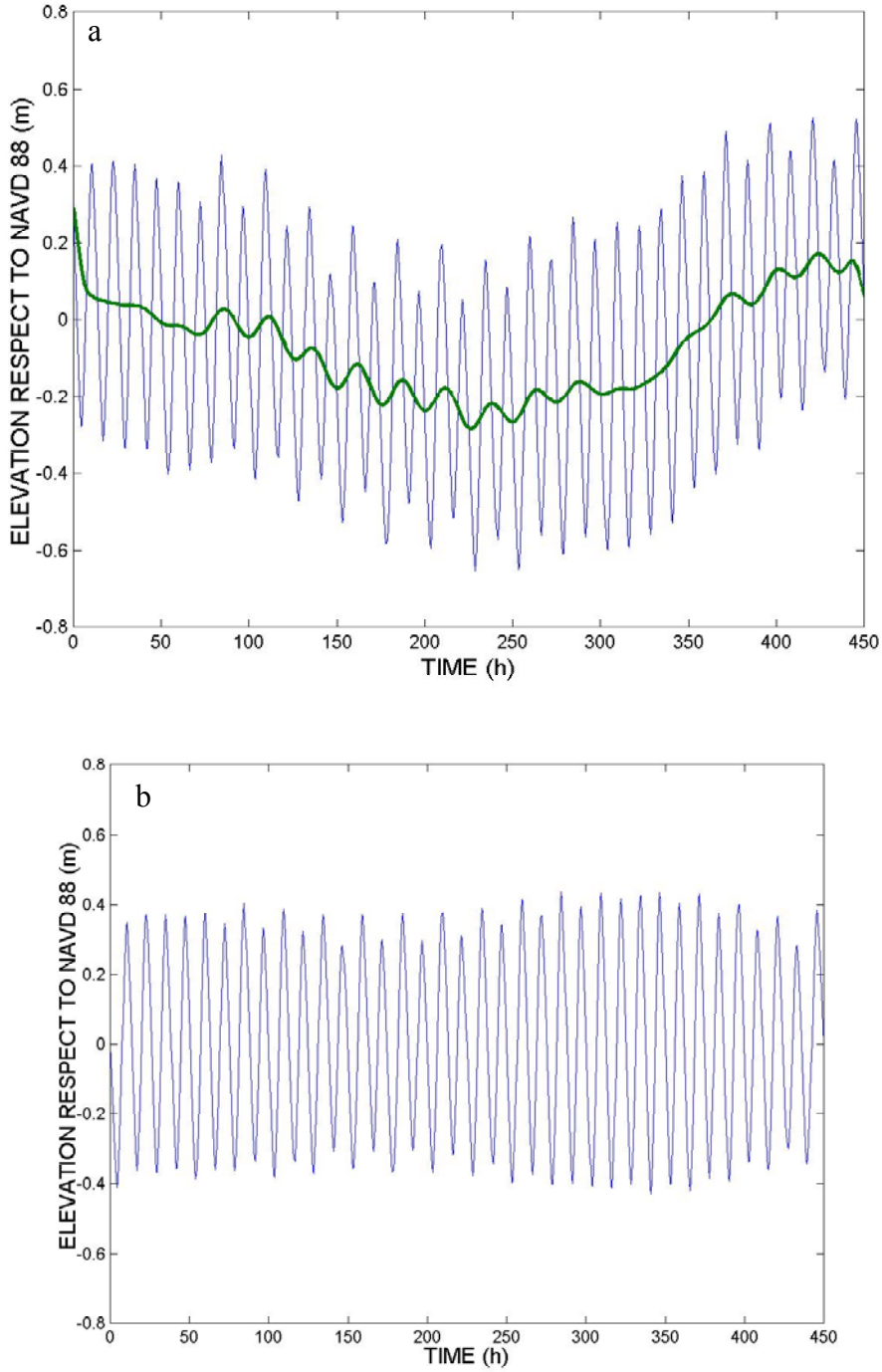

Figure 4.3 Tidal time series from UFG1, 09/14/00-10/13/00, a) Raw data, b) Tidal plot after the mid-tide trend is removed. Time origin 12:00 am.

In Figure 4.3a the raw tidal time series is shown along with the tidal trend and in Figure 4.3b the tidal time series is shown after subtracting the mean-tide trend. The eastern boundary accordingly used this water surface elevation boundary condition.

For the boundary in the C-18 canal, two sets of boundary condition data were available. The daily average flow time series of the S-46 structure and the water surface elevation time series. The elevation time series was obtained from the tide gauge UFG 3 (same period as at UFG 1) installed in the Southwest Fork (Figure 2.10). In order to make these data usable at the flow boundary (S-46 Structure) amplitude corrections were carried out by trial and error till both predicted and measured time series matched. In order to calculate the phase correction (lag) following calculations were carried out assuming shallow water conditions. The tidal wave celerity C is given by,

$$C = \sqrt{gh} \tag{4.23}$$

where, g is the acceleration due to gravity and h is the water depth. Then the phase shift ΔT is given by,

$$C = \sqrt{gh} = \frac{\Delta L}{\Delta T}; \qquad \Delta T = \frac{\Delta L}{C} \tag{4.24}$$

where, ΔL is the distance for which the water depth is considered uniform, accordingly the phase lag for the distance between the UFG 3 gage station and the S-46 structure was calculated and verified (0.13 hour). Figure 4.4 gives the plot of the raw data collected at UFG 3, including the mean trend and the amplitude with trends removed. It was hypothesized that these data, corrected for the phase and amplitude could be applied as boundary condition to simulate actual flow conditions.

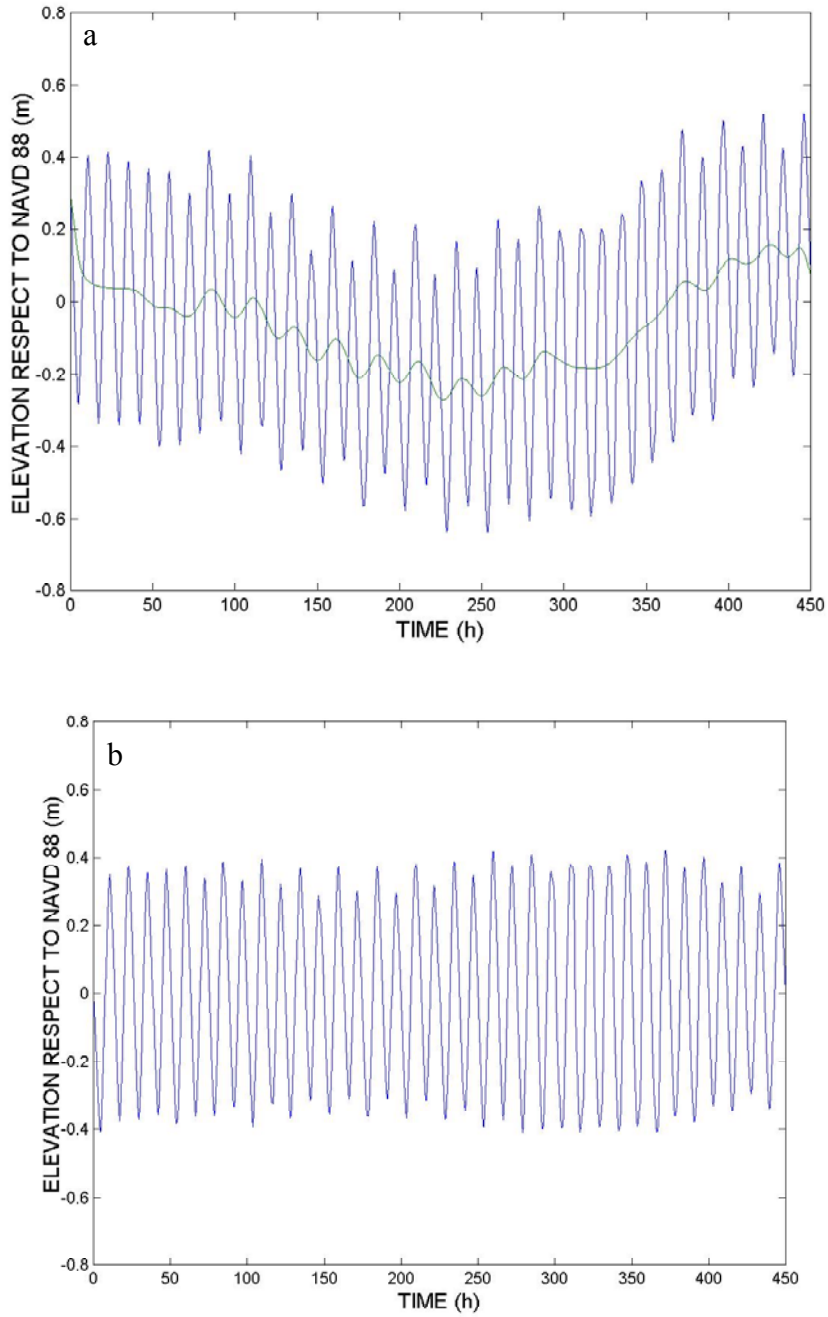

Figure 4.4 Tidal time series from UFG3, 09/14/00-10/13/00, a) Raw data, b) Tidal plot after the mid-tide trend is removed. . Time origin 12:00 am

Note that the flow discharge time series (Figure 4.5) from the S-46 structure was selected, as the model is known to be giving better simulation results under discharge boundary condition.

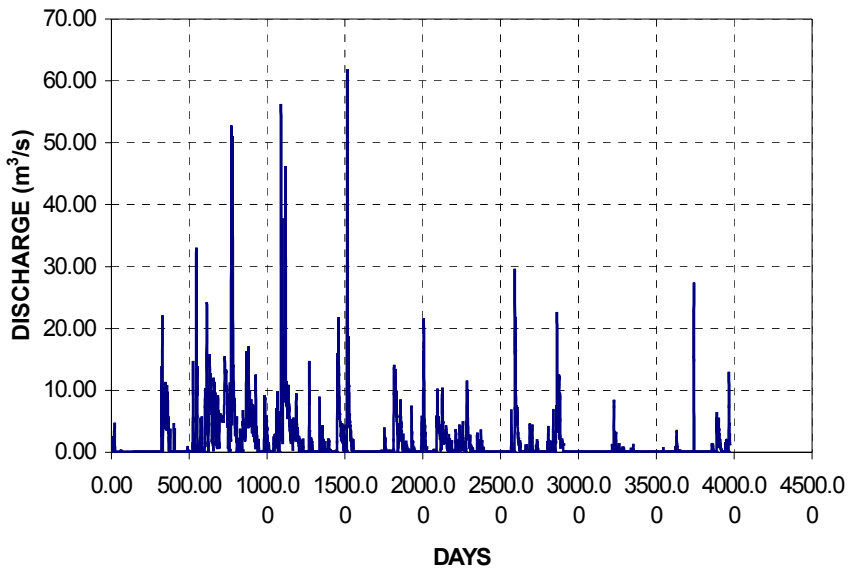

Figure 4.5 Flow time series applied at S-46 boundary

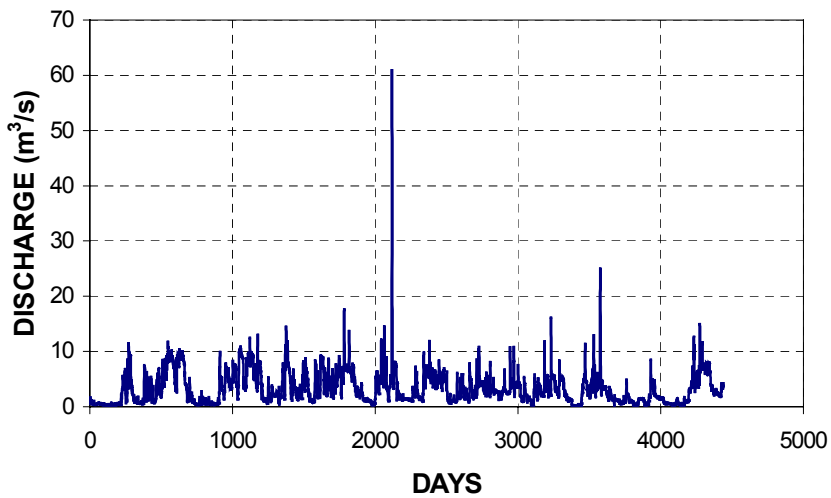

Figure 4.6 Flow time series applied at Northwest Fork boundary

In the Northwest Fork boundary as well, two sets of boundary conditions, namely, the water surface elevation boundary condition (obtained from transferring the collected data of the tidal station UFG 2) and flow discharge boundary condition were evaluated. The flow time series used is shown in Figure 4.6.

Table 4.2 Amplitude and phase correction factor for the tides

Boundary	Amplitude factor	Phase correction
C-18	1.14	0.13 hour
Northwest Fork	1.18	0.042 hour

Per U.S. Geological Survey Report 84-4157 (Russell and McPherson, 1984) the majority (77.3 %) of the fresh water flow in to the estuary enters through the Northwest Fork. Therefore, the flow discharge boundary condition for this tributary was considered as most appropriate as opposed to the water surface elevation. The corrected water surface elevation data from UFG 2 tide gage was used for calibration.

The North Fork carries the least discharge (2.2%) of the total freshwater flow in to the estuary in the mean, (Russell and McPherson, 1984)) hence at this boundary also flow discharge boundary condition is applied. The flow discharge was worked out from the Northwest boundary data applying a constant multiplier ($\frac{2.2}{77.3} = 0.0285$).

4.5 Model Calibration and Validation

4.5.1 Calibration

In general calibration of the model aims at simulating conditions identical or close to that in the prototype so that prototype conditions can be accurately replicated and reproduced. Calibration involves matching multiple parameters, which is often times, is practically impossible. However, depending on the nature experiments and the results desired, the type of calibration differs. Since the present model simulation aims to relate the velocity and the associated stress field to the erosion/accretion of the sediments in the estuary, it would be highly desirable to calibrate the model with comparison of the flow velocities. But current data for the model simulation period, between September 14th 2000 and 18th October 2000 was not available and therefore, it was decided to calibrate the model using the data collected at the instrument station located in the Southwest Fork (Figure 3.1) between November 26th and May 15th 2003 for which current as well as

water surface elevation data was available. The amplitude multiplier and phase lag factors are given in Table 4.2.

Accordingly a simulation for this period was carried out using flow discharge boundary conditions for the Southwest, the Northwest and North tributary boundaries and water surface elevation boundary condition for the East boundary. For the eastern boundary the tidal data from Miami Harbor were "transferred" to the FECRR bridge boundary by applying suitable correction factors for the amplitude and the phase lag. This procedure was carried out in two steps. In the first step, the Miami harbor data for the period 14th September 2000 to 18th October 2000 were transferred to the boundary with application of recommended coefficients (for method of calculation refer to NOS Tide Tables for year 2000). The calculated tidal elevations were compared with the UFG 1 data and the final multiplication correction factor was obtained as 1.023. For the model simulation period in year 2002 the same correction factor was used to transfer tidal elevations of Miami harbor to the flow boundary.

Model calibration began with an initial run for 48 hours (referred to as 'cold start') in order to make the tide and discharge mutually compatible throughout. In addition, the flow attains stability in this period. The results of the cold start period were compared with the current velocities as well as the water surface elevations obtained from the instrument tower. The process was continued by changing the variable component of the bottom friction coefficient (one component of z_0) (applicable uniformly throughout the model domain), until an approximate match of the current magnitude and phase was obtained. In the second step *RESTART.OUT* and *RSWT.OUT*, the two output files of the cold start were used as input, and model run was performed for a longer period (15days)

in order to obtain simulation for final calibration. The predicted and measured currents were then compared and is given in Figure 4.7a (Cold start) and 4.7b (Hot start) for a variable bottom friction factor of 0.027. It can be seen that the agreement is very good for the current, with a maximum error of 1.8% of the total current amplitude. The water surface elevation however differs by about 2.8 cm, which is about 3% of the tidal amplitude. Since current is in better agreement with the measured data the calibration was considered accurate enough for simulation. In addition, comparison of the predicted and measured current direction exhibited good agreement as indicated in 4.8.

4.5.2 Model Validation

Model validation was carried out using the same calibrated parameters and simulating the flow conditions of year 2000 (between September 14th and October 18th). The measured as well as the model results at both the tidal gage stations after cold start as well as hot start periods are compared and reproduced as Figures 4.9 and 4.10. As indicated in the figure 4.10, the agreement is fairly accurate with a maximum variation of 2.7 cm, which is about 3.4% of the maximum tidal amplitude reported in the estuary. Similar validation was also carried out using the Northwest Fork data collected between September 3rd and September 12th which also showed equally good agreement as shown in Figure 4.11.

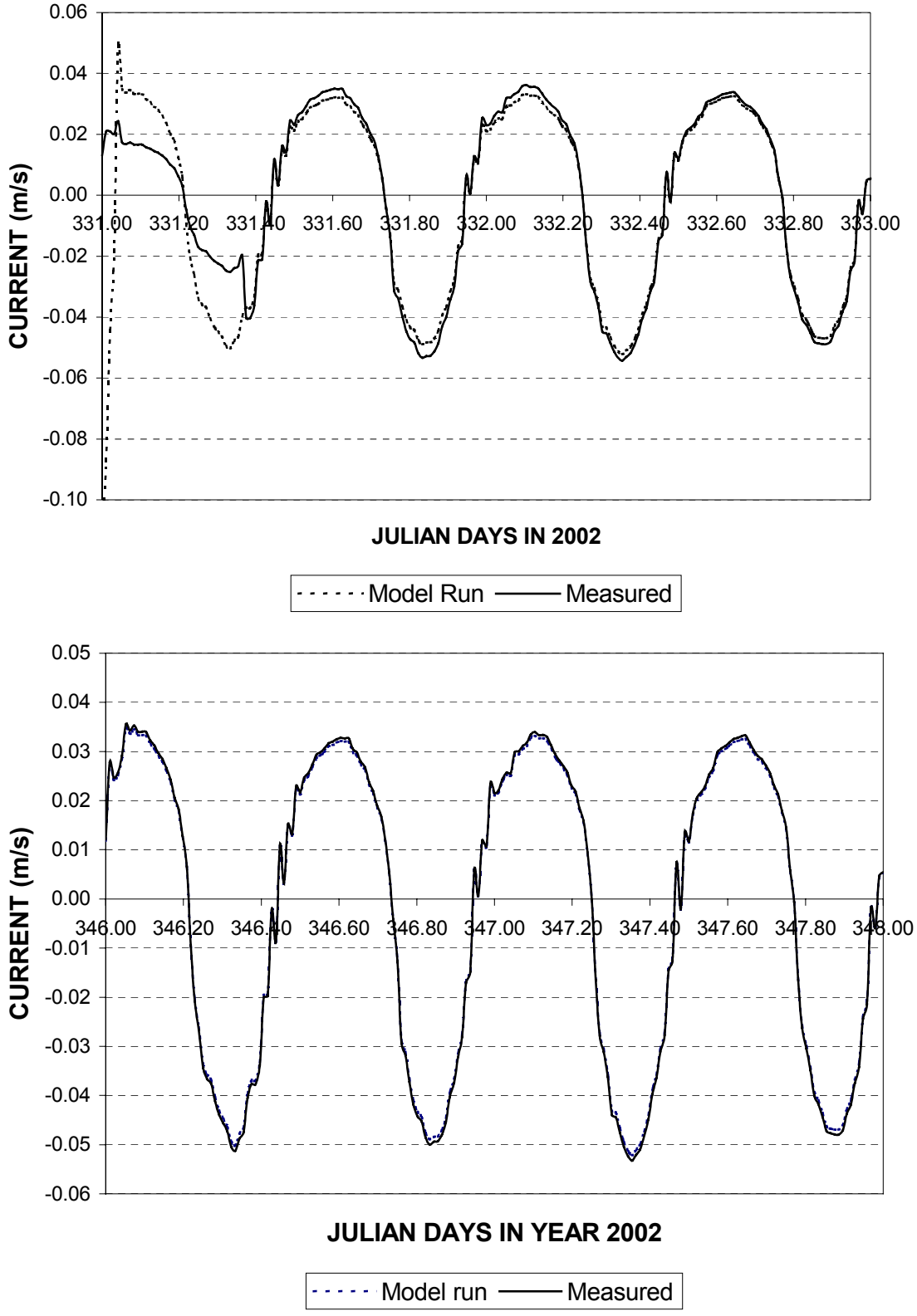

Figure 4.7 Model calibration measured vs. predicted current, a) Cold Start, b) Hot Start.

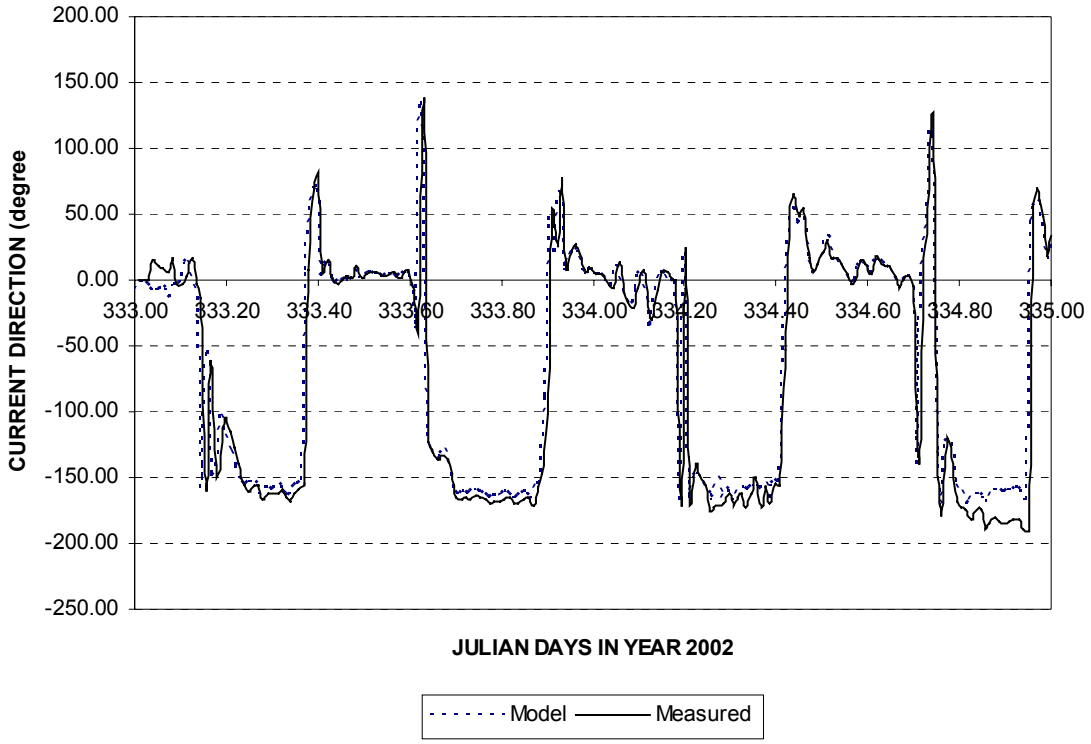

Figure 4.8 Model calibration measured vs. predicted current direction.

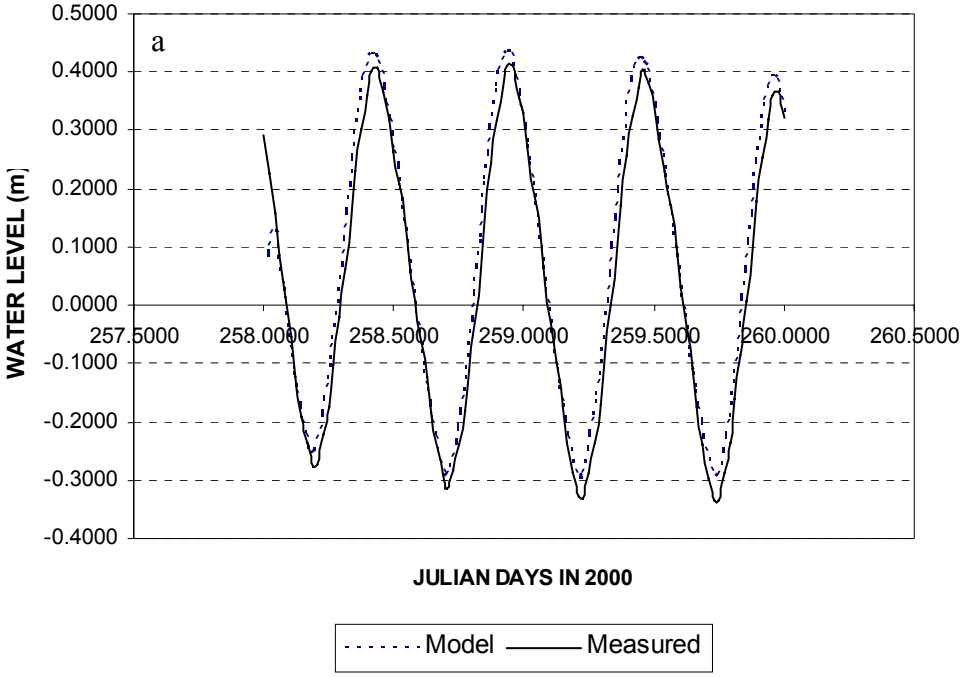

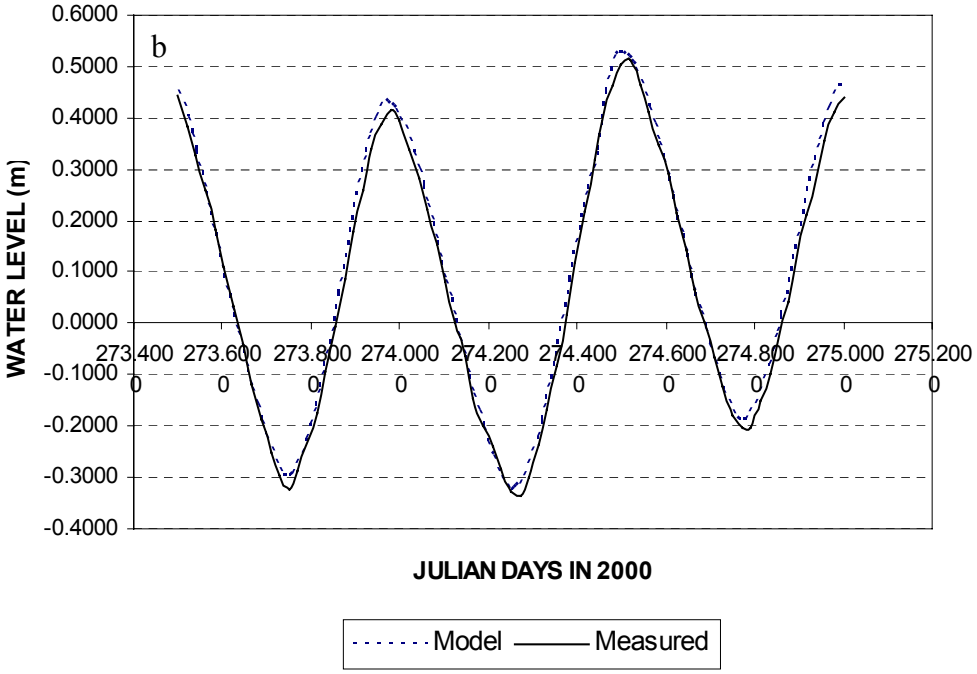

Figure 4.9 Model calibration measured vs. predicted water surface elevation (UFG2) Year 2000, a) Cold Start, b) Hot start.

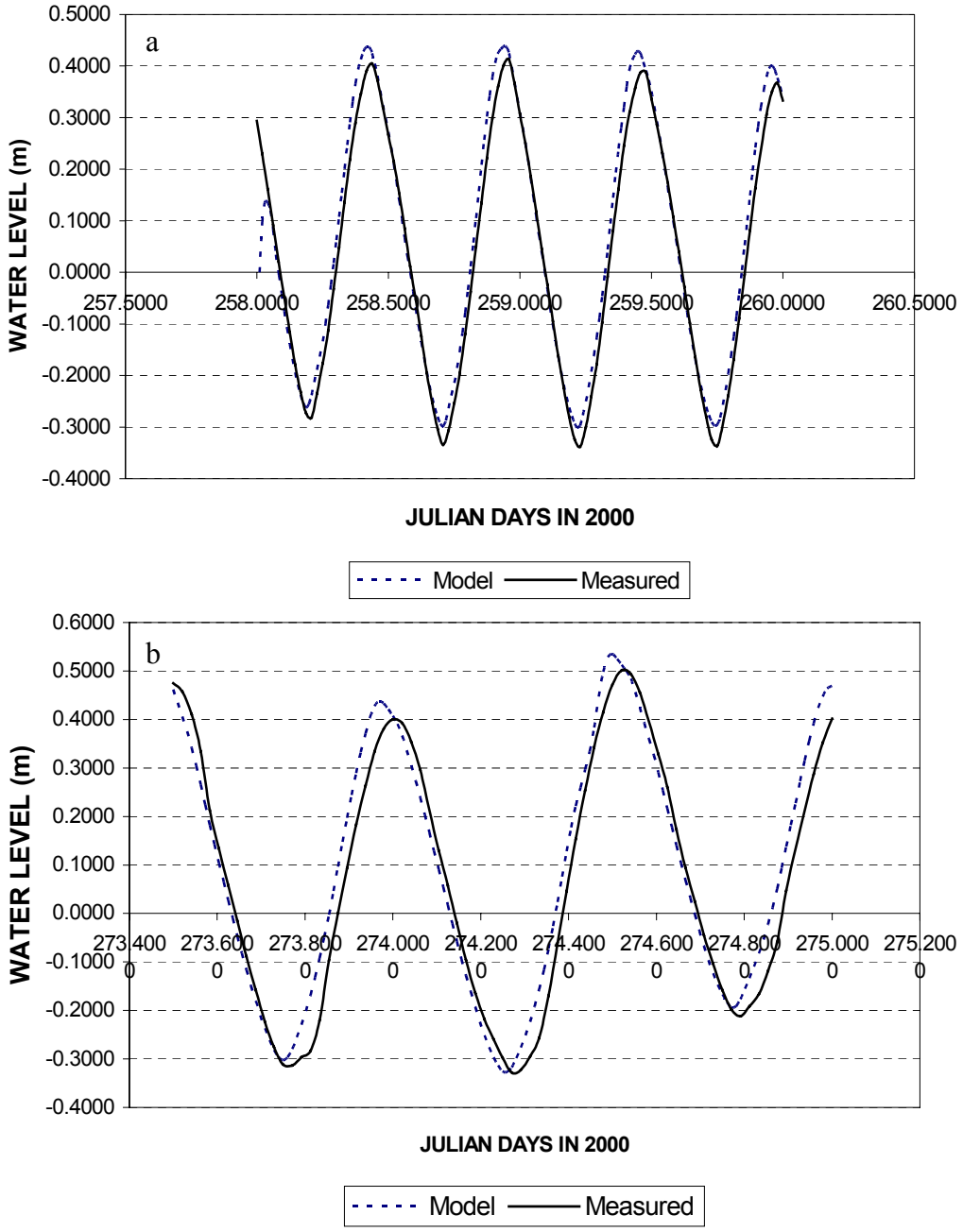

Figure 4.10 Model calibration measured vs. predicted water surface elevation (UFG3) Year 2000, a) Cold Start. b) Hot start.

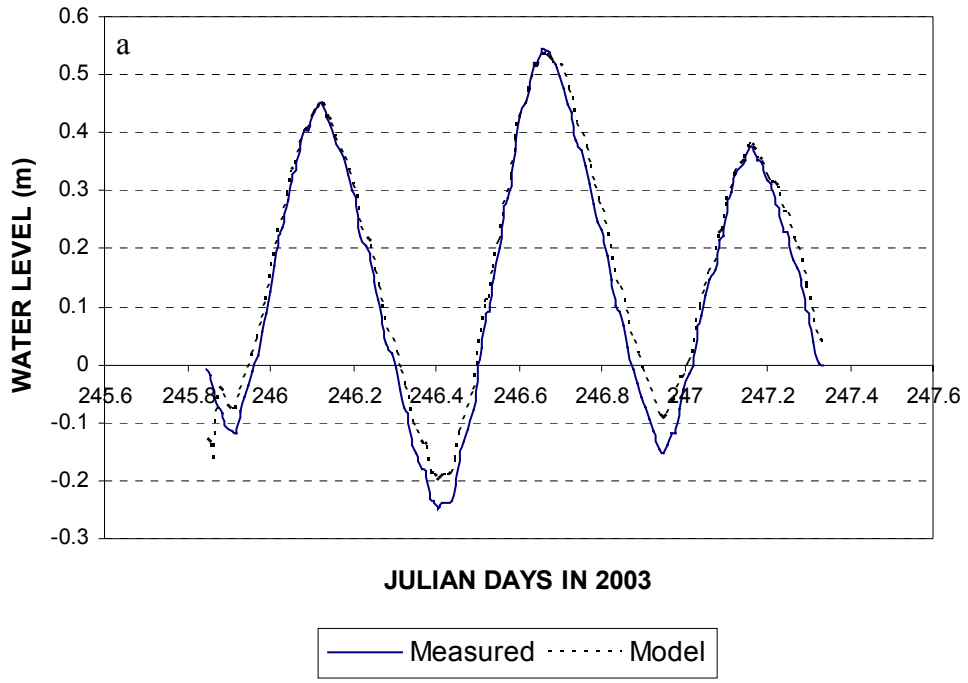

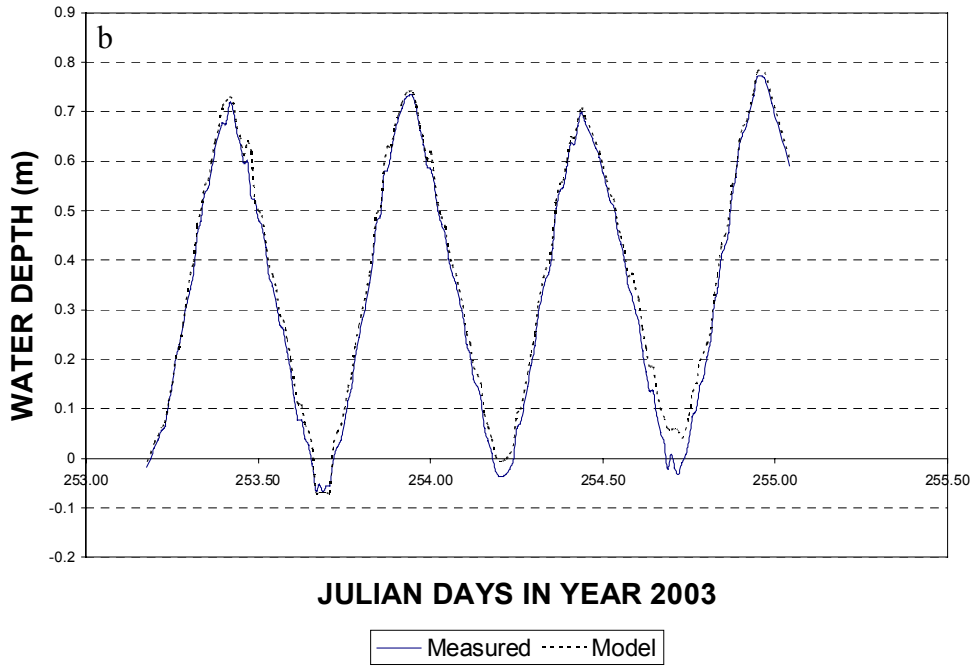

Figure 4.11 Model calibration measured vs. predicted water surface elevation (Northwest Fork) Year 2003, a) Cold Start, b) Hot start.

4.5.3 Simulation of trap scheme of Ganju, 2001

As noted, Ganju et al., (2001) carried out the model simulations by installing a trap in the C-18 canal. The trap was located 480m down stream of the S-46 structure and was 180 m long, 60 m wide and dredged 3 m from the existing bed level. The same scenario was simulated in the present model in order to revalidate data and have a check on the model results. The simulations indicated a 60% reduction in the current magnitude against 67% reported by Ganju, 2001. The results of the simulation (current) are given as Figure 4.12. With this final validation, it was considered that the model is calibrated for the estuary and therefore ready for the actual simulations.

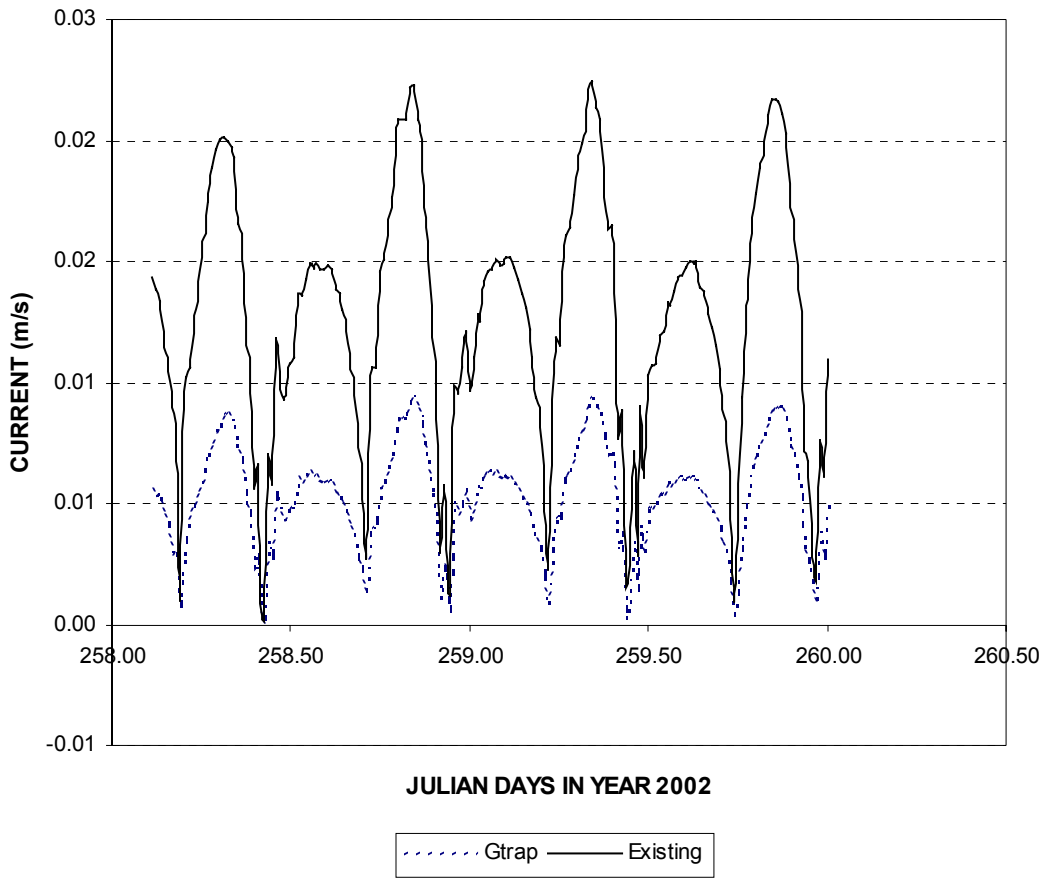

Figure 4.12 Validation results using trap used by Ganju, 2001.

CHAPTER 5
EVALUATION OF SEDIMENTATION CONTROL ALTERNATIVES

5.1 Design Basis

5.1.1 General Principle

Two concepts for management of sediment are adopted with respect to the central embayment, as shown schematically in Figure 5.1**.** These include sediment entrapment (Figure 5.1a,c) and sediment self-cleaning by channelization (Figure 5.1b,d).

5.1.1.1 Sediment Entrapment

For sediment entrapment an area of the submerged bottom is deepened to a depth greater than the surrounding bottom (Figure 5.1a,c). This works on the simple concept of decreasing the velocity by increasing the flow area. The carrying capacity of the flow being proportional to its velocity, a reduction in the velocity would reduce the carrying capacity and thereby result in sedimentation. This in turn would allow maintenance dredging to be performed at a specific location (the trap), rather than over a broad submerged area. There is an existing sand trap of this nature at Jupiter Inlet, as shown in Figure 2.9.

Trap efficiency is defined as the percent by which the effluent suspended solid load is reduced with respect to the influent load. In a tidal situation, the seaward edge of the trap will be the influent side during flood flow and the effluent side during ebb, and vice versa for the landward edge.

5.1.1.2 Self-cleaning Channel

The concept of a channel designed in such a way that the flow through it is in non-silting non-scouring (or self-cleaning) equilibrium can be employed where it is desired that the sediment flows through without net deposition (Figure 5.1b,d). In an ideal setup the trap efficiency of such a channel would be zero.

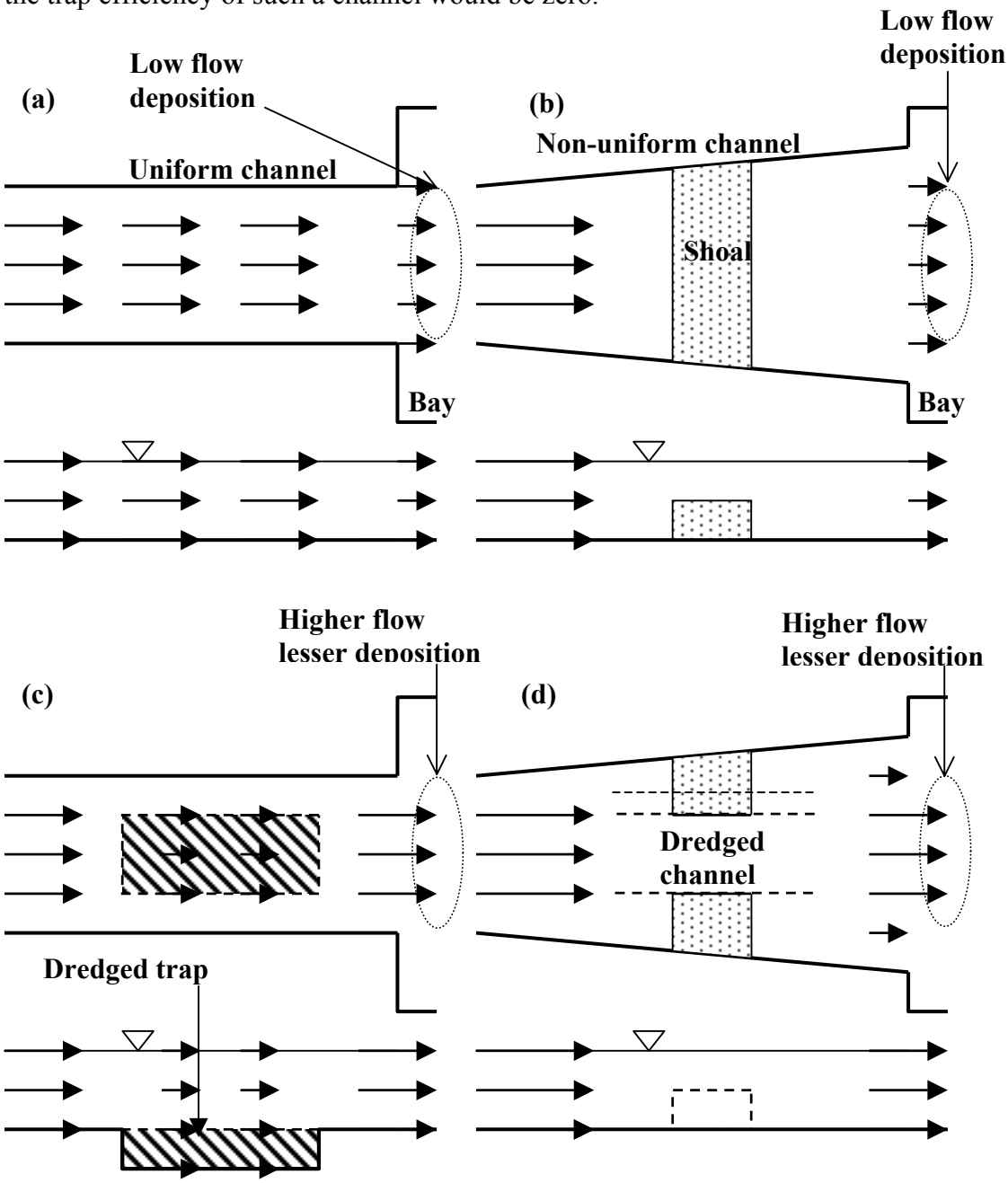

Figure 5.1 Design concepts for sediment management.

Trap and the channel are incorporated in the model by changing the bottom profile file (*dxdy.inp*). Accordingly, the depths and elevations of the grid cells in the designated area are changed per design.

5.1.2 Design Alternatives

Alternative schemes indicated in Table 5.1 were formulated and studied for their efficiency and function. Note that Alternatives 6 and 7 were introduced to determine if there was an interactive effect of multiple alternatives implemented simultaneously. However, simulations showed that this was not the case, i.e., there was no measurable impact of an alternative on others. As a result, only the first five were investigated further. General locations of Alternatives 2 through 5 are shown in Figure 5.2. Detailed drawings are shown later in the chapter. The basis of selection and design for each alternative (considering the existing "no-action" condition as Alternative no. 1) is described next.

Table 5.1 Alternative schemes for evaluation

Alternative no.	C-18 Canal Trap	Bay Channel	Bay Y-channel Channel	Northwest Fork Channel
1	Existing ("no-action") condition			
2	X			
3		X		
4			X	
5				X
6	X	X		X
7	X		X	X

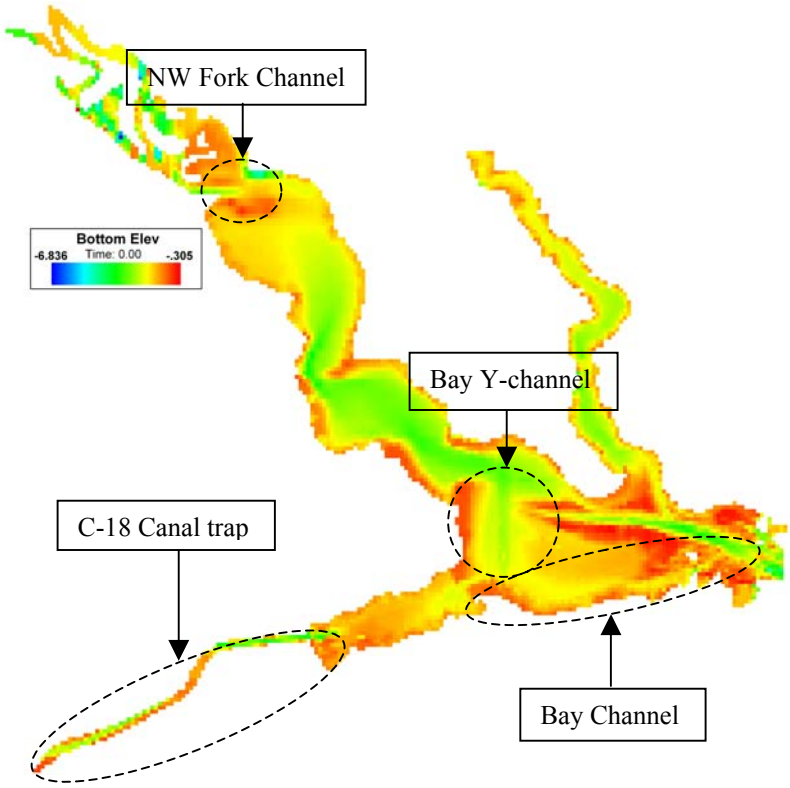

Figure 5.2 Alternatives considered, with existing bathymetry.

5.1.2.1 Alternative No. 2: C-18 Canal Trap

The design sediment trap includes the entire stretch of the C-18 canal downstream of the S-46 structure, in order to take care of the drawback of a much shorter trap of Ganju (2001), which was shown to trap only 60% of the sediment under all conditions of S-46 discharge. In addition, the sensitivity to sediment concentration, flow velocity and location were also found to be pronounced in that analysis. Accordingly, it was decided to dredge the entire length of the canal to -3.5 m (with respect to NAVD 88). The trap was considered to have a width equal to that of the canal. The dredged section is shown in Figure 5.3.

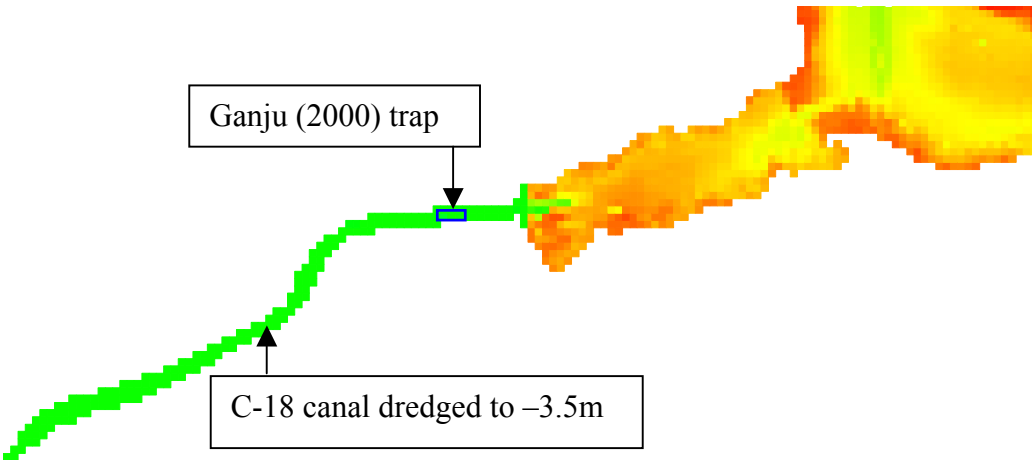

Figure 5.3 Dredged bathymetry of the C-18 canal with plan form view of the proposed trap. Trap considered by Ganju (2001) is also shown.

5.1.2.2 Alternative No. 3: Bay Channel

A self-cleaning channel close to the south bank of the bay (Figure 5.4) was adopted in order to improve the flow in that portion of the bay, which is weaker than in the existing channel. It was considered that such a channel along the ebb flow path would concentrate the flow and thereby flush out incoming fine sediment arriving from the Southwest Fork. In addition, this channel would improve small-craft navigation, provided it was designed appropriately.

The design depth in the channel was based on the California Department of Boating and Safety (1980), which stipulates a minimum depth of 0.9 m below the deepest draft of the vessel or 1.5 m, which ever is greater. Considering 1.5 m as the minimum depth for navigation plus 0.63 m for sedimentation and allowance for over-depth dredging, the final dredged depth of the channel works out to 2.13 m.

The California Department of Boating Safety stipulates a minimum width of 23 m at the design depth. The existing navigation channel (Figure 5.5) is maintained at 33 m at the design depth of 2.2 m. However, with a side slope of 1 : 3 m, the top width

works out to 23 m + 13.2 m = 36.2 m. Considering that cell dimensions are fixed at 25 m x 25 m, a self-cleaning channel width of 50 m was adopted in the model.

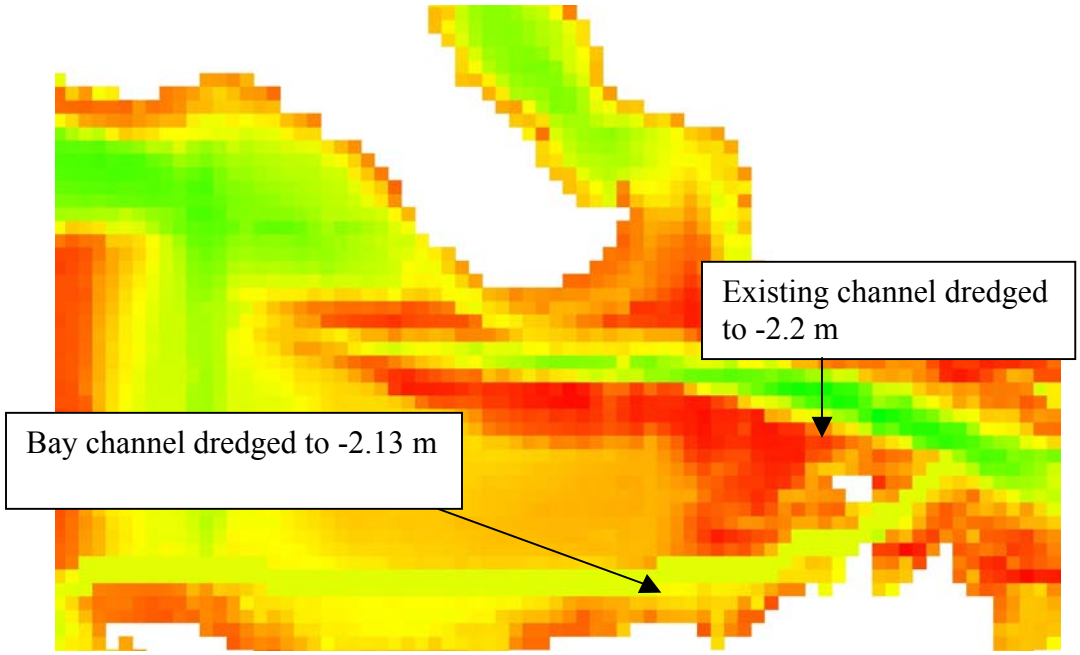

Figure 5.4 Planform view of the proposed self-cleaning channel in the bay.

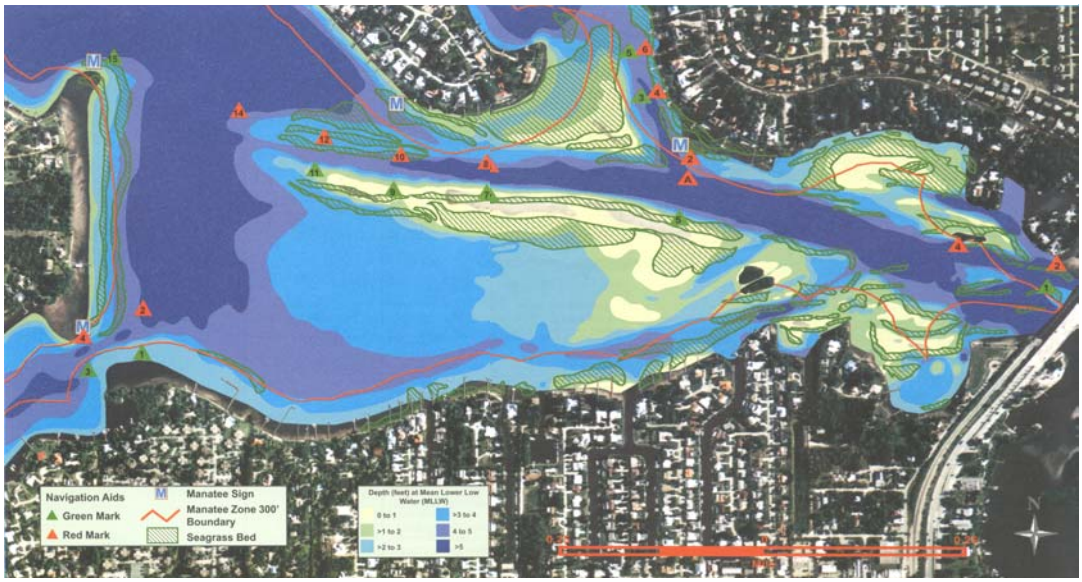

Figure 5.5 Location of the sea grasses indicated in model with increased roughness.

The channel was designed with three bends. Per design stipulations (Bruun, 1989), the bend angle should not be more than 30° and radius of curvature not less than 1,500 m. Also, at bends widening is generally carried out. For the model the width at the bends were widened by 25 m (one extra cell). As seen from Figure 5.4 and 5.5 the channel is largely outside the zones where sea grass beds occur.

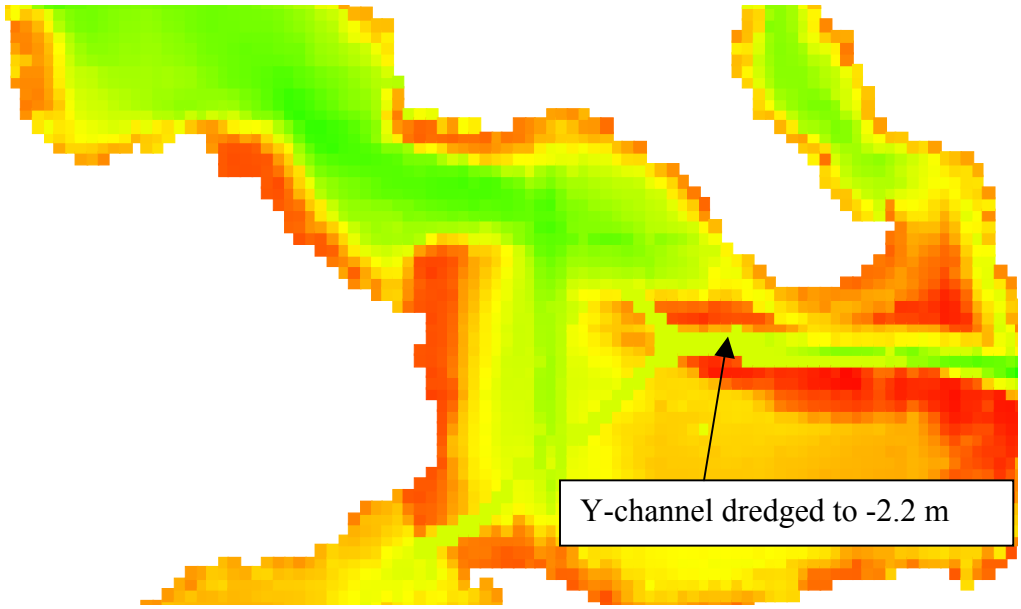

Figure 5.6 Planform view of the proposed self-cleaning Y-channel in bay.

5.1.2.3 Alternative No. 4: Bay Y-channel

The proposed Bay Y-channel originates from the existing navigation channel, and bifurcates into the Southwest and Northwest Forks (Figure 5.6). The width of the channel must be equal to that of the exiting channel, i.e., 30.5 m at the design depth of 2.2 m. The same depth is adopted for the extension. With a side slope of 1:3 and a depth of 2.2 m, the width at the top works out to 30.5 + 2x3x2.2 = 43.2 m. Hence in the model a two-cell wide (50 m) channel was simulated. At the bifurcation a total channel width of 100 m (four cell widths) was chosen for navigation purposes.

5.1.2.4 Alternative No. 5: Northwest Fork Channel

This alternative is located in fairly shallow depths and is devised to channelize the flow into a deeper channel so that mud would be prevented from depositing under increased velocity. Accordingly, the channel would be self-cleaning and thereby reduce the cost of maintenance. The location of the channel, shown in Figure 5.7, goes around a shoal. The width of the channel is maintained at 50 m with a (navigable) depth of 2.13 m and side slopes of 1:3. The widths at the bends are increased by one cell width for navigational purpose.

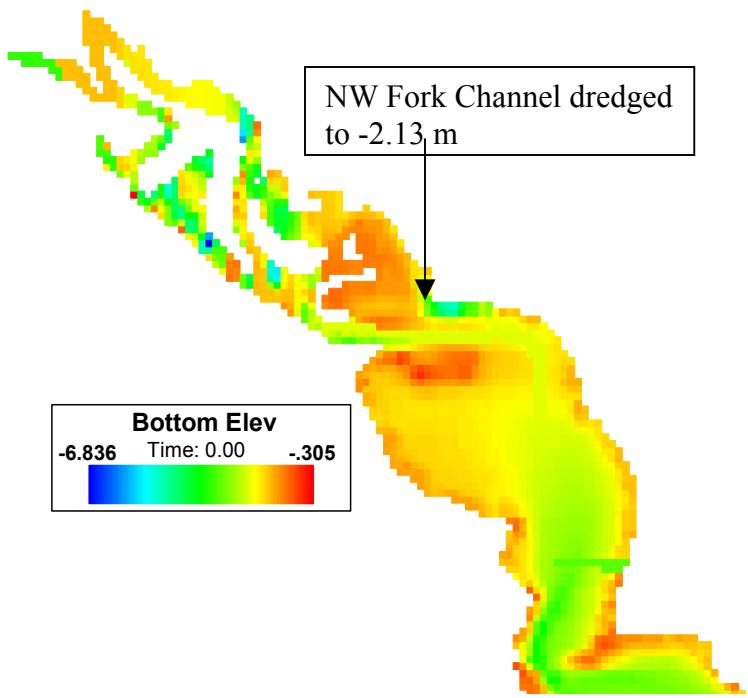

Figure 5.7 Planform view of the proposed self-cleaning channel in the Northwest Fork.

5.1.3 Efficiency Analysis

5.1.3.1 Velocity Vector Calculation

The direction θ of the resultant flow velocity vector is calculated from

$$\theta = \tan^{-1}\left(\frac{u}{v}\right)\frac{180}{\pi} \tag{5.1}$$

where u and v are the two measured velocity components. The corresponding magnitude, $\bar{u}$, is obtained from

$$\bar{u} = \sqrt{u^2 + v^2}\,\frac{u}{|u|} \tag{5.2}$$

5.1.3.2 Sediment Deposition Calculation

The rate of mass deposition rate under flow is given by

$$D = \left(1 - \frac{\tau_b}{\tau_c}\right) W_s CLW; \quad \tau_b < \tau_c \tag{5.3}$$

where τ_b is the bed shear stress, τ_c is the critical shear stress for erosion, W_s is the settling velocity, C is the suspended sediment concentration, and L and W are the length and width of the trap or channel, respectively and deposition D is given in kg/sec. The bed shear stress in the model is calculated from

$$(\tau_{bx}, \tau_{by}) = c_b \sqrt{u_1^{\,2} + v_1^{\,2}}\,|u_1, v_1| \tag{5.4}$$

where

$$c_b = \left(\frac{\kappa}{\ln(\Delta_1 / 2z_o)}\right)^2 \tag{5.5}$$

and where $\Delta_1 = 0.25$, $z_0 = 0.047\,\text{m}$ and the Karman constant $\kappa = 0.4$. Substituting these values in Equation (5.5) gives $c_b = 0.167$.

The critical bed shear stress of erosion is determined based on the type of sediment, i.e., sand or fine-grained. These values are determined next.

Fine sediment: For the fine sediment, a τ_c value of 0.1 Pa is selected for calculation of the critical velocity for erosion, u_c (Mehta and Parchure, 2000). From Equation (5.4) τ_c is given as

$$\tau_c = c_b u_c^{\ 2} \tag{5.6}$$

Therefore, with $c_b = 0.167$, $u_c = 0.247$ m/s is obtained.

Sand: For sand, u_c can be calculated from the Shields' relationship, under fully rough turbulent flow, which is given by (Buckingham and Mehta, 1985)

$$u_c = 0.0133[(\gamma_s - \gamma)d_{50}]^{0.5} \tag{5.7}$$

where γ_s is the unit weight of sand (= 2,650 kg/m^3), γ is the unit weight of estuary water (= 1,020 kg/m^3) and d_{50} is the median grain diameter, which ranges between 0.1 and 0.4 mm (Jaeger et al., 2001). For calculations three median diameters were considered, namely, 0.1, 0.2 and 0.3 mm. The corresponding critical velocities from Equation (5.7) are given in Table 5.2. In connection with these values, we note that the shear stress being proportional to the square of flow velocity under turbulent flows, Equation (5.3) may be expressed as

$$D = \left(1 - \frac{u^2}{u_c^{\ 2}}\right) W_s CLW \tag{5.8}$$

where u is the current velocity.

Table 5.2 Critical velocities for sand

Median Diameter, d_{50} (mm)	Critical Velocity, u_c (m/s)
0.1	0.17
0.2	0.24
0.3	0.29

Deposit thickness: The calculation for sand deposition is carried out using Equation (5.8). For that purpose, the mass of sand m was converted into the corresponding volume using relation

$$V = \frac{m}{\rho_s(1-n)} \tag{5.9}$$

where, V is the sand volume, ρ_s is the sand granular density, and n is the porosity. For the present calculations, ρ_s=2,650 kg/m^3, and n=0.4. Conversion of volume of sand deposited into sedimentation thickness D_r can be accomplished from

$$D_r = \frac{V}{A} = \frac{m}{\rho_s (1-n) A} \tag{5.10}$$

where A is the area of deposit.

With regard to fine sediment the same calculations were performed and the total sedimentation rate was calculated. The deposit volume was calculated from

$$V = \frac{m}{\rho_d} \tag{5.11}$$

where ρ_d is the sediment dry density, which was calculated with 15% organic content (OC) from the relation

$$\rho_d = 1900 \exp(-0.156 OC) + 80 \tag{5.12}$$

with 15% OC (Ganju, 2000) the density works out to 263 kg/m^3.

5.1.3.3 Trap Efficiency

Trap efficiency is defined in terms of the sediment removal ratio r given by

$$r = \frac{(q_s)_i - (q_s)_e}{(q_s)_i} \tag{5.13}$$

where $(q_s)_i$ is the influent sediment load, and $(q_s)_e$ is the effluent load. Efficiencies for different trap scenarios were examined by Ganju et al. (2001). Accordingly, sediment flux calibration was carried out using those results, so that the r values could be determined on a consistent basis. Separate calculations were carried out for sand and for fine sediment.

5.1.3.4 Channel Efficiency

The method of calculation of the efficiency of the self-cleaning channel is similar to the one given above. In the present analysis an ideal self-cleaning channel is defined as one in which the removal ration r = 1 (or 100%). Erosion of channel, as might occur under very high flows, was not explored separately because the environment in question is largely a depositional one.

5.2 Design Simulations

5.2.1 Design Flows

Model simulations were carried out under three tributary flow scenarios – flows used for model calibration, median (50 percentile) flows and peak (98 percentile) flows, following Ganju (2000). The discharges are listed in Table 5.3.

Table 5.3 Design flows in tributaries

Tributary	Southwest Fork	Northwest Fork	North Fork
Calibration discharge (m^3/s)	14.5	32	0.3
Median discharge (m^3/s)	1.3	0.7	0.1
Peak discharge (m^3/s)	32	61	1.9

5.2.2 Alternative 1

Water surface elevation time series at the three tidal stations (UFG1, UFG2, and UFG3) were available for a period of 34 days (09/14/2000 to 10/18/2000). As noted, data from UFG1 were used at the eastern boundary, and data from other two stations were used for verification of model accuracy. Accordingly, model runs were restricted to these 34 days. Simulation with the existing bathymetry, i.e., Alternative 1, was intended to observe the present flow regime and compare the same with results from changed bathymetry under other alternatives. This would enable the calculation of the change in

velocity and bottom shear stress due to depth change at a trap or a channel (see, for example, Figure 5.8).

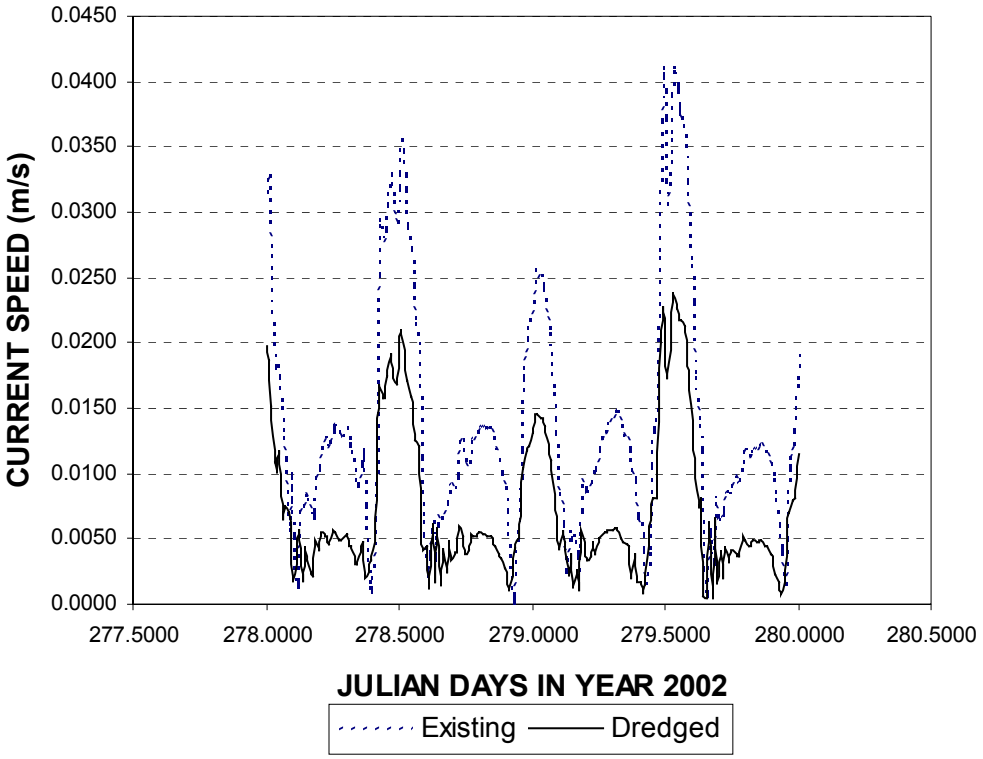

Figure 5.8 Current comparisons for a model cell at the upstream end of the Northwest Fork channel: calibration discharges.

5.2.3 Alternatives 2, 3, 4 and 5

Under calibration discharges in the tributaries, the maximum peak flood and ebb velocities are compared in Table 5.4 for the four alternatives. For each alternative, the three values (upstream, mid-point and downstream) have been averaged and given for all three tributary discharge scenarios (calibration, median and peak) in Table 5.5. Figure 5.9 shows the current velocity vectors for the maximum flood flow condition at spring tide over the model domain. Figure 5.10 shows the corresponding ebb flow vectors.

Table 5.4 Maximum currents at alternatives: calibration discharges

Alternative	Condition	Upstream		Mid-point		Downstream	
		Ebb (m/s)	Flood (m/s)	Ebb (m/s)	Flood (m/s)	Ebb (m/s)	Flood (m/s)
C-18 canal	Non-dredged	0.03	0.025	0.05	0.028	0.05	0.03
	Dredged	0.01	0.008	0.035	0.021	0.04	0.03
Bay channel	Non-dredged	0.30	0.23	0.26	0.12	0.12	0.08
	Dredged	0.21	0.17	0.14	0.12	0.10	0.07
Y-channel	Non-dredged	0.30	0.26	0.23	0.20	0.08	0.08
	Dredged	0.21	0.16	0.10	0.09	0.04	0.04
NWF channel	Non-dredged	0.06	0.04	0.04	0.04	0.05	0.04
	Dredged	0.03	0.027	0.02	0.02	0.025	0.02

Table 5.5 Maximum currents at alternatives: Different discharges

Alternative	Condition	Calibration discharge		Median Discharge		Peak discharge	
		Flood (m/s)	Ebb (m/s)	Flood (m/s)	Ebb (m/s)	Flood (m/s)	Ebb (m/s)
C-18 trap	Non-dredged	0.07	0.05	0.03	0.01	0.16	0.11
	Dredged	0.06	0.04	0.04	0.03	0.11	0.10
Bay channel	Non-dredged	0.30	0.23	0.21	0.18	0.29	0.26
	Dredged	0.21	0.17	0.18	0.14	0.35	0.30
Y-channel	Non-dredged	0.30	0.28	0.22	0.20	0.21	0.20
	Dredged	0.21	0.20	0.17	0.16	0.32	0.30
NWF channel	Non-dredged	0.06	0.04	0.04	0.03	0.10	0.06
	Dredged	0.03	0.027	0.02	0.02	0.09	0.06

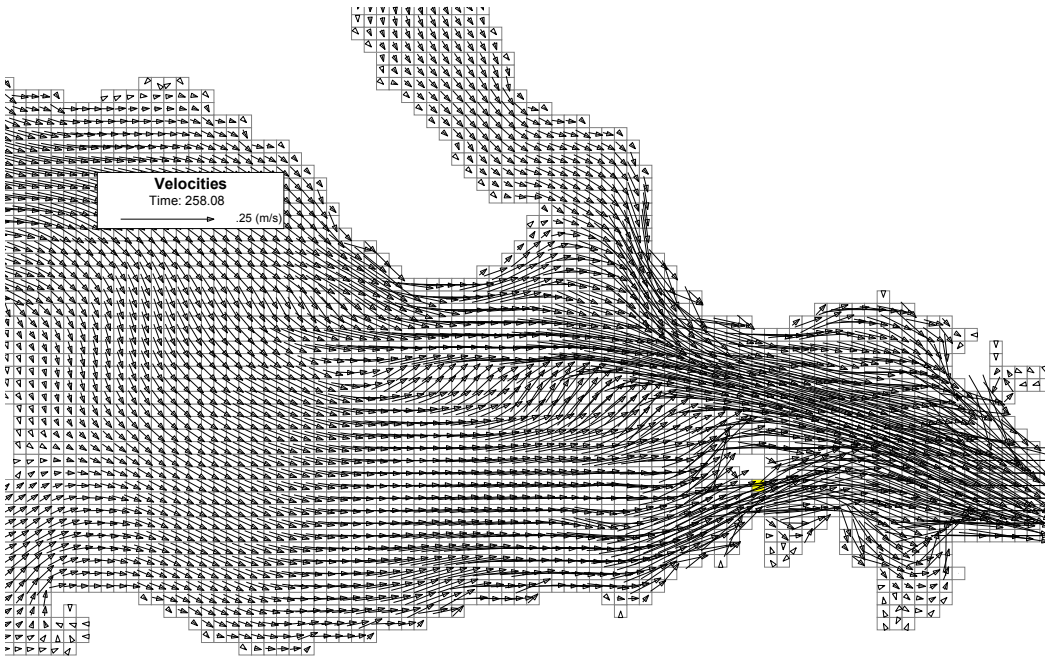

Figure 5.9 Current velocity vectors over the modeled domain; maximum flood velocities at spring tides.

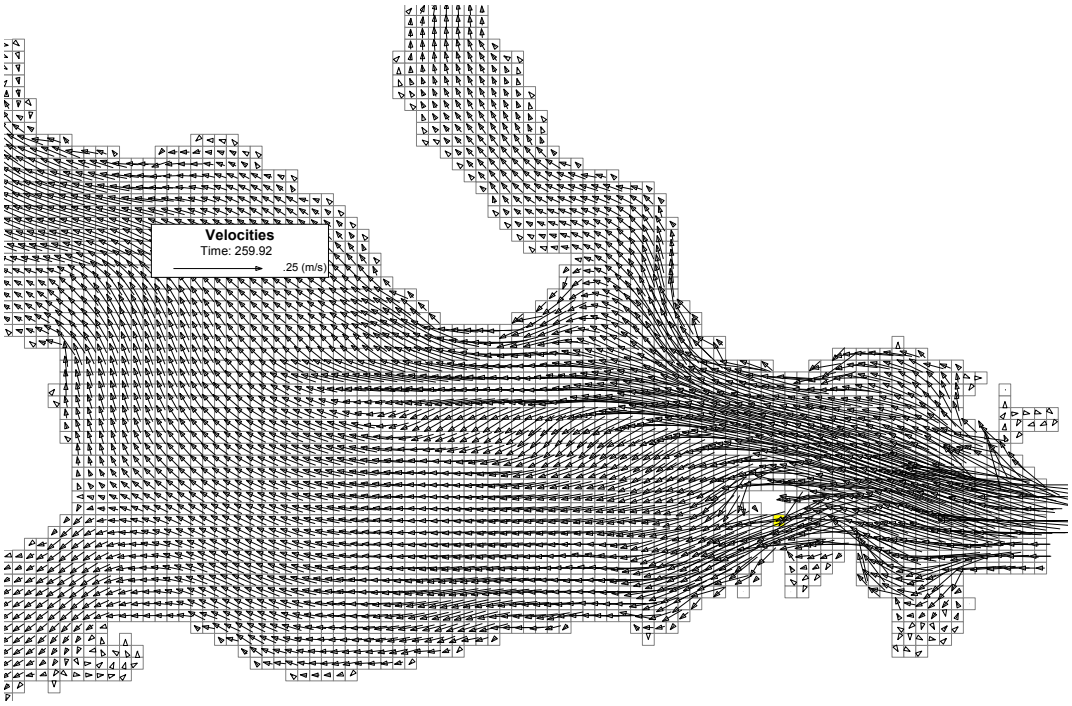

Figure 5.10 Current velocity vectors over the modeled domain; maximum ebb velocities at spring tide.

5.3 Deposition Equation Calibration

In order to apply Equation (5.3), it must be calibrated against existing deposition rates within the modeled domain. This is described next.

5.3.1 Calibration for Sand

Taking the bay channel as an example, we note that Ganju et al. (2001) reported entry of 9.2 Mkg (5,786 m^3) of sand into the central embayment from the inlet. Accordingly, the report calculates a uniform deposition of 3.25 mm/year. Since the bay area is 1,780,308 m^2, using Equation (5.3) and a uniform (non-dredged condition; calibration discharge) current of 0.12 m/s (average of all cells), the sand settling flux can be worked out as follows:

3. Rate of sedimentation per unit bed area = 9.2 Mkg/ 1,780,310 m^2 = 5.16 kg.
4. For 0.1 mm diameter sand, critical velocity = 0.17 m/s (Eq.5.7).
5. Using Equation (5.8), sand settling flux = 2.81×10^{-7} kg/m^2 s.

Table 5.6 provides all results based on such calculations.

5.3.2 Fine Sediment

Table 5.6 Calibration for sediment fluxes

Alternative	Total supply (Mkg)	Area of deposit (m^2)	Unit deposition (kg/m^2)	Deposition flux (kg/m^2 s)
C-18 canal	Sand = 0.0 Fines = 1.27	577,560 577,560	0.00 2.20	0.0 8.72×10^{-8}
Bay channel	Sand = 9.20 Fines = 0.46	1,780,310 1,780,310	5.16 0.26	2.81×10^{-7} 9.36×10^{-9}
Bay Y-channel	Sand = 9.20 Fines = 0.46	1,780,310 1,780,310	5.16 0.26	2.81×10^{-7} 9.36×10^{-9}
Northwest Fork	2.00	1,949,890	0.87	3.42×10^{-8}

Similar calculation for fine sediment was carried out. As an example, for the bay channel, the total inflow of fine sediments is 0.46 Mkg. So the total volume works out to

1,749 m^3. Accordingly, the sediment flux works out to 9.36 x 10^{-9} kg/m^2 s. Table 5.6 provides all results.

5.4 Sand Deposition due to Alternatives

5.4.1 Bay Channel

Table 5.7 gives the sand deposition flux in the bay channel averaged over the entire length for the three discharge scenarios – calibration, median and peak. In these calculations the channel length is taken as 1,430 m, and width 50 m. The respective mean sediment concentration values are 0.04, 0.02 and 0.10 kg/m^3.

Table 5.7 Rate of sand deposition in bay channel

Median diameter (mm)	Deposition flux (kg/m^2 s)		
	Calibration discharge	Median discharge	Peak discharge
0.1	8.80×10^{-6}	9.67×10^{-6}	5.64×10^{-6}
0.2	1.32×10^{-5}	2.76×10^{-5}	1.14×10^{-5}
0.3	3.52×10^{-5}	4.06×10^{-5}	2.74×10^{-5}

5.4.2 C-18 Canal

Table 5.8 Rate of sand deposition in C-18 cana

Median diameter (mm)	Deposition flux (kg/m^2 s)		
	Calibration discharge	Median discharge	Peak discharge
0.1	1.38×10^{-5}	2.62×10^{-5}	0.89×10^{-5}
0.2	2.07×10^{-5}	3.68×10^{-5}	1.24×10^{-5}
0.3	3.64×10^{-5}	5.06×10^{-5}	2.26×10^{-5}

In this case, for the calibration discharge case the mean sediment concentration in the C-18 canal was taken as 0.048 kg/m^3, as recorded at the Southwest Fork tower. For the median and peak discharges the respective values are 0.020 and 0.10 kg/m^3. The percent of fines is taken as 15. The 1,890 m long canal is considered having a uniform width of 50 m. Results are given in Table 5.8.

5.4.3 Bay Y-channel

Deposition fluxes for the 850 m (stem plus one arm) long and 50 m wide channel are given in Table 5.9.

Table 5.9 Rate of sand deposition in Y-channel

Median diameter (mm)	Deposition flux (kg/m^2 s)		
	Calibration discharge	Median discharge	Peak discharge
0.1	4.41×10^{-6}	5.76×10^{-6}	3.08×10^{-6}
0.2	8.80×10^{-6}	3.16×10^{-6}	6.24×10^{-6}
0.3	1.38×10^{-5}	3.06×10^{-5}	0.74×10^{-5}

5.5 Fine Sediment Deposition due to Alternatives

Table 5.10 gives the fine sediment budget based on the concentration reported in the data collection in Southwest and Northwest Forks. The results compare well with those of the values predicted in Ganju et al. (2001).

Table 5.10 Rate of fine sediment deposition in alternatives

Alternative	Deposition flux		
	Calibration discharge	Median discharge	Peak discharge
C-18 canal	2.25×10^{-5}	2.75×10^{-5}	1.45×10^{-5}
Bay channel	2.26×10^{-6}	2.87×10^{-6}	1.38×10^{-6}
Bay Y-channel	2.26×10^{-6}	2.87×10^{-6}	1.38×10^{-6}
NW Fork channel	4.06×10^{-6}	5.16×10^{-6}	2.76×10^{-6}

5.6 Sediment Removal

5.6.1 Calculation of Deposition

Deposition in the trap and the channels was calculated using the above results. The removal ratio from Equation (5.13) was calculated by adopting the sediment load in the tributaries reported by Ganju et al. (2001). Tables 5.11 and 5.12 give the annual sand budget and the Tables 5.13 and 5.14 the fine sediment budget in the channel for calibration and peak discharge cases (leaving out median discharges for illustration.

Table 5.11 Annual sand budget: Calibration discharge

Alternative	Rate of deposition (mm/s)	Total deposition (mm)	Total deposition (kg)
Bay channel	8.81×10^{-6}	8.30	943,590
Bay Y-channel	4.40×10^{-6}	8.83	989,780

Table 5.12 Annual sand budget: Peak discharge

Alternative	Rate of deposition (mm/s)	Total deposition (mm)	Total deposition (kg)
Bay channel	5.64×10^{-6}	5.32	604,800
Bay Y-channel	3.08×10^{-6}	5.81	585,000

Table 5.13 Annual fine sediment budget: Calibration discharge

Alternative	Rate of deposition (mm/s)	Total deposition (mm)	Total deposition (kg)
C-18 canal	2.25×10^{-5}	17.5	286,400
Bay channel	2.26×10^{-6}	1.93	38,730
Bay Y-channel	2.26×10^{-6}	1.93	20,400
NW Fork channel	4.06×10^{-6}	7.50	62,220

Table 5.14 Annual fine sediment budget: Peak discharge

Alternative	Rate of deposition (mm/s)	Total deposition (mm)	Total deposition (kg)
C-18 canal	1.45×10^{-5}	11.30	184,570
Bay channel	1.38×10^{-6}	1.17	23,630
Bay Y channel	1.38×10^{-6}	1.17	12,440
NW Fork channel	2.76×10^{-6}	5.10	42,310

5.6.2 Calculation of Channel Efficiency

For an assessment of the efficiencies of the trap/channels, we will assume that the two channels in the bay accumulate sand only, whereas C-18 canal and the Northwest Fork accumulate fine sediment only. On that basis, Table 5.15 summarizes the annual load and shoaling (rounded to nearest mm) in the canal and channels. From these results that while the C-18 canal trap acts as such, the three channels are unlikely to be self-cleaning. On the other hand we note that the performance of the channels improves at peak discharges, which, in general, highlights the sediment-flushing role of high river discharges, as at all estuaries in their natural state.

Table 5.15 Annual sediment loading

Alternative	Calibration discharge		Peak discharge	
	Load (metric tons)	Shoaling (mm)	Load (metric tons)	Shoaling (mm)
C-18 canal	286	18	185	11
Bay channel	944	8	605	5
Bay Y-channel	990	9	585	6
NW Fork channel	62	8	42	5

5.6.3 Removal of Bay Sediment

The role of proposed alternatives as sediment traps, especially under typical prevailing flow conditions in the estuary lends itself to an assessment of these alternatives as a means to reduce sedimentation in the bay. This is noted next.

As mentioned, Ganju et al. (2001) reported entry of 9,200 (metric) tons of sand into the central embayment, corresponding to a uniform shoaling thickness of 3.3 mm/year (accurate to tenth of mm). Since the bay channel would remove 940 tons (at calibration discharge), the net shoaling would reduce to 2.9 mm/year.

Similar calculation for fine sediment removal by the C-18 canal trap plus the Northwest Fork channel can be shown to reduce the deposition of 0.78 mm/year of fine sediment in the bay to 0.57 mm/year.

5.7 Assessment of Alternatives

It is instructive to make a qualitative assessment of the proposed alternatives based on their roles in improving water quality (by trapping fine sediment) and navigation (by trapping sand). Based on assignment of numbers: +1 (good), 0 (no effect) and -1 (negative impact), Table 5.16 provide the assessment.

Table 5.16 Assessment of impacts of proposed alternatives

Alternative	Sedimentation control	Navigation	Overall	Comment
1 No-action	-1	-1	-2	-2, however does not mean that the present condition is severe
2 C-18 canal	+1	0	+1	If fine organic-rich sediment continues to accumulate in to the central bay, this option should be considered
3 Bay channel	+1	+1	+2	Should be considered for implementation; careful design will be required so that sea grass beds are not disturbed
4 Y-channel	-1	+1	0	Despite its effectiveness as a trap, shoaling may be rapid because it would cut existing and active shoal
5 NWF channel	+1	0	+1	If fine sediment accumulation continues, this option should be considered

CHAPTER 6
CONCLUSIONS

6.1 Summary

The objective of this study was to assess the implementation of schemes for sediment entrapment and self-cleaning channels in the micro-tidal (< 2 m range) estuarine environment containing both sand and fine sediment. The central embayment of the Loxahatchee River estuary on the east (Atlantic) coast of Florida was chosen as the candidate location due to its unique characteristics with respect to the influx of fine sediment and sand in the central embayment, and the concerns that have arisen in recent years due to the potential for long term impacts on the system due to this influx. The spring tidal range in the central embayment is 0.8 m, and three main tributaries feed the bay; Southwest Fork/C-18 canal, Northwest Fork and North Fork. Bay sediment is a mixture of sand, silt and clay along with organic detritus.

An ideal sediment trap captures all of incoming sediment, i.e., the removal efficiency is 100%. A self-cleaning channel allows no net deposition or erosion of incoming sediment, which passes through, so that its removal efficiency is 0%. In addition to the "no-action" present condition in the study area, four alternatives were examined: a sediment trap in the C-18, a self-cleaning channel in the central bay itself, a (self-cleaning) Y configured extension of the existing navigation channel in the bay and a self-cleaning channel in the Northwest Fork. All the self-cleaning channels were designed to meet the minimum depth and width required for the shallow draft vessels plying the area.

The basis for the introduction of the sediment trap was to capture sediment arriving from the S-46 sluice-gate structure at the head of the C-18 canal, prevent the material from settling in the Southwest Fork and the central embayment. The overall rationale for the introduction of the self-cleaning channels was to ease the passage of sediment, especially the fine-grained component from the tributaries, so as to prevent its deposition in the central embayment, and thereby enable it to exit to the Atlantic from Jupiter Inlet.

Hydrodynamic flow modeling was carried out using the Environmental and Fluid Dynamic Code (EFDC) to calculate water elevations, velocities, and bed bottom shear stresses in the estuarine domain. The model was calibrated using data on water levels, currents and suspended sediment concentration collected in years 2002/2003 at a site in the Southwest Fork. Validation was then carried out using data collected in 2000 in the central embayment and in the Northwest Fork in 2003.

Following model validation, model runs were carried out for the selected alternatives, and their efficiencies were calculated by relating the sediment settling flux with change in flow momentum and hence bed shear stress. The results of these simulations and conclusions are discussed in the following section.

6.2 Conclusions

1. Calculations indicate that the concepts of sediment entrapment and of self-cleaning can operate only partially in the study area due to the weak prevailing forcing by tide and the episodic nature of the freshwater discharges in the tributaries.

2. The simulations indicated that under conditions of typical discharges from the tributaries, with the introduction of Bay channel and Bay Y-channel, annually 1,930 (metric) tons of sand out of the total 9,200 tons entering the bay could be captured. The Bay channel would reduce the sand load by 940 tons, thus lowering the present bay-mean 3.3 mm/year shoaling thickness by 0.4 mm/year. The addition of the Y-channel would reduce shoaling by 0.9 mm/year. Also, these two channels could entrap about 68 tons of fine sediments, thus reducing the present 0.78 mm/year fine sediment shoaling thickness by 0.11 mm/year. Simulations

under peak discharges showed reduced entrapment by the two channels, because under high discharges their self-cleaning performance improved. For sand, the Bay channel reduced the shoaling thickness by 0.4 mm/year, and the two channels together by 0.8 mm/year. Similarly, the two channels would reduce fine sediment shoaling by 0.11 mm/year. Note however that such flows do not occur frequently in the study area.

3. On account of its length (same as that of the canal), the C-18 trap was found function better than the short (60 m long) trap of Ganju (2001), with annual entrapment increasing from 159 tons to 290 tons under typical discharge sequence from the S-46 structure, and reduced to 190 tons under peak discharge.

4. The Northwest fork channel did not function per expectation. Although the percent-wise flow velocity reduction was found to be the least (40%) in this channel of all the alternatives, as a result of velocity reduction self-cleaning was not achieved. The annual entrapment of fine sediment was about 62 tons. Under peak discharge this value would reduce to 42 tons.

5. From the simulations it can be concluded that while the C-18 canal trap acts as such, the three channels are unlikely to be self-cleaning. On the other hand, the performance of these channels improves at peak discharges, which highlights the sediment flushing role of the high river discharges, as at all estuaries in their natural state.

6. The implementation of C-18 trap, the Bay channel and the Northwest Fork channel could collectively reduce bay-mean sedimentation from as much as 3.3 mm/year to 2.9 mm/year from sand and from 0.78 mm/year to 0.47 mm/year for fine sediment.

7. A qualitative assessment of the proposed alternatives based on their roles in improving water quality (by trapping fine sediment) and navigation (by trapping sand) was carried out based on the assignment numbers, +1 for good, 0 for no effect and –1 for negative impact. This assessment leads to the following observations.

8. Although the present condition in the study area with respect to sedimentation does not appear to be severe (in comparison with numerous estuaries elsewhere), implementation of the one or more of the above alternatives may be considered at a future date, if necessary.

9. Fine sediment accumulation in the central bay due to ingress of sediment from upland discharge and erosion of existing and old deposits could be reduced with the installation of C-18 trap, as it accounts for more than half of the total fine sediment entering the bay. Periodic dredging of the canal would then remove the trapped sediment.

10. Bay channel (close to the southern bank of the central embayment) appears to be a good option. Since it would act as an efficient ebb flow channel, it could improve

bay flushing as well as navigation and serve to reduce bay-wide sedimentation. Under peak river discharges the channel appears to possess a degree of self-cleaning capability for fine sediment and, accordingly, it may require low maintenance dredging. However, careful design considerations with regard to its alignment will be required to stay clear of sea grass beds in the area.

11. The Y-channel, despite having good sand trapping capability, is likely to shoal up with sand rapidly, as it cuts through active shoals. Also, this channel is not effective for trapping of fine sediment partly due to its cross-flow orientation (70-110) with respect to the direction of the prevailing flows.

12. It appears that while the Northwest Fork channel will not be able to draw additional flow into it, it would assist in trapping fine sediment, and may be considered for implementation if the present rate of accumulation of fine sediment in that area continues.

6.3 Recommendations for Future Work

Trap efficiency modeling would be more accurate if based on a sediment model linked to EFDC. Simulations can then be extended to calculate sediment transport by accounting for the role of sediment composition in greater detail and with greater accuracy.

Sources of sediment internal to the modeled domain may have to be simulated in order to identify the internal movement of sediment and formation of shoals in the Northwest Fork and the central embayment. Long-term simulation of flows and sediment transport on the order of years (at least one year) is required to evaluate the net sediment movement necessary for a more effective examination of the efficiency of traps and channels.

LIST OF REFERENCES

Antonini, G.A., Box, P.W., Fann, D.A., and Grella, M.J., 1998. Waterway evaluation and management scheme for the south shore and central embayment of the Loxahatchee River Florida. *Technical Paper TP-92,* Florida Sea Grant College Program, Gainesville, Florida,.

Brunn, P., *Port Engineering,* Fourth Edition, 1989, Gulf Publishing Company, Houston, Texas

Buckingham, W.T., Mehta A.J., 1985. Physical Modeling of Tidal entrances: a case study. *Proceeding of the First National Conference on Dock and Harbor Engineering*, Vol. 2, Indian Institute of technology, Mumbai, E.39-E.47

Department of Army, U.S. Army Corps of Engineers, 1984, *Shore Protection Manual,* U.S. Government Printing Office, Washington, D.C.

Ganju, N.K., 2001. Trapping of organic-rich fine sediment in an estuary. M.S. Thesis, University of Florida, Gainesville, Florida

Ganju, N.K., Mehta, A.J., Parshukov, L.N., and Krone, R.B., 2001. Loxahatchee River , Florida Central Embayment: Sediment budget and trap evaluation. *Coastal and Oceanographic Engineering Program, Report no UFL/COEL-2001/008* University of Florida

Goodwin, C.R., and Russell, M.G., 1984. Simulation of tidal flow and circulation patterns in the Loxahatchee River estuary, southeastern Florida. *Water-Resource Investigation Report 87-4201,* U.S. Geological Survey, Tallahassee, Florida.

Hamrick, M.J., 1992. Three dimensional fluid dynamics computer code: Theoretical and computational aspects, *Special Report No 317 in Applied Marine Science and Ocean Engineering,* Virginia Institute of Marine Science, Gloucester Point, Virginia

Ippen, A.T. and Harleman, D.R.F., 1966. Tidal dynamics in estuaries. In: *Estuary and Coastline Hydrodynamics*, A.T. Ippen, ed., Engineering Societies Monographs, McGraw Hill, New York,

Jaeger, J. M., and Hart, M., 2001. Sedimentary processes in the Loxahatchee River Estuary: 5000 years ago to the present. *Final Report*, submitted to the Jupiter Inlet District Commission, Jupiter, Florida, Department of Geology and Geophysics, University of Florida, Gainesville, Florida.

Jupiter Inlet District, 1999. Environmental restoration program for the Loxahatchee River central embayment. *JID Report*, Jupiter Inlet District Commission, Jupiter, Florida.

Lambe, T.W., and Whitman R.V., 1969., *Soil Mechanics*, Wiley, New York.

Marsh-McBirney, 2001 Electromagnetic Current meter (Model 585 OEM), Operation Manual., USA

McPherson, F.B., and Sonnetag, H.W., 1984. Sediment concentrations and loads in the Loxahatchee River estuary, Florida, 1980-82. *Water-Resource Investigation Report 84-4157,* U.S. Geological Survey, Tallahassee, Florida.

Mehta, A.J., and Parchure, T.M., 2000. Surface erosion of fine-grained sediment revisited. In: *Muddy Coast Dynamics and Resource Management*, B.W. Flemming et al. eds., Elsevier, Amsterdam.

Mehta, A.J. and Li., 2003., Coastal Cohesive Sediment Transport Class notes, *Principles and Process-modeling of Cohesive Sediment Transport,* University of Florida, Florida

Moustafa., J. and Hamrick M.J., 1995. A three-dimensional environmental fluid dynamics computer code: Theoretical and computational aspects. *Special Report 317.* The College of William and Mary, Virginia Institute of Marine Science, Virginia, USA.

Nakamura, S., 2001. *Applied Numerical Methods with Software*. Prentice Hall, Englewood Cliffs, New Jersey

Ochi, M.K., 1990. *Applied Probability and Stochastic Processes*. John Wiley and Sons, New York.

Russell, M.G., and McPherson, F.B., 1982. Freshwater runoff and salinity distribution in Loxahatchee River estuary, Southeastern Florida, 1980-82. *Water-Resource Investigation Report 83-4244,* U.S. Geological Survey, Tallahassee, Florida.

Simpson, M.R., and Oltmann, R.N., 1993. Discharge-measurement system using an acoustic Doppler current profiler with applications to large rivers and estuaries. *Water Supply Paper 2395*, U.S. Geological Survey, Sacramento, California.

Sonnetag, H.W., and McPherson, F.B., 1984. Nutrient input from the Loxahatchee River environmental control district sewage-treatment plant to the Loxahatchee River estuary, southeastern Florida. *Water-Resource Investigation Report 84-4020,* U.S. Geological Survey, Tallahassee, Florida.

Vito, A.V., Editor, 1975. *Sedimentation Engineering. ASCE Manuals and Reports on Engineering Practice – No 54*, PWS-KENT Publishing Company, Boston, USA

Wanless, H., Rossinsky, V., Jr, and McPherson, F.B., 1984. Sedimentologic history of the Loxahatchee River estuary, Florida. *Water-Resource Investigation Report 84-4120,* U.S. Geological Survey, Tallahassee, Florida.

BIOGRAPHICAL SKETCH

Rashmi Ranjan Patra was born in Bhubaneswar in the state of Orissa, India, to Mrs. Sabitri and Dr. Gouranga Ch. Patra. After schooling in M.K.C. High School and M.P.C. College in Baripada, Orissa, the author went to the Indian Institute of Technology, Kharagpur, for a bachelor's degree in civil engineering. During initial years after graduation, he worked as a design engineer for the development of the first dry-dock project in India for Keppel Shipyards, Singapore, and then for Water and Power Consultancy Services (India) Limited before joining the coastal engineering program of the Department of Civil and Coastal Engineering at the University of Florida for the master's degree. Upon obtaining the degree the author plans to practice as a professional and continue the work he has been doing, and thereby contribute to the field, which is so fascinating.